

ACCEPTED MANUSCRIPT

Measuring Glacier Mass Changes from Space - A Review

To cite this article before publication: Etienne Berthier *et al* 2023 *Rep. Prog. Phys.* in press <https://doi.org/10.1088/1361-6633/acaf8e>

Manuscript version: Accepted Manuscript

Accepted Manuscript is “the version of the article accepted for publication including all changes made as a result of the peer review process, and which may also include the addition to the article by IOP Publishing of a header, an article ID, a cover sheet and/or an ‘Accepted Manuscript’ watermark, but excluding any other editing, typesetting or other changes made by IOP Publishing and/or its licensors”

This Accepted Manuscript is © 2023 IOP Publishing Ltd.

During the embargo period (the 12 month period from the publication of the Version of Record of this article), the Accepted Manuscript is fully protected by copyright and cannot be reused or reposted elsewhere. As the Version of Record of this article is going to be / has been published on a subscription basis, this Accepted Manuscript is available for reuse under a CC BY-NC-ND 3.0 licence after the 12 month embargo period.

After the embargo period, everyone is permitted to use copy and redistribute this article for non-commercial purposes only, provided that they adhere to all the terms of the licence <https://creativecommons.org/licenses/by-nc-nd/3.0>

Although reasonable endeavours have been taken to obtain all necessary permissions from third parties to include their copyrighted content within this article, their full citation and copyright line may not be present in this Accepted Manuscript version. Before using any content from this article, please refer to the Version of Record on IOPscience once published for full citation and copyright details, as permissions will likely be required. All third party content is fully copyright protected, unless specifically stated otherwise in the figure caption in the Version of Record.

View the [article online](#) for updates and enhancements.

Measuring Glacier Mass Changes from Space - A Review

Etienne Berthier¹, Dana Floriciou², Alex S. Gardner³, Noel Gourmelen⁴⁻⁵⁻⁶, Livia Jakob⁵, Frank Paul⁷, Désirée Treichler⁸, Bert Wouters⁹⁻¹⁰, Joaquin Belart^{11,12}, Amaury Dehecq¹³, Ines Dussailant⁷, Romain Hugonnet¹⁻¹⁴⁻¹⁵, Andreas Kääh⁸, Lukas Krieger², Finnur Pálsson¹², Michael Zemp⁷

1 LEGOS, Université de Toulouse, CNES, CNRS, IRD, UPS, Toulouse, France

2 Remote Sensing Technology Institute (IMF), German Aerospace Center (DLR), Oberpfaffenhofen, Germany

3 Jet Propulsion Laboratory, California Institute of Technology, Pasadena, California

4 School of GeoSciences, University of Edinburgh, Edinburgh, EH8 9XP, UK

5 Earthwave Ltd, Edinburgh, EH1 2EL, UK

6 IPGS UMR 7516, Université de Strasbourg, CNRS, Strasbourg, 67000, France

7 Department of Geography, University of Zurich, Zurich, Switzerland

8 Department of Geosciences, University of Oslo, Norway

9 Department of Physics, Institute for Marine and Atmospheric Research, Utrecht University, Utrecht, Netherlands

10 Department of Geoscience and Remote Sensing, Delft University of Technology, Delft, the Netherlands

11 National Land Survey of Iceland, Stillholt 16-18, 300 Akranes, Iceland

12 Institute of Earth Sciences, University of Iceland, Reykjavik, Iceland

13 Univ. Grenoble Alpes, CNRS, IRD, Grenoble INP, IGE, Grenoble, France

14 Laboratory of Hydraulics, Hydrology and Glaciology (VAW), ETH Zürich, Zürich, Switzerland

15 Swiss Federal Institute for Forest, Snow and Landscape Research (WSL), Birmensdorf, Switzerland

Abstract

Glaciers distinct from the Greenland and Antarctic ice sheets are currently losing mass rapidly with direct and severe impacts on the habitability of some regions on Earth as glacier meltwater contributes to sea-level rise and alters regional water resources in arid regions. In this review, we present the different techniques developed during the last two decades to measure glacier mass change from space: digital elevation model differencing from stereo-imagery and synthetic aperture radar interferometry, laser and radar altimetry and space gravimetry. We illustrate their respective strengths and weaknesses to survey the mass change of a large Arctic ice body, the Vatnajökull Ice Cap (Iceland) and for the steep glaciers of the Everest area (Himalaya). For entire regions, mass change estimates sometimes disagree when a similar technique is applied by different research groups. At global scale, these discrepancies result in mass change estimates varying by 20 to 30%. Our review confirms the need for more thorough inter-comparison studies to understand the origin of these differences and to better constrain regional to global glacier mass changes and, ultimately, past and future glacier contribution to sea-level rise.

Abstract

1. Introduction

2. Importance of an accurate glacier inventory

3. Differencing of digital elevation models

1

4

6

9

1

1	3.1. Principle	10
2	3.2. DEM from optical stereo-imagery	11
3	3.2.1. Stereo sensors with decametric (5-15 m) resolution	11
4	3.2.2. Stereo sensor with metric to submetric resolution	13
5	3.2.3. Future missions with stereo capabilities	14
6	3.3. DEM from radar imagery	14
7	3.3.1. Elevation data from spaceborne bistatic InSAR systems	15
8	3.3.2. Limitations and challenges of InSAR DEMs for elevation change mapping	17
9	3.3.3. Future missions with single pass InSAR capabilities	18
10		
11		
12		
13	4. Radar altimetry	19
14	4.1. Radar altimetry data	19
15	4.2. Principle to assess glacier changes	21
16	4.3. Limitations and challenges	21
17	4.4. Outlook	22
18		
19		
20		
21	5. Laser altimetry	22
22	5.1. Laser altimetry data from ICESat and ICESat-2	22
23	5.2. Principles to assess glacier changes	24
24	5.2.1. Methods for calculating elevation change from near-repeat observations	24
25	5.2.2. Methods for non-repeat observations and rough surfaces	25
26	5.3. Outlook	26
27		
28		
29	6. Gravimetry	26
30	6.1. GRACE and GRACE-FO data	27
31	6.2. Glacier mass balance from GRACE	28
32	6.3. Limitations and challenges	29
33	6.4. Outlook	31
34		
35		
36		
37	7. Strengths and weaknesses of the different techniques	31
38	7.1. Comparison over the Vatnajökull Ice Cap - Iceland	31
39	7.2. Comparison over the Everest area - Himalaya	36
40	7.3. Synthesis of the pros and cons of each method	38
41		
42		
43	8. Conclusion	41
44		
45	Acknowledgments	42
46		
47	Author contribution statement	42
48		
49	References	43
50		
51		
52		
53		
54		
55		
56		
57		
58		
59		
60		

1. Introduction

Glaciers are an iconic symbol of climate change (Oerlemans, 2005). Their geometry responds to changes in temperature and precipitation at yearly to decadal time scales in ways that are easily perceived by humans. Their rapid present-day shrinkage has direct, and sometimes severe, consequences on some inhabited areas on Earth as their meltwater contributes significantly to rising sea level (Cazenave et al., 2018; Frederikse et al., 2020; Meier, 1984) and alters regional water resources in arid regions (Pritchard, 2019; Huss and Hock, 2018). Glacier retreat also has a distinct effect on biodiversity, tourism and glacier hazards (Cauvy-Fraunié and Dangles, 2019; Haeberli and Whiteman, 2015; Salim et al., 2021).

This review deals with all glaciers on Earth, i.e. the more than 200'000 ice bodies disconnected from or weakly connected to the Greenland and Antarctic ice sheets (Pfeffer et al., 2014; RGI Consortium, 2017). Their cumulative size ($\sim 700'000 \text{ km}^2$) is rather modest compared to the two giant ice sheets. Their overall volume is such that, if they were to melt entirely, sea level would rise by about 30 cm (Millan et al., 2022; Farinotti et al., 2019), which is one to two orders of magnitude smaller than the same quantity for the two ice sheets. However, being highly sensitive to climate fluctuations (Oerlemans, 2001; Cuffey and Paterson, 2010), even a small climate imbalance leads to rapid mass change. Glacier mass change remains one of the least-constrained components of the global water cycle, and was identified as a critical research gap in the 2019 Intergovernmental Panel on Climate Change (IPCC) Special Report on the Ocean and Cryosphere in a Changing Climate (Portner et al., 2019).

The glacier-wide mass balance rate is a key variable to characterise the state of health of glaciers, their contribution to river runoff and sea level rise (Zemp et al., 2019; Hugonnet et al., 2021; Marzeion et al., 2014). It is defined as the change of mass of an entire glacier (or an entire glacierized region) and expressed in gigatons per year (Gt/yr = total mass balance in this review). For improved comparability between glaciers or regions of contrasting sizes, this quantity is often divided by the glacierized area and is expressed as metre water equivalent per year (m w.e./yr = specific mass balance), which is equivalent to the water layer gained or lost on average during one year (Cogley et al., 2011).

Traditionally, and during most of the 20th century, glacier mass balance has been derived from pointwise field observations performed on a few dozen glaciers by repeatedly measuring the melt at ablation stakes and the snow accumulation from pits or cores in the accumulation area (Thibert et al., 2008; Zemp et al., 2015). These in situ measurements of the surface mass balance were sometimes complemented with repeat airborne photogrammetric flights to measure multi-year volume change and validate/calibrate the field measurements (Zemp et al., 2013; Andreassen et al., 2016). Global mass change estimates were then derived by extrapolating these few tens of measurements to the entire glacier sample (Meier, 1984; Kaser et al., 2006), leading to large uncertainties or even biased estimates (Gardner et al., 2013). Since the start of the 21st century, the launch of novel spaceborne sensors has fostered the emergence of remote sensing methods to measure glacier mass changes at local, regional and global scales (Bamber and Rivera, 2007; IGOS, 2007; Marzeion et al., 2017; Haeberli et al., 2021; Taylor et al., 2021).

This review aims at presenting and comparing these modern satellite-based techniques (Figure 1), i.e. digital elevation model (DEM) differencing (section 3), repeat radar (section 4) and laser (section 5) altimetry, and gravimetry (section 6). This review does not address the input/output (or component) method. This method estimates the glacier mass change as the difference between the surface mass balance and the ice discharge (Noël et al., 2018). In this method, the only mass balance component effectively measured from space is the frontal ablation, which in general is a modest part of the overall mass budget (McNabb et al., 2015; Van Wychen et al., 2016; Błaszczyk et al., 2009; Kochtitzky et al., 2022). The input/output method is thus too heavily based on in situ measurements or models to estimate the surface mass balance (Bamber et al., 2018) to be considered in the present review.

Because all the satellite-based techniques rely at some point on the availability of a global inventory of glacier outlines, the review starts with a presentation of the state-of-the-art on glacier mapping from space (section 2). In a final section (section 7), we compare the ability of the different techniques to depict the elevation changes and mass balance of a large Arctic ice cap (Vatnajökull, Iceland), steep glaciers in the Everest area and discuss their respective strengths and weaknesses with a regionally-differentiated perspective. Our goal is not an exhaustive overview of the Earth observation satellite missions used in glaciology, i.e. we only consider the satellite missions that have been used specifically in glacier mass balance studies (Figure 2).

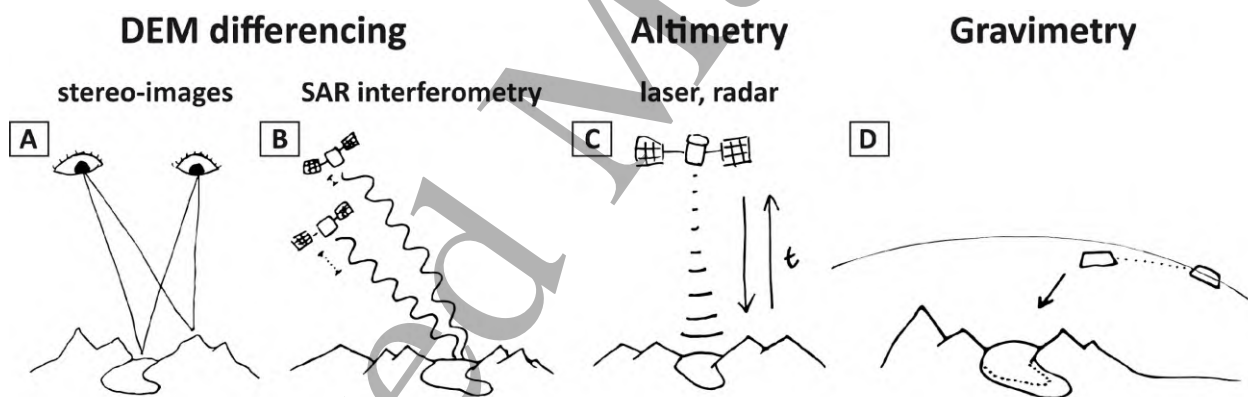


Figure 1: Sketch of the main techniques used to estimate glacier mass change from space. DEM differencing and altimetry (A-C) first determine glacier volume changes through repeat measurement of the glacier elevations. The sources of elevation data are usually DEMs, commonly derived from (A) satellite stereo images, where two satellites "see" the terrain in 3D just as humans do with their two eyes, or (B) SAR interferometry, which reconstructs the surface terrain from the phase difference of the recorded microwave signal at two SAR satellites that fly very close together. Other sources or point/profile-based elevation data are (C) radar and laser altimetry, which determines the surface elevation directly under the satellite by means of the two-way travel time of a radar/laser pulse. (D) Satellite gravimetry is used to detect mass changes directly: two satellites on the same orbit are connected with a ranging system that detects acceleration/deceleration of the satellites relative to each other caused by changes in the gravimetric force. These changes include, among others, glacier mass change between different satellite overpasses. Source of A, B and C: Treichler (2017).

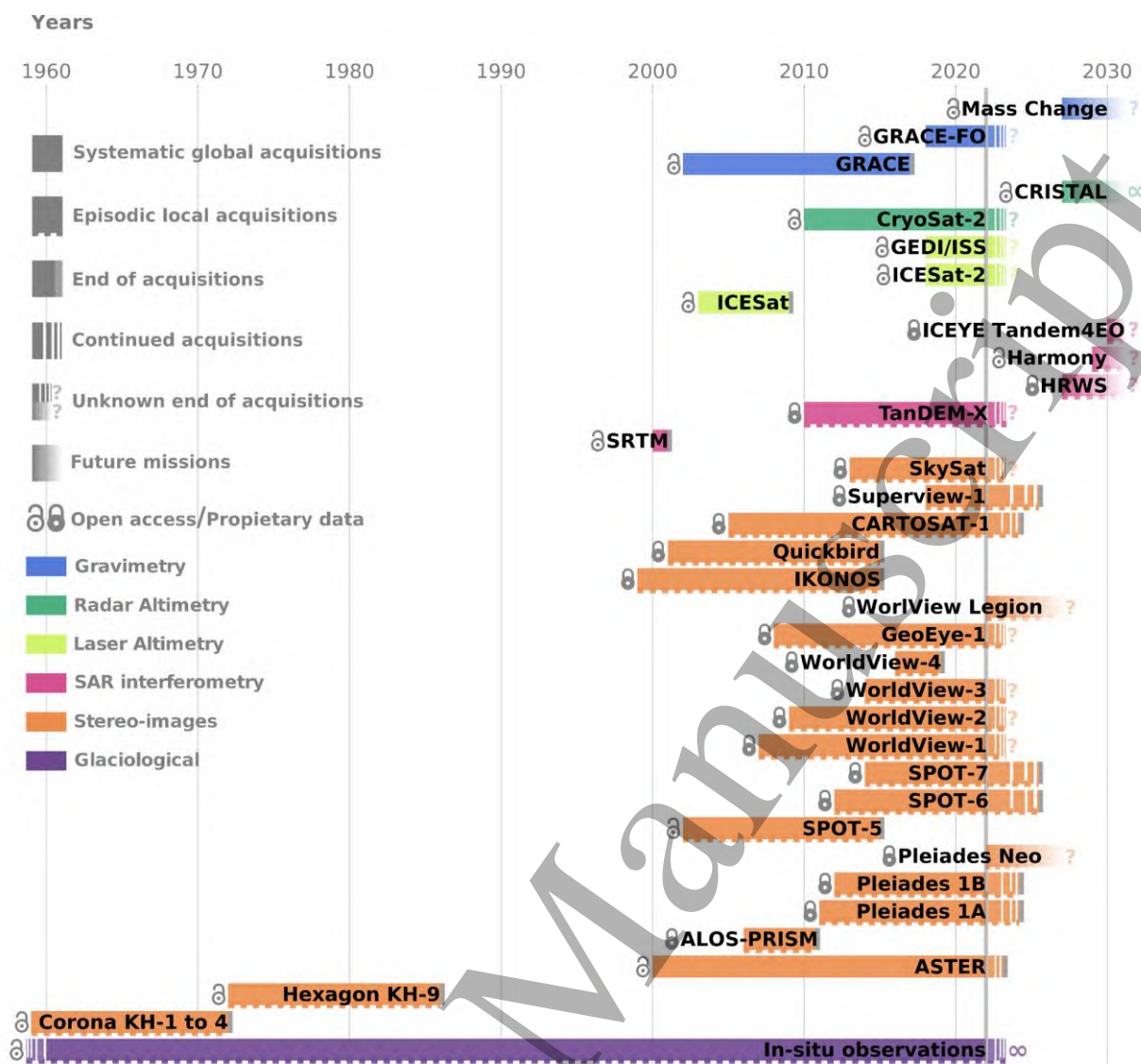


Figure 2: Overview of the lifetime of the main satellite missions used in glacier mass balance studies (as of October 2022). The colours distinguish different types of satellite sensors. The “?” is used when the decommission date is not known and “∞” for long term (i.e. operational) monitoring without a specific end date. A distinction is also made between missions that provide systematic “global” coverage and others that make “local” acquisitions on demand. “Open access” missions are those for which the data are fully open access to all users. Conversely, “proprietary” is used for commercial missions or missions for which the access is limited to certain users, for example upon acceptance of a research proposal. The list of future missions is not exhaustive but aims at illustrating a potential gaps for certain categories of data (notably, laser altimetry and “open access” stereo-images with global coverage).

2. Importance of an accurate glacier inventory

The main purpose of a glacier inventory is to characterise the area covered by glaciers (i.e. where are they?) and the volume or mass of ice they store (i.e. how much ice do they contain?). Whereas glacier outlines define the region covered by glacier ice, glacier area distribution with elevation (i.e. glacier hypsometry) is of key importance for numerical modelling of glacier evolution and for hydrological models. Glacier volume is derived from a range of methods and needed for water resources assessment as well as calculation of glacier contribution to sea-level rise. With glacier changes (in length, area and volume) being widely accepted as key indicators

of climate change (Bojinski et al., 2014; Trewin et al., 2021; Oerlemans, 2005), a glacier inventory also provides a base for change assessment when mapped outlines are available for at least two points in time. Related assessments over longer time periods also provide information about glacier health. For example, glaciers losing area at their highest elevations are in a strong disequilibrium with climate and will ultimately disappear (Pelto, 2010; Carturan et al., 2020).

When glacier outlines are combined with a DEM, a wide range of glacier-specific topographic characteristics can be derived (Kienholz et al., 2015), which allows calculating further metrics to describe a glacier (Haeberli and Hoelzle, 1995). For example, glacier median (or mean) elevation is widely used as a proxy for the equilibrium line altitude (ELA) for a glacier with a zero mass balance (Braithwaite and Raper, 2009). When this so-called balanced-budget ELA_0 is known, a rough climatic classification of glaciers can be derived (Ohmura et al., 1992) which opens a wide range of further calculations, including details about precipitation in high mountains regions (Sakai et al., 2015). And, most importantly, glacier outlines spatially constrain glacier-specific calculations such as elevation changes, flow velocities and debris-covered fractions (Scherler et al., 2018). For the former two, glacier outlines also constrain where “off glacier” terrain is. These stable regions can be used for several steps in the data processing (e.g. DEM co-registration) and for the uncertainty assessment (e.g., Nuth and Kääb, 2011). In short, glacier outlines are required for nearly all glacier-related calculations (Kargel et al., 2005). But how are glacier outlines measured?

Nowadays, scientists use inventories readily available, most frequently from the Global Land Ice Measurements from Space (GLIMS) glacier database (which is multi-temporal) or the Randolph Glacier Inventory (RGI), which provides a single snapshot of glacier extents and is available in a globally near complete version since 2011 (Pfeffer et al., 2014). Since then, the RGI has been continuously improved and is now available in its version 6 (RGI Consortium, 2017). Outlines available in the GLIMS database and from the RGI have been freely provided by the scientific community on a voluntary basis as an outcome or by-product of diverse research projects. This means that updating and filling of the database is slow and is so far uncoordinated. Today, a working group¹ of the International Association of Cryospheric Sciences (IACS) is coordinating glacier data compilation and redistribution. The group also prepares the release of RGI version 7.

As glacier outlines are mostly derived from optical satellite images, the opening of the Landsat archive in 2008 (Wulder et al., 2012), with free access to orthorectified imagery, started a new era in global glacier mapping and change assessment. Semi-automated mapping of glaciers from multi-spectral satellite data using previously developed methods (Hall et al., 1987; Bayr et al., 1994; Paul et al., 2002) were applied to large samples of glaciers all over the world (Bolch et al., 2010; Frey et al., 2012; Guo et al., 2015). The most popular method is based on a simple red (noted R, or near infrared, NIR) / short wave infrared (noted SWIR) band ratio that increases contrast between ice and snow as their reflection is close to zero in the SWIR band. This allows distinguishing snow and ice from all other terrains or clouds with a simple threshold th applied to the ratio image, e.g.

1 <https://cryosphericssciences.org/activities/working-groups>

$$glaciers = where \left(\frac{R}{SWIR} > th \right)$$

To achieve the best possible results, the threshold value (e.g. $th = 1.5$) has to be selected and optimised manually for individual regions and scenes, in general balancing the inclusion of dark ice in cast shadow and excluding bare rock (Paul et al., 2016). The resulting binary image is transformed to polygons using raster to vector conversion (Figure 3). Remaining omission (ice hidden by clouds or debris cover) and commission errors (water, bare rock, seasonal snow, lake and river ice) have to be manually corrected during post-processing. In regions with many debris-covered glaciers, this last step is very laborious and time consuming (Racoviteanu et al., 2022). Debris cover on glaciers is thus the bottleneck of global glacier mapping efforts and hinders rapid and easy updates of the global datasets with its >200'000 glaciers. Once glacier outlines with debris cover are mapped, the extent of debris cover can be determined as a residual from automated clean ice mapping (Scherler et al., 2018; Herreid and Pellicciotti, 2020). Other problematic factors are remaining seasonal snow and clouds hiding the glacier perimeter. Both require that only the most appropriate scenes are selected from the archives for glacier mapping. In maritime regions with abundant clouds and late lying seasonal snow, high-quality glacier extents can thus only be mapped occasionally, typically every 5-10 years. This has improved a bit with the more frequent observations from Sentinel-2 (at least every 5 days, even more often towards higher latitudes), as the chance for cloud-free images acquired at the end of the ablation period has considerably increased.

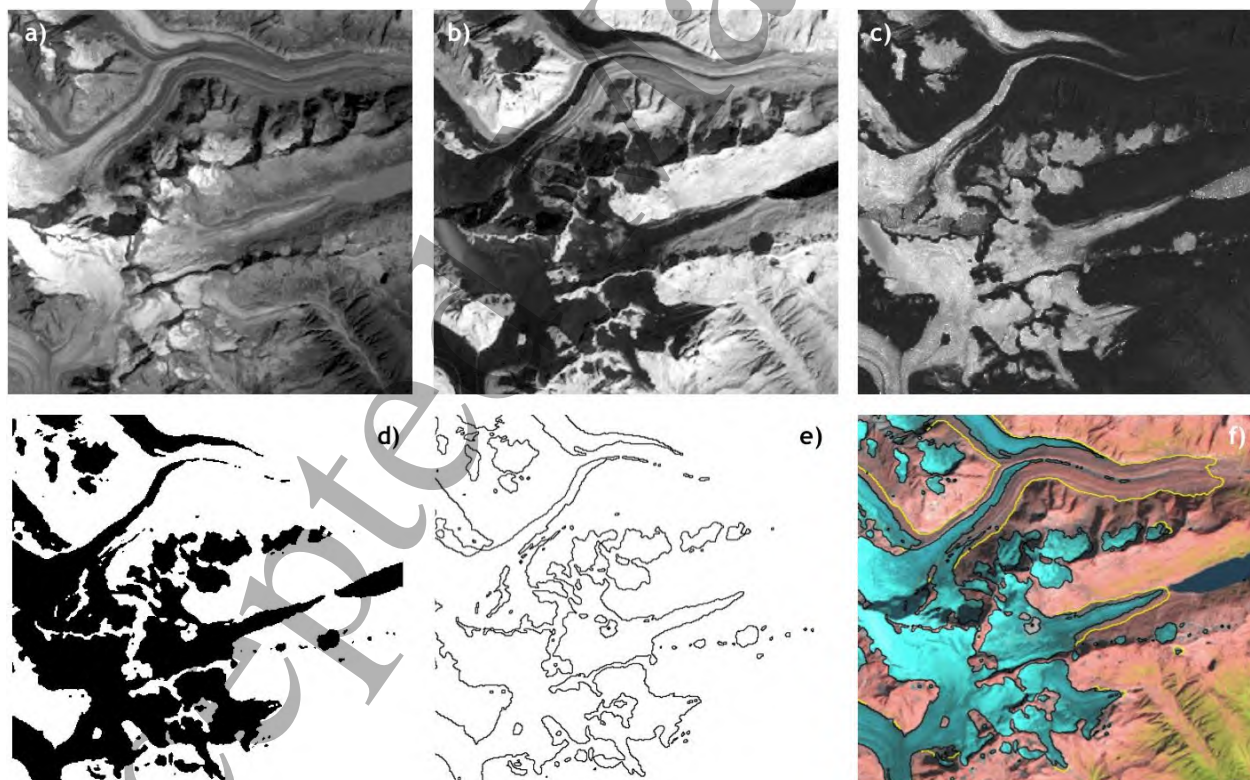


Figure 3: Glacier mapping with the band ratio method applied to Landsat Thematic Mapper (TM) images of Unteraar (upper glacier in the image) and Oberaar (the one in the centre) glaciers in the Bernese Alps, Switzerland. a) TM band 3 (red), b) TM band 5 (shortwave infrared), c) band ratio TM3/TM5, d) the resulting binary glacier map after applying a threshold to c), e) glacier outlines after raster-vector conversion of d), and f) overlay of the outlines seen in e) in black with manually corrected extents in yellow, adding the unmapped glacier area under debris cover. The background image in f) is a false-

1 *colour composite with TM bands 5, 4, and 3 as red, green and blue, showing ice and snow in light blue,*
2 *bare rock in pink to brown and vegetation in green to yellow. Landsat-5 image acquired 31 August 1998.*
3 *Landsat-5 image courtesy of the U.S. Geological Survey. Source: glovis.usgs.gov.*
4

5 An important issue when using glacier outlines for elevation change calculation is good spatial
6 and temporal matches. The outlines should refer to the larger glacier extents, e.g. for retreating
7 glaciers the date of the first DEM. As many DEM differencing studies use the Shuttle Radar
8 Topography Mission (SRTM) DEM (February 2000) or the first Advanced Spaceborne Thermal
9 Emission and Reflection Radiometer (ASTER) DEMs (from 2000 or 2001) as a starting point, and
10 because the vast majority of glaciers are shrinking worldwide (Zemp et al., 2015), glacier outlines
11 derived from satellite images acquired around the year 2000 are preferable. Most outlines in
12 RGI version 6 have been acquired between 2000 and 2010, but several regions only offer much
13 older (1960s to 1980s) or more recent extents. It might thus be required to correct these
14 manually. A manual correction is also needed in the case of surging glaciers so that the rapid
15 volume gain at their advancing terminus is not missed (Berthier and Brun, 2019). A poor spatial
16 match can arise when the DEM used for orthorectification of the satellite images is different
17 from —or of a lesser quality than— the DEMs used to obtain elevation changes (Kääb et al.,
18 2016). The related horizontal shifts cannot easily be corrected as they are non-systematic.

19 The specific mass balance is computed as the total mass balance divided by the mean glacier
20 area over the study period (Fischer et al., 2015; Cogley et al., 2011). Thus, in principle, two sets
21 of glacier outlines should be available, one at the start and one at the end of the study period.
22 Practically, this is often not the case, especially for studies with a regional or global scope that
23 mostly use the RGI (Zemp et al., 2019; Hugonnet et al., 2021). Uncertainties due to the lack of a
24 repeat inventory or to low quality of some outlines in the RGI can be assessed in regions where
25 state-of-the-art and repeat inventories are available (e.g. Section 7 in the supplementary
26 material of Dussaillant et al. (2019)). As glacier area loss is fast, sometimes over 1% per year
27 (Paul et al., 2020), repeat regional and global inventories are needed.

28 Finally, differences in how to interpret/identify which parts belong to a glacier can have an
29 impact on mass balance estimates. Again, debris-covered glacier parts introduce the largest
30 uncertainty in interpretation (Paul et al., 2013) and can, moreover, easily be confused with rock
31 glaciers. These might look morphologically very similar and the transition to a debris-covered
32 glacier can be gradual as in cold/dry climates some rock glaciers might have developed from
33 heavily debris-covered glaciers (Janke et al., 2015). Depending on which glacier extent is used
34 and how strong the changes are in the uncertain glacier zone, clear differences in the specific
35 mass balance (and to a lesser extent the total mass balance) can occur across different studies
36 (Ferri et al., 2020). This needs to be homogenised, but until then, a precise description of the
37 glacier inventory used (and the modifications applied) is required to allow intercomparison of
38 results from different studies.

3. Differencing of digital elevation models

39 The comparison of multi-temporal DEMs, often referred to as the geodetic method, has been

used for decades to build maps of glacier elevation changes (dh). Division by the time separation between the two surveys gives elevation change rates (dh/dt) that can then be converted to mass balance using an assumption on the density of the material gained or lost. Initially applied to DEMs derived from maps (e.g., Adalgeirsdóttir et al., 1998; Nuth et al., 2007; Pálsson et al., 2012), aerial photographs (Thibert et al., 2008; Finsterwalder, 1954) and more recently to airborne Lidar data (Abermann et al., 2010; Echelmeyer et al., 1996), the technique has been used since the early 2000s with satellite DEMs, often in conjunction with older maps (Berthier et al., 2004; Kääb, 2008; Rignot et al., 2003). We first describe the principle of the method (3.1) before presenting the two main sources of satellite DEMs, optical stereo-imagery (3.2) and interferometric SAR data (3.3).

3.1. Principle

The method consists in coregistering and then differencing two DEMs, i.e. two grids representing the elevation of the glacier surface at two epochs in time. Since 2012, the method has also been modified to tackle time series of DEMs, either using a simple linear regression through the elevation time series (Willis et al., 2012; Nuimura et al., 2012) or using a more advanced statistical framework to resolve non linearities in the glacier elevation change signal (Hugonnet et al., 2021).

A key preprocessing step is the relative adjustment of the different DEMs on the stable terrain surrounding the glaciers. The compared DEMs must share the same map projection and, importantly, be referenced to the same elevation datum (geoid or ellipsoid, see <https://doi.org/10.5194/tc-2021-197-CC1>). A first and mandatory step is to correct the horizontal and vertical shifts between the DEMs using, for example, the coregistration method from Nuth and Kääb (2011). In the case of spy satellite images (presented below), an affine transformation (rotation, scaling) or more complex non linear shifts may have to be corrected beforehand (Maurer and Rupper, 2015; Dehecq et al., 2020). After applying this translation vector, some sensor-specific artefacts may remain and need to be modelled to approach an unbiased elevation change estimate (Nuth and Kääb, 2011). For example, undulations in the DEMs in the along-track direction, related to the jitter of the platform, are common in optical imagery (Girod et al., 2017). In other cases, tilts or along/cross track biases between the DEMs have to be corrected (Shean et al., 2016). If DEMs of different original resolutions are compared, some biases related to the terrain morphology may also persist. Terrain curvature proved to be a good proxy for correcting the latter biases (Gardelle et al., 2012). After relative adjustment, DEMs can be subtracted (or processed as a time series) to map elevation changes.

There are two final hurdles before obtaining the glacier-wide total mass balance, two issues which are shared with the altimetry-based estimates discussed in sections 4 and 5 of this review. (1) The first one is the need to fill in data gaps in the map of elevation changes. These gaps are often distributed unevenly and thus, if not filled properly, may lead to biased estimates. For example, native stereo sensors from the late 1990s or early 2000s such as ASTER or Satellite Pour l'Observation de la Terre (SPOT) 5 acquired imagery using 8-bits sensors (for which images are made of 2^8 , i.e. 256 digital numbers) leading to poor radiometric dynamics in the bright, textureless accumulation area of glaciers, and hence a concentration of data gaps. As these upper regions often experience attenuated elevation changes than the lower reaches

(Schwitter and Raymond, 1993; Belart et al., 2019), filling these gaps with a glacier-wide average value would bias the mass balance estimate. Several approaches have been developed to fill data gaps (Seehaus et al., 2020), one of the best performing and robust being the local hypsometric approach that exploits the fact that elevation changes are often correlated with altitude (McNabb et al., 2019). (2) The second hurdle is the conversion of the volume change to mass change. This requires an estimate of the density conversion factor (Cuffey and Paterson, 2010). Here again, various strategies have been used. Assuming an unchanged vertical density profile (the so-called Sorge's law), many studies (e.g., Bader, 1954; Arendt et al., 2002) used a single ice density (900 kg/m^3). Others (e.g., Haag et al., 2004) have favoured separating the ablation area (where ice is lost at a density of 900 kg/m^3) and accumulation area, where they used an average density for the firn (often 500 to 600 kg/m^3), assuming, implicitly, a change in the vertical density profile. Huss (2013) used a firn densification model calibrated with in situ measurements of firn density to show that a single density of $850 \pm 60 \text{ kg/m}^3$ was a good compromise for glacier-wide estimates over a measurement period longer than 3 years (and ideally longer than 5 years). Improvements in this volume to mass conversion are still needed as it remains the largest source of errors in a recent estimate of global glacier mass change (Hugonnet et al., 2021).

Due to these uncertainties in the volume to mass conversion and the precision of the elevation change measurements, DEM differencing is typically applied over periods of 5 to 10 years, although dense time series of DEMs can also allow exploring short term, seasonal elevation changes (Seehaus et al., 2015; Belart et al., 2017; Beraud et al., 2022). The temporal resolution and timeliness of the geodetic mass balance record can be improved with ancillary data such as in situ mass balance measurements (Zemp et al., 2019, 2020) or snow line satellite observations (Barandun et al., 2021; Davaze et al., 2020).

3.2. DEM from optical stereo-imagery

The principle of DEM generation from a stereoscopic pair is simple and has been used for decades by national mapping agencies to chart the Earth's land topography using overlapping aerial photographs. It consists of estimating the distortions (also called the parallax) between pair, triplet or more images acquired from different viewpoints. If the acquisition geometry (position, pointing angles) of the images are known, the parallax can be converted to terrain elevation. For an historical background, the reader is referred to a review (Toutin, 2001) describing the early days of DEM generation from optical satellite images.

The main drawback of optical (visible or near infra-red) images, compared to radar data, is that they are weather dependent. No DEM can be derived during the (polar) night or when clouds obscure the Earth's surface. Another notorious limitation is that DEMs derived from these images often concentrate data gaps and exhibit more noise in the snow-covered accumulation areas. We will see below that this is however not true anymore for modern stereo-imagery.

In the following, we distinguished two generations of stereo sensors depending on their resolution. We focus on the sensors that have been most used for estimating glacier elevation changes and do not aim at an exhaustive overview.

3.2.1. Stereo sensors with decametric (5-15 m) resolution

Early satellite multispectral sensors (Landsat, SPOT) did not have built-in stereo capabilities. However, the SPOT1-4 satellites could point across track so that stereo pairs were assembled on-demand using images acquired a few days or weeks apart from different orbits. DEMs have been derived from such image pairs (AlRousan et al., 1997), including for alpine glacier tongues in the 1990s or early 2000s (Berthier et al., 2004). A severe limitation of these across-track stereo acquisitions was the loss of visual similarities between images acquired several days apart, the increased risks of clouds and the fact that glacier surface displacement between the two acquisitions could bias the measurement of the parallax. In the SPOT1-4 image catalogue, the number of such opportunistic stereo pairs is limited.

The sparse availability of stereo pairs from civil satellites before 2000 can be compensated by the declassification of spy satellite images from the 1960s, 70s and 80s acquired by missions such as Corona and Hexagon (Surazakov and Aizen, 2010). They provide very useful data to measure multi-decadal glacier mass balance and put the recent changes (i.e. post-2000) in a longer perspective as done for the Himalaya and the Tibetan Plateau (Maurer et al., 2019; Zhou et al., 2018; Holzer et al., 2015). The recent development of open-source tools to calculate DEMs from these images (Dehecq et al., 2020; Belart et al., 2019; Ghuffar et al., 2022) should further increase their use in the future.

In the civil domain, native stereo capabilities emerged in the early 2000s with the ASTER sensor on board the Terra satellite (Hirano et al., 2003) and the High Resolution Stereoscopic (HRS) instrument on board SPOT5 (Gleyzes et al., 2012). Both sensors are made of two telescopes, one pointing forward (or toward the nadir for ASTER) and the other backward. Stereo pairs are thus systematically acquired along track within a few tens of seconds, resulting in a large archive of scenes suitable for DEM generation. Members of the GLIMS project were involved in the ASTER Science team and ensured that glaciers were among the priority targets for ASTER (Raup et al., 2000). Importantly, the GLIMS team also tuned the gain setting to avoid saturation of the images over the bright snow-covered areas. Numerous glaciological studies exploited the ASTER stereo-capabilities following some promising early results (Kääb, 2002; Kargel et al., 2014). Since April 2016, ASTER images have been freely available which boosted their use by the scientific community. As of writing, ASTER is still acquiring stereo pairs but the end of the mission is planned for September 2023 and, unfortunately, ASTER will not be replaced.

The SPOT5-HRS archive (2002-2015) has been publicly opened recently (June 2021) as part of the SPOT World Heritage program from the French Space Agency, CNES. Before that, access to the images was restricted to the French mapping agency and the French defence. Only during the international polar year (IPY), 2007-2009, a dedicated image acquisition program took place over the polar regions. The SPIRIT (Spot5 stereoscopic survey of Polar Ice: Reference Images & Topographies) initiative distributed 40-m DEMs and 5-m ortho-images of glaciers and ice sheet margins to the scientific communities (Korona et al., 2009). The SPOT5-HRS archive is large and almost unexploited. Outside the SPIRIT period, this mission did not benefit from a fine gain setting for glacier and ice sheets (contrary to ASTER) so that many images in the catalogue may be too saturated for DEM generation.

1 The Panchromatic Remote-sensing Instrument for Stereo Mapping (PRISM), onboard the ALOS
2 satellite, also has native stereo capabilities (triplet of images acquired along track) together with
3 a promising 2.5 m resolution and a 60-km swath. SPOT6 and SPOT7 have a similar swath but
4 even higher resolution (1.5 m). DEMs derived from PRISM or SPOT6/7 have been less used by
5 the glaciological community (Ragetti et al., 2016; Lamsal et al., 2011; Berthier and Brun, 2019),
6 likely because data access is not as straightforward as for ASTER. The same also applies to
7 Cartosat-1 (Pieczonka et al., 2011).
8
9

10 Various software has been used to generate DEMs from the stereo-pairs. Up to a few years ago,
11 most of the processing was done using commercial software such as PCI Geomatica (Toutin,
12 2001) or ERDAS (Bolch et al., 2008). Recently, open-source tools such as MicMac, SETSM or ASP
13 have been developed to process high resolution images (Beyer et al., 2018; Rupnik et al., 2018;
14 Noh and Howat, 2015) and were also adapted to medium resolution images (Girod et al., 2017;
15 Shean et al., 2020).
16
17
18
19

20 **3.2.2. Stereo sensor with metric to submetric resolution**

21
22 In the second part of the 2000s and during the 2010s, a novel generation of high resolution
23 satellites was launched, including Worldview (WV, DigitalGlobe, now Maxar) and Pléiades (CNES
24 and Airbus Defence & Space). These satellites have a sub-metre resolution and are
25 characterised by a high agility so that stereo pairs (or triplet) can be formed from along-track
26 acquisitions a few tens of seconds apart. Two characteristics have dramatically increased the
27 quality of the DEMs that can be derived from these modern sensors over snow and ice. First,
28 the radiometric depth has evolved from 8 bits for ASTER, SPOT1-5 (and others) to 11 or 12 bits
29 (2048 or 4096 digital numbers) for WV1-4 and Pléiades (and SPOT6/7). Second, the sub-metre
30 resolution means that fine scale features of the terrain can be resolved. Both characteristics
31 lead to images with a lot of contrast even in the snow-covered accumulation areas and almost
32 no saturation. This implies that (i) the entire archives are useful for glaciology (without any
33 special gain setting) and (ii) the correlation between the stereo-pair works efficiently so that
34 almost complete DEMs can be constructed even over ice sheets (Shean et al., 2016; Howat et
35 al., 2019) or the glacier accumulation areas (Berthier et al., 2014). The higher spatial resolution
36 and the good knowledge of the orbits also results in a higher vertical precision of the DEMs. The
37 improvement in resolution and precision between ASTER and Pléiades is illustrated for the
38 Meighen Ice Cap (Figure 4). As a rule of thumb, the vertical DEM precision is on the order of the
39 image resolution.
40
41
42
43
44
45
46
47
48
49
50
51
52
53
54
55
56
57
58
59
60

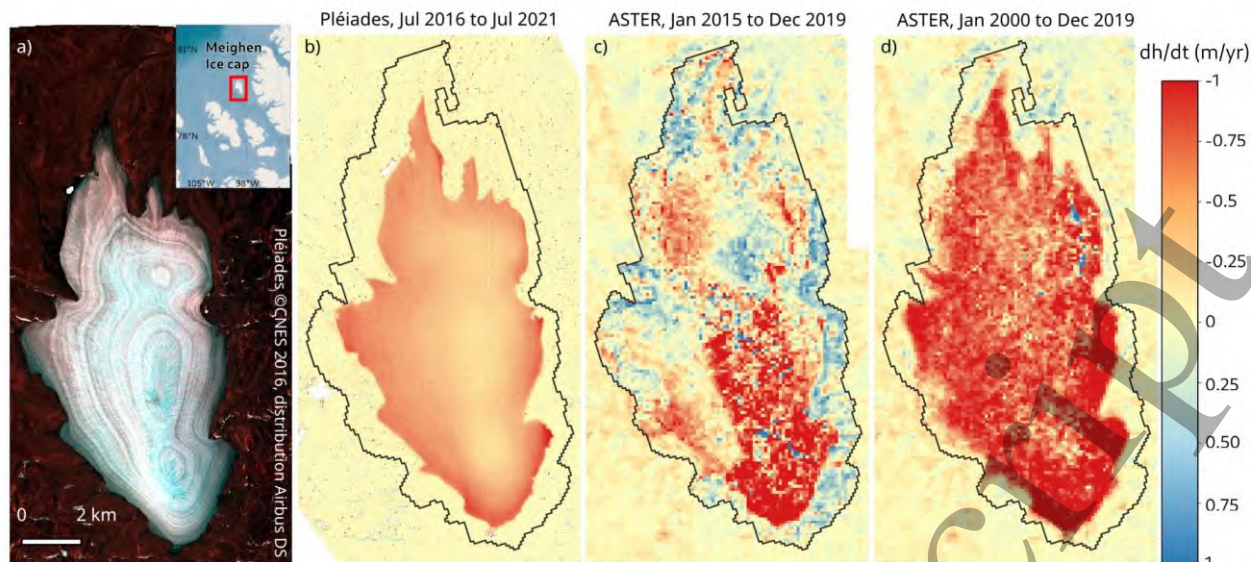


Figure 4: a) False color (near-infrared) image of Meighen Ice cap, Canadian Archipelago (Burgess and Danielson, 2022), from a Pléiades scene acquired in July 2016 (©CNES 2016, distribution Airbus DS). b-d: Rate of elevation change (dh/dt in m/yr) for the Meighen Ice Cap (RGI60-03.00691) during 5 years periods, from two Pléiades stereo-pairs acquired 29 July 2016 and 19 July 2021 (b, this study), from all ASTER stereo-images acquired (c) between 1 January 2015 and 31 December 2019 (Hugonnet et al., 2021) and (d) during the 20 year period from 1 January 2000 to 31 December 2019 (Hugonnet et al., 2021). The black polygon is the RGIv6 outline, derived from 1999-2003 imagery according to the RGI handbook, although these elevation change maps suggest that the outlines were derived from older imagery. Note the sharply reduced noise level from very high resolution 12-bit Pléiades stereo-imagery compared to ASTER (8-bit images) and also the need for an updated glacier inventory to properly estimate the specific mass balance of this ice cap.

The sub-metre resolution is obtained at the cost of relatively narrow swaths (~10-20 km) compared to, for example, ASTER (60 km) or SPOT-HRS (120 km). This means that several images, often acquired over the course of several days or weeks, need to be mosaicked to cover a large ice cap or an entire mountain range. Another drawback is that these sensors are commercial, which complicates data accessibility for the scientific community. They mostly acquire images on-demand and contrary to ASTER, they do not continuously build a vast archive of stereo images. Exceptions to this rule are the numerous, time-stamped WV DEMs freely available in the Arctic (ArcticDEM, Porter et al., 2018), Antarctic (REMA DEMs, Howat et al., 2019) and in High Mountain Asia (Shean et al., 2020). Dedicated acquisition campaigns are also performed by the French Space Agency (CNES) through the Pléiades Glacier Observatory².

3.2.3. Future missions with stereo capabilities

Several space agencies are on the way or have projects to launch more satellites with improved stereo capabilities such as Pléiades Neo from Airbus or WorldView Legion for Maxar. In 2023, CNES and Airbus DS will launch the CO3D constellation³ with the main goal to build a global high resolution DEM. However, none of these missions is open-access and scientifically driven.

² <https://www.legos.omp.eu/pgo/>

³ <https://labo.obs-mip.fr/multitemp/co3d-the-very-high-resolution-mission-dedicated-to-3d/>

1 A game changer would be a future satellite stereo mission with a high resolution (on the order
2 of 1-2 metres), capable of covering a large extent of terrain in a short period of time and
3 continuously acquiring freely available images. Such a concept, currently named Sentinel-HR⁴, is
4 being promoted by scientists from several disciplines and explored further by the French Space
5 Agency (Iliopoulos et al., 2022).
6
7
8
9

10 **3.3. DEM from radar imagery**

11 Spatially-distributed surface elevation information can also be gained from single-pass across-
12 track interferometric (InSAR) data. In this case, a radar system with spatial separation (baseline)
13 between transmitter and receiver is required for the data acquisition, with one antenna
14 transmitting and both receiving the complex SAR signal. This so-called bistatic instrument
15 configuration enables the generation of high quality interferograms that are not affected by
16 temporal decorrelation and ice motion and with reduced atmospheric effects (Rosen et al.,
17 2000; Bamler and Hartl, 1998).
18
19
20
21
22

23 The cross-track technique is based on the evaluation of phase differences measured by the two
24 SAR antennae. While in a single SAR image the location of each surface point is reduced to the
25 range distance, this technique is a means to measure also the radar look angle allowing to recover
26 the point's location in space. The interferometric phase difference of every pixel is used to
27 determine the difference between the two range distances to the SAR antennae which in turn
28 can be considered a measure of the radar look angle (Bamler and Hartl, 1998). A sensitivity
29 measure of the interferometrically derived elevation is the height resulting from a phase change
30 of one fringe (2π) which represents one ambiguity cycle. This height of ambiguity is inversely
31 proportional to the perpendicular component of the baseline, the effective baseline. A larger
32 effective baseline leads to a dense fringe pattern, hence higher precision but also more difficult
33 unwrapping. Conversely, a smaller baseline leads to a noisier DEM but a more robust unwrapping.
34 Additionally, the radar wavelength also has a directly proportional influence, a low frequency SAR
35 (e.g. L-band, 1.25 GHz) generates larger heights of ambiguities and thus less sensitive DEMs than
36 a C- or X-band SAR system (5.3 GHz and 9.6 GHz, respectively).
37
38
39
40
41
42
43

44 **3.3.1. Elevation data from spaceborne bistatic InSAR systems**

45 To date, two spaceborne InSAR missions have been launched with the primary objective of
46 measuring Earth's topography.
47
48

49 The first single-pass interferometer, the Shuttle Radar Topography Mission (SRTM) was flown
50 from 11 to 22 February 2000 and was a unique experiment with two antennae on the same
51 platform, the second antenna located on the end of a 60-m long mast (Farr et al., 2007). Thus,
52 the SAR data were acquired with a known, constant baseline during the mission. The coverage of
53 the resulting DEM is, however, principally limited to a latitude range from 56°S to 60°N due to
54 the inclined orbit of the Space Shuttle and its mapping geometry. The good vertical accuracy
55 (better than 9 m) and the short temporal baseline provided a snapshot of the glacierized areas
56
57
58
59
60

4 <https://labo.obs-mip.fr/multitemp/category/sentinel-hr/>

1 within these latitudes. The SRTM C-band DEM (processed by the National Aeronautics and Space
2 Administration, NASA), obtained by combining overlapping ascending and descending strip data,
3 has been widely used due to its completeness and it is available for free download in various
4 versions, the latest being released in February 2020 by the Land Processes Distributed Active
5 Archive Center (LPDAAC). The SRTM X-band DEM, processed by the German Aerospace Center
6 (DLR), is also available but has wide gaps due to the narrower swath and is therefore less used.
7
8

9 The second mission, TanDEM-X (TerraSAR-X add-on for Digital Elevation Measurements), is
10 currently in orbit and consists of the coordinated operation of two almost identical satellites —
11 TerraSAR-X (TSX) and TanDEM-X (TDX), the latter named similarly as the mission— flying in close
12 helix formation (Krieger et al., 2007). The mission has been operational since December 2010. The
13 primary objective of the TanDEM-X mission is the generation of a worldwide, consistent, timely,
14 and high precision DEM which was released in 2018 (Wessel et al., 2018). Operational data
15 acquisition for DEM generation is performed using the bistatic InSAR stripmap mode (30 km
16 swath width): either the TSX or TDX satellite is used as a transmitter to illuminate a common radar
17 footprint on the Earth's surface. The scattered signal is then recorded by both satellites
18 simultaneously. Both satellites act as a large single-pass radar interferometer with the
19 opportunity for flexible baseline selection. Prerequisites for bistatic operation of this fully active
20 system are the PRF (Pulse Repetition Frequency) synchronisation and the relative phase
21 referencing between the two satellites.
22
23
24
25
26
27
28

29 The global DEM product of the TanDEM-X mission (DLR-EOC, 2018), whose performances are
30 analysed in Rizzoli et al. (2017) and Wessel et al. (2018), is the result of the combination of 4 years
31 (from December 12, 2010 to January 16, 2015) of bistatic data acquisitions with different
32 baselines and geometries. In order to compensate residual offsets and tilts after the
33 interferometric processing, this product is calibrated to selected ICESat points except in
34 Greenland and Antarctica. Hence the global TanDEM-X DEM is not suitable for the derivation of
35 surface elevation changes, but rather as a reference DEM for various purposes. Instead, individual
36 bistatic TanDEM-X acquisitions can be processed to timestamped DEMs and used to generate
37 time series of surface elevations at yearly or multiyear intervals over regions with high mass
38 losses (Abdel Jaber et al., 2019; Braun et al., 2019). Compared to early volume change
39 assessments for which DEMs from different sensors were combined, the TanDEM-X single-pass
40 interferometer offers significant improvement in terms of spatial resolution (typically 5 to 10 m)
41 and vertical accuracy. Typically, elevation changes are measured within +/- 1 m if ice free areas
42 are available for proper adjustment of the DEMs.
43
44
45
46
47
48
49

50 The map of surface elevation change rate over the Western Vatnajökull Ice Cap (Iceland) obtained
51 from two TanDEM-X 30 km-wide strips is shown in Figure 5. The 2012 DEM is composed of
52 ascending acquisitions in August (western strip) and June (eastern strip). The second coverage
53 was achieved with ascending acquisitions in winter 2016, with the western strip from December
54 and the eastern from November. The DEMs were vertically coregistered over ice free areas. The
55 decrease in elevation from 2012 to 2016 can be clearly observed at the outlet glacier termini,
56 while higher on the ice cap the surface elevation is almost constant or slightly increases. The
57 obvious large spot of surface lowering in the Northwest of the ice cap is caused by the
58 Bárðarbunga caldera collapse in 2014/2015 (Gudmundsson et al., 2016). The slight elevation
59
60

change discrepancy at the boundary between the different DEMs is visible as a linear feature only on the ice cap and may be due to seasonal elevation changes or variable radar penetration.

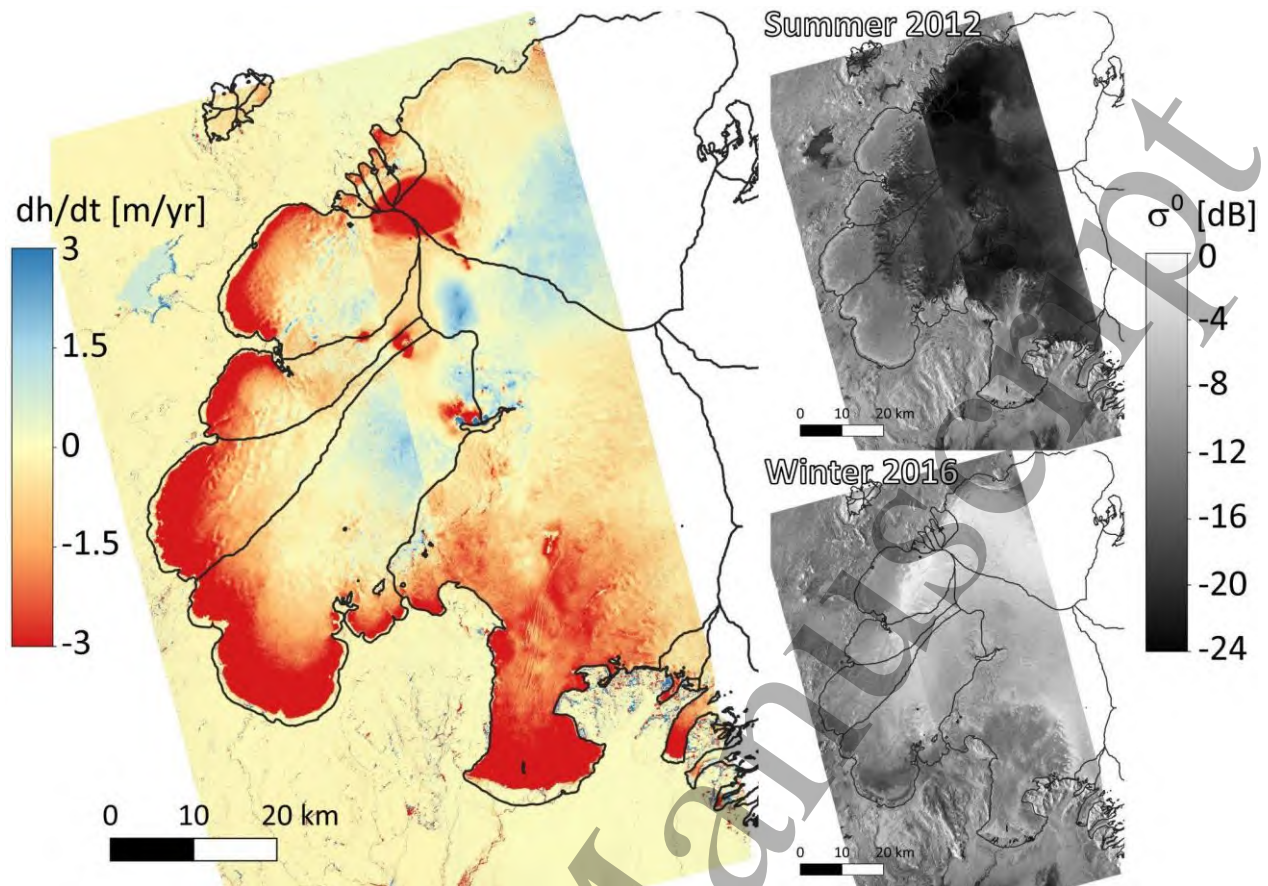


Figure 5: Surface elevation change rate [m/yr] over Vatnajökull Ice Cap (Iceland) from TanDEM-X bistatic acquisitions in summer 2012 and winter 2016. The right panels show the backscatter images [dB] for these two periods, illustrating the strong seasonal contrast and the need for correcting the varying radar penetration into snow and firn. A larger penetration depth is expected in the cold winter snow and firn (high backscatter) compared to the wet summer firn (low backscatter).

For large basins and on the flat areas at the interior of the ice sheets, TanDEM-X elevation change maps can be complemented with interpolated Cryosat-2 elevation changes at crossover locations (Krieger et al., 2020).

3.3.2. Limitations and challenges of InSAR DEMs for elevation change mapping

DEM processing and phase unwrapping errors. The ruggedness of the topography of many glacierized regions with steep mountains and intricate water bodies poses a significant difficulty for the interferometric processor algorithms of phase unwrapping and absolute elevation determination (Rossi et al., 2012). Most of these issues can be overcome by exploiting a robust external reference DEM like the global TanDEM-X DEM in case of multitemporal TanDEM-X DEM generation.

DEM coregistration. The reference and secondary DEMs may be affected by vertical biases with respect to each other. These can be constant (offset), linear (tilt) or even varying with low frequency (e.g., Malz et al., 2018; Abdel Jaber et al., 2019). They can furthermore be affected by

horizontal shifts causing an additional slope- and aspect-dependent elevation bias in the surface elevation change, which couples with the vertical bias, resulting in a systematic error with high potential impact on the volume change rate estimated over large areas.

Signal penetration. For the analysis and interpretation of interferometric elevation over snow and ice, the effects of signal penetration have to be considered (Lambrecht et al., 2018; Rott et al., 2021; Dehecq et al., 2016; Sommer et al., 2022). These effects become more prominent with increasing radar wavelength so that comparison of DEMs derived from SAR sensors operating at different wavelengths can be challenging. The elevation difference bias can also be large if SAR DEMs are compared to DEMs derived from optical images as the former are subject to radar penetration whereas the latter map the glacier surface (Li et al., 2021). The surface inferred from InSAR elevation data refers to the position of the scattering phase centre in the snow/firn medium, which may result in an elevation bias versus the actual surface (Dall, 2007). Ideally, the InSAR data over temperate glaciers should be acquired in warm seasons in order to reduce the SAR signal penetration. The status of the snow and firn surface of a glacier in respect to wetness and possible effects of radar signal penetration can be assessed through the analysis of backscattering coefficients measured by the active SAR and included in the systematic error budget (Abdel Jaber et al., 2019). However, on the rough crevassed termini of temperate glaciers, the surface scattering is dominating and the SAR signal penetration is minimal.

Imaging geometry. In complex topography areas, information in SAR images is lost due to radar layover and shadow effects. This can be partially compensated by combining data acquired from ascending and descending orbits. In the case of InSAR DEMs because the incidence angle on the glacier surface varies in range direction, it cannot be identical in the opposite viewing geometries and leads to differences in SAR signal penetration. Besides, few areas are always either in layover or shadow and can never be resolved in the SAR image.

Seasonal changes. Ideally, data acquisitions should be at the end of the ablation season (also the end of the glaciological year) when the glacier surface is at its lowest, but most importantly the two coverages should be acquired at the same time of year in order to minimise seasonal changes, which can be significant in certain glacier regions (Sommer et al., 2022). Since in general data availability restricts the ability to fulfil this criterion, the residual temporal gap has to be compensated for, and taken into account in the systematic error budget.

3.3.3. Future missions with single pass InSAR capabilities

The German Space Agency (DLR) plans to release TanDEM-X DEM 2020 in 2024, a new global DEM which will combine bistatic TanDEM-X data acquisitions between 2017 - 2020. Beforehand a 30 m change map indicating regions with significant height changes to the TanDEM-X DEM (released in 2018) will be made available in 2023.

The High Resolution Wide Swath (HRWS) DLR mission aims at continuing the X-band series and is programmed to be launched in 2026/27 (Moreira et al., 2021). HRWS consists of a main high-resolution X-band radar satellite and 3 small, receive-only satellites in formation flight. The small satellites, following the MirrorSAR concept (Krieger et al., 2018), have a reduced functionality compared to classical receiver satellites and allow an effective, low-cost implementation of a multistatic interferometric system for high-resolution DEM generation and for secondary mission

objectives such as ocean currents, traffic flow monitoring, river and ice flow monitoring using along-track interferometry. The multistatic mission goal will be a global digital elevation model at 4-m posting with a relative elevation accuracy of 2 m. The flexibility of HRWS's multistatic mission design will allow the generation of on-demand local to regional DEMs.

Harmony, selected as ESA's Earth Explorer 10 will be launched in 2029 to address key scientific questions related to ocean, ice and land dynamics. It is envisaged as a mission with two receive-only C-Band SAR satellites that orbit in two alternative formations with the Copernicus Sentinel-1D satellite as transmitter. In the cross-track interferometry constellation planned for years 1 and 5 of the mission, and perhaps intermediate periods, Harmony will produce interferometric DEMs over virtually all glaciers globally and with the same repeat as Sentinel-1D, i.e. nominally 12 days.

Two European companies, ICEYE and SATLANTIS, announced recently preliminary plans to develop and manufacture a Tandem for Earth Observation (Tandem4EO) constellation consisting of two radar and two VHR optical satellites, each capable of under 1-m resolution imaging. The satellites are to be flown in a sun-synchronous orbit, with two ICEYE SAR imaging spacecraft flying in a bistatic formation, and two SATLANTIS very high-resolution optical imaging spacecraft trailing behind. With closely coordinated operations, the constellation intends to support, among other themes, environmental monitoring at land and sea as well as precise SAR Interferometry (InSAR) change detection, thus being also of interest for glacier studies.

4. Radar altimetry

Earth observing radar altimetry has traditionally been used to derive time-dependent elevation over oceans and ice sheets. The large (~10 km) footprint of conventional radar altimetry has limited its application over regions of more complex topography. The launch of CryoSat-2⁵ (Wingham et al., 2006) by the European Space Agency in 2010 changed this however, allowing the monitoring of glaciers outside the two large ice sheets (McMillan et al., 2014; Gray et al., 2015; Foresta et al., 2016; Jakob et al., 2021).

4.1. Radar altimetry data

Radar altimetry for Earth Observation was initially developed for observing ocean topography and is one of the main instrumental records of ocean topography with applications in marine geoid, ocean currents, and sea level change. Its use is now ubiquitous across the cryosphere and inland water. Radar altimeters are nadir-looking instruments recording time between pulse emission and reception, which is then converted to distance. This distance is usually that of the point-of-closest approach (POCA), obtained via retracking of the recorded waveform (Davis and Moore, 1993; Wingham et al., 1986; Martin et al., 1983). Over sloping terrain, POCA is situated off-nadir and requires special procedures to properly relocate the echo (Brenner et al., 1983). CryoSat-2 operates a beam-forming radar altimeter which improves the along-track footprint resolution, and its interferometric mode allows accurate echo-location in the across-track

⁵ CryoSat-2 data can be obtained from <https://cs2eo.org/> and <https://cryotempo-eolis.org/>

direction (Figure 6).

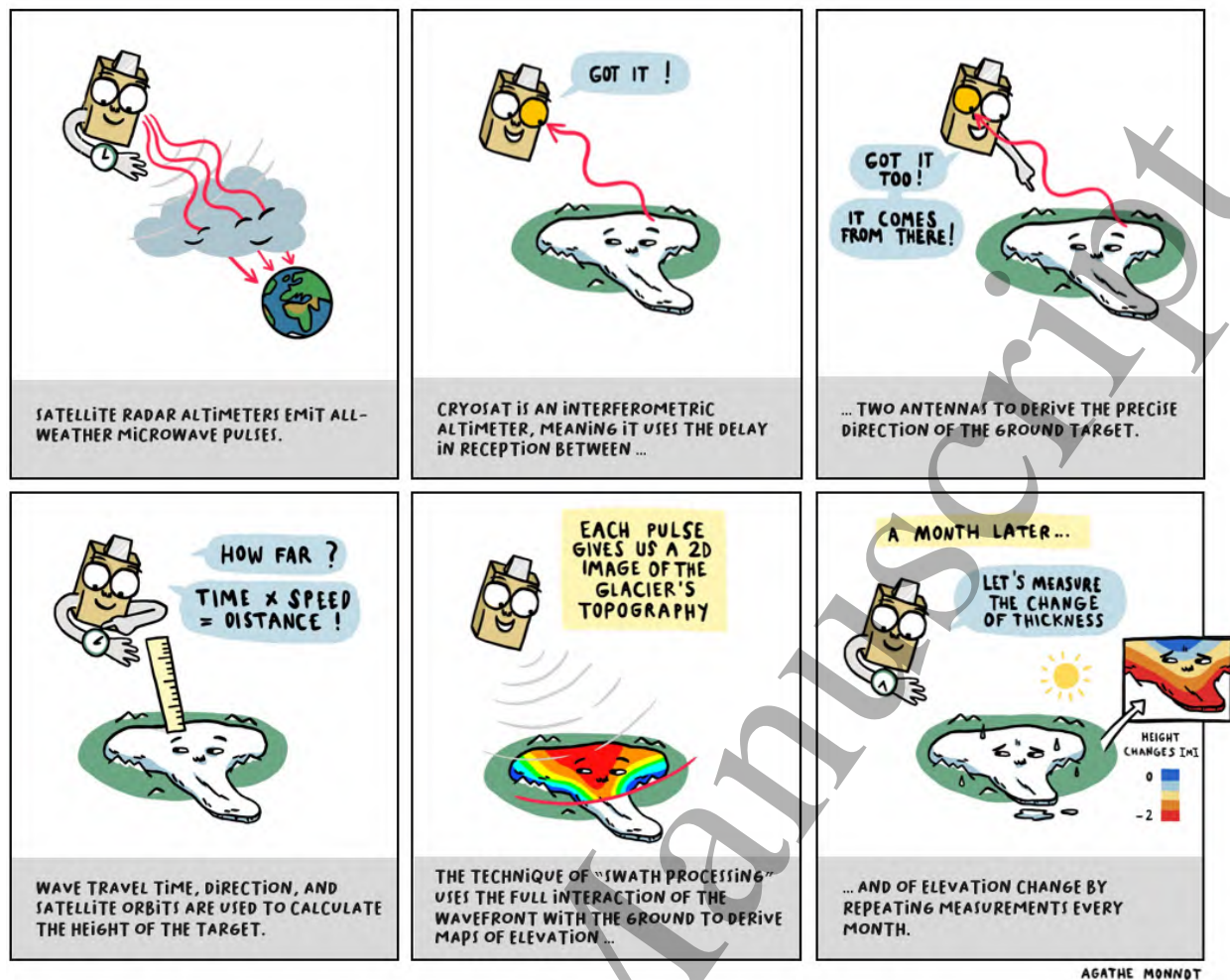


Figure 6: Principles of Cryosat-2 interferometric radar altimetry and swath processing.

This revolutionary design led to a paradigm shift in how radar signal is processed for elevation retrieval. In the presence of sloping terrain, CryoSat-2 is akin to the geometry of a side-looking SAR, with the ability to retrieve elevation information beyond the POCA (Wingham et al., 2006). The potential of the so-called swath processing has been demonstrated with data acquired by the airborne ASIRAS radar system (Hawley et al., 2009) and then by CryoSat-2 (Gray et al., 2013; Gourmelen et al., 2018), generating between 1 and 2 orders more measurements than POCA from conventional waveform retracking. For a detailed description of swath processing, we refer to Gray et al. (2013) and Gourmelen et al. (2018). Apart from an increase in the number of elevation measurements retrieved from CryoSat-2, swath processing allows a better sampling of low-lying terrain as the POCA tends to be located in topographic highs (Foresta et al., 2016). This leads to a more complete hypsometric coverage of small ice bodies and thus a more representative sampling of ice elevation changes that tends to be strongly correlated with elevation. In addition, since it does not rely on waveform retracking, swath processing allows retrieval of elevation even when the waveform leading edge is difficult to identify such as for high surface slopes and high terrain roughness. The improved spatial coverage coupled with a monthly repeat cycle gives CryoSat-2 unique spatio-temporal capabilities to monitor changes in glacier volume, and ultimately mass.

4.2. Principle to assess glacier changes

To assess linear rates of change from swath elevations, the method follows a generic approach developed over ice sheets. The swath elevation data is binned into a grid, with cell resolution typically set around 500 m as a trade-off between spatial resolution and robustness, and then a plane-fit approach is applied in each grid cell (Foresta et al., 2016, 2018). The plane-fit algorithm is a simple regression, modelling elevation (z) with the parameters easting (x), northing (y) and time (t). The coefficient for time (t) resolves a constant rate of surface elevation change and is retrieved from the plane-fit model of each individual grid cell, resulting in gridded maps of dh/dt . Several improvements to the method have been made by applying outlier removal, quality filtering and quality weighting methods (Foresta et al., 2016, 2018; Jakob et al., 2021; Morris et al., 2020, 2022). The maps of elevation changes typically have coverage of between 60% and 87% (Foresta et al., 2016, 2018; Morris et al., 2020; Tepes et al., 2021). Different gap filling methods have been applied over the years, including spatial interpolation and hypsometric averaging at different spatial scales (Nilsson et al., 2015b). Similar to the DEM differencing and laser altimetry methods, the elevation changes are then converted into mass changes, using the glacierized area from glacier masks (section 2) and a volume-to-mass conversion factor (section 3.1).

In regions with highly complex terrain, such as High Mountain Asia and the Gulf of Alaska, the data rate is usually lower due to limitations with closed-loop onboard-tracking (Dehecq et al., 2013) and decreasing data quality with higher surface slopes. Larger grid cells are therefore necessary, and since for larger grid cells the plane-fit approach is a too simplistic representation of topography, an auxiliary baseline DEM is required to remove the terrain-related elevation change within each cell (Jakob et al., 2021; Käab et al., 2012).

Besides providing linear change over a time-period, CryoSat-2's monthly repeat cycle has enabled multiple studies to resolve time-dependent changes, giving insights into annual and seasonal changes (Foresta et al., 2016, 2018; Morris et al., 2020; The IMBIE Team, 2020; Gray et al., 2015; Jakob et al., 2021). For monthly change in elevation, additional spatial averaging is needed and resolution is typically set from 2 km for relatively regular surfaces (The IMBIE Team, 2020) up to larger glacier units (Jakob et al., 2021). Several methods for time series generation exist, from simple monthly averaging (Foresta et al., 2018) to more robust statistical weighted mean (Davis and Segura, 2001; Malczyk et al., 2020; Gray et al., 2015).

4.3. Limitations and challenges

Limitations related to other elevation change methods (DEM differencing, laser altimetry) are also applicable to radar altimetry-based studies. These include the uncertain volume-to-mass conversion, the need for gap-filling or data interpolation, and reliance on correct glacier masks for generating volume change and mass balance.

Further, Ku-band radar signal scatters within the snow and firn volume, with the potential to impact the accuracy of time-dependent elevation, with spectacular examples over the interior of the Greenland Ice Sheet after extreme melt events (Nilsson et al., 2015a). This spectacular case study however stems from the combination of a thick and dry firn, and of the absence of

1 repeated and frequent melt events. Studies conducted over a large range of settings have
2 demonstrated the consistency between radar-altimetry and airborne laser or field-based multi-
3 annual elevation change (Gray et al., 2015; Foresta et al., 2016; Gourmelen et al., 2018; Tepes
4 et al., 2021), as well as ways to identify change in penetration and to correct for its impact
5 (Nilsson et al., 2015a; Slater et al., 2019; Gray, 2021). Scattering properties can also induce
6 elevation biases at a seasonal timescale (Gray et al., 2019; Morris et al., 2022), and efforts are
7 underway to understand and address their impact and exploit the potential of radar altimetry
8 for mapping seasonal change.
9

10 11 12 **4.4. Outlook**

13
14 Over the course of the last decade, CryoSat-2 has demonstrated that beam-forming,
15 interferometric, radar altimetry can monitor glacier change globally, providing a unique blend of
16 spatial and temporal resolution. It offers the possibility to analyse glacier change in response to
17 complex atmospheric and oceanic forcing. The combination of radar altimetry with other
18 available techniques and constantly improving glacier and climate models should lead to more
19 accurate mass balance estimates and better process understanding.
20
21

22
23
24 Importantly, the European Commission Copernicus expansion mission concept CRISTAL (Kern et
25 al., 2020), a radar altimeter inspired by CryoSat-2 and AltiKa, and due to launch in 2027, will be
26 the first operational mission with a primary objective to monitor glaciers globally for decades to
27 come (Figure 2).
28
29

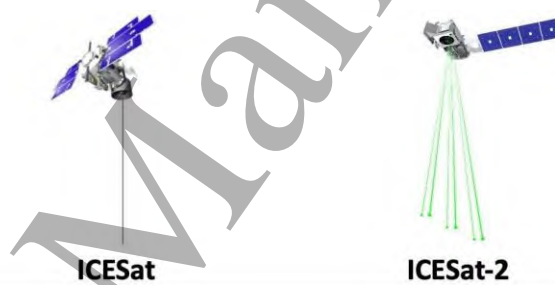
30 31 32 **5. Laser altimetry**

33
34 Spaceborne laser altimeters can measure the elevation of the Earth's surface at very high
35 accuracy over a small spatial footprint. They emit a short laser pulse at a known time that
36 reflects off of the Earth surface and back to the instrument telescope, where its arrival time is
37 recorded and the total travel time is computed. Knowing the speed at which the laser pulse
38 travels, the time of flight can be converted to range. With additional knowledge of the
39 spacecraft position and orientation, range measurements can be converted to elevation
40 measurements geolocated to a point on the Earth surface. Laser sensors record profiles of
41 individual elevation measurements rather than spatially continuous DEMs such as from imaging
42 sensors. There have been three Earth-orbiting satellite laser altimeter missions (Table 1):
43 NASA's Ice, Cloud and land Elevation Satellite (ICESat, 2003-2009), ICESat-2 (2018-), and GEDI
44 (2018-). The latter is the laser altimeter on board the International Space Station (Dubayah et
45 al., 2020). It has not been extensively used so far in glaciology and is not described further here.
46
47
48
49
50
51
52
53

54 55 **5.1. Laser altimetry data from ICESat and ICESat-2**

56 The main goal of ICESat was to measure the elevation change of the ice sheets to determine
57 their contribution to sea level change (Schutz et al., 2005). Despite design limitations that
58 shortened the operational lifetime of the lasers (Abshire et al., 2005), the mission provided
59 global surface elevation measurements of unprecedented accuracy during its seven year
60

mission life (2003-2009). ICESat recorded data during two to three month-long campaigns per year. The data consists of full-waveform 1064 nm laser returns of an ~65 m elliptical laser footprint (Schutz et al., 2005). The mission operated in a 91-day repeat orbit and a 94 degree inclination that covered latitudes up to $\pm 86^\circ$, with precision pointing employed in polar regions to steer the laser footprints to within ± 300 m of reference ground tracks. In lower latitudes, the reference ground track pattern was not repeated with as good accuracy. The along-track distance between measurements is 172 m, but the distance between reference ground tracks ranges from ~6 km close to the poles up to 89 km at the equator. For land ice studies, there exist preprocessed level-2 data products: GLAH12 (optimised for ice sheets), GLAH14 (commonly used for mountain glaciers), and GLAH06 (level 1B, used for smooth polar glaciers). In addition to an elevation value for each footprint, these products include numerous attributes and corrections. The latest release of the data, 2014, is version 34. ICESat's revolutionary data provided multiple glaciological insights, in particular for volume changes of ice sheets (Pritchard et al., 2009; Sørensen et al., 2011) and glaciers (Gardner et al., 2011; Kääb et al., 2012). The success of ICESat led to the follow-up mission ICESat-2, launched 8 years after the end of the ICESat mission. To bridge the gap between the two missions, NASA'S Operation IceBridge provided annual airborne altimetry data for selected areas in the Arctic and Antarctic (MacGregor et al., 2021).



	ICESat	ICESat-2
wavelength	1064 nm	532 nm
spot diameter (ground)	65 m	11 m
along-track sample distance	172 m	0.7 m
# of beams	1	6 (3 pairs)
operation strategy	19 8-37 day campaigns	continuous
across slope measurement	no	yes
near-exact repeat	@ poles	@ poles
repeat cycle	91 days	91 days
pointing control	35 -100 m	3 - 25 m
sensor technology	analog	photon-counting
latitude coverage	$\pm 86^\circ$	$\pm 88^\circ$

Table 1: Main characteristics of the ICESat and ICESat-2 missions.

ICESat-2 was launched in September 2018, and had a minimum mission lifetime of 3 years (Markus et al., 2017) met in December 2021. Unlike its predecessor, ICESat-2 uses a digital photon counting detector and 10 kHz micro-pulse laser, providing a greatly increased number of elevation measurements with 0.7m along-track spacing between pulses (Neumann et al., 2019). ICESat-2 operates in a 91-day repeat orbit, like ICESat, but with a latitude coverage up to $\pm 88^\circ$.

1 The laser micro-pulse is split into 3-beam pairs (6 beams total), with each pair consisting of a
2 weak ($\frac{1}{4}$ strength) and strong beam (full strength). Within each pair, beams are separated on
3 the ground by 90 m and the beam pairs by 3.3 km (Markus et al., 2017). The surface footprint of
4 each beam is approximately 11 m in diameter (Luthcke et al., 2021; Magruder et al., 2021). Data
5 is collected nearly continuously globally but the satellite only operates in exact repeat mode in
6 polar regions, with a pointing control of 4.4 m (Luthcke et al., 2021). At lower latitudes the
7 mission off-points the instrument to prioritise vegetation coverage over repeat observations.
8 Level 2A Geolocated Photons (ATL03) is the ICESat-2 product of primary interest for studies of
9 detailed glacier features such as crevasses (Herzfeld et al., 2021) or supraglacial lakes (Fair et al.,
10 2020). Most suitable for glacier change studies are Level 3A Land Ice Height (ATL06) and L3B
11 Annual Land Ice Height (ATL11, corrected for surface slope), that are binned in the along-track
12 in 40 m and 60 m segments, respectively. Level 3B gridded ice height and height change data
13 (ATL14, ATL15) were made public in late 2021.

14 The 1064 nm laser on board ICESat led to little multiple scattering within snow and ice and
15 therefore no elevation bias (Smith et al., 2018). ICESat-2 uses a 532 nm laser that, under certain
16 conditions, can experience a large degree of multiple scattering within the snow and ice. The
17 magnitude of this elevation bias depends on snow conditions and the method of identifying the
18 surface height from the photon cloud (Smith et al., 2018). It can be as large as 24 cm in extreme
19 cases (e.g. pure snow/ice with extremely large grains). However, for most applications, the bias
20 is negligible (2-5 cm) and largely cancels for repeat measurements under similar snow
21 conditions.

22 **5.2. Principles to assess glacier changes**

23 ICESat was only capable of pointing to the same location on the ground (i.e. reference ground
24 track) to within 10s to 100s of metres and measurements were made every ca. 170 m along-
25 track. This makes it challenging to directly compare near-repeat elevation measurements, as
26 elevation changes will be convolved with differences in elevation due to changes in
27 measurement location (Figure 7). This is often referred to as the “slope error” and must be
28 corrected for. ICESat-2 has far superior pointing control (3-25 m) and closely spaced beam pairs
29 (90 m) that make correcting for “slope error” robust and straightforward. In steeper or rougher
30 terrain or in the mid-latitudes without quasi-exact repeat tracks, different ground tracks may
31 not be directly comparable altogether without an additional reference elevation dataset and
32 the use of spatial statistics (Figure 7). In all cases, the sampling is rather sparse at the scale of
33 individual glaciers or ice caps, and most of the times uneven between the ablation and
34 accumulation areas, such that a careful extrapolation to the entire ice body is required.

35 Whatever the method, accurate glacier masks are required to correctly classify individual
36 surface elevation measurements (section 2). Inclusion of measurements on stable terrain
37 outside glaciers (e.g. when an outdated glacier inventory is used) will lead to almost unbiased
38 volume change estimates (the off glacier elevation changes will sum up to almost 0) but an
39 underestimate of glacier thickening/thinning area-averaged rates because the correct total
40 volume change is divided by an area which is too large.

5.2.1. Methods for calculating elevation change from near-repeat observations

All methods to estimate elevation change from ICESat data aim at removing the influence of sloping terrain between slightly shifted repeat ground tracks (Figure 7a). Moholdt et al. (2010) provide an overview and comparison of the most common methods summarised hereafter. The most accurate way to retrieve elevation change is to compare elevation profiles at locations where ascending and descending tracks intersect (i.e. crossover locations) (Brenner et al., 2007), but crossover locations can be sparse. Another set of methods use along-track planes formed by segments of repeat ground tracks, relying on redundancy from several years of laser altimetry measurements. In this approach linear regression is used to simultaneously estimate the local surface slope and elevation change from ice thinning/thickening (Fricker and Padman, 2002; Howat et al., 2008). Most variants of this method assume that the surface slope and rate of elevation change are constant over several years, though higher order models can also be fitted (Nilsson et al., 2016). This approach can be sensitive to how the tracks are ordered in space. Schenk and Csatho (2012) found that higher-order fitting surfaces better captured the more complicated thinning/thickening signal in the rapidly changing coastal areas of the ice sheets. A third method relies on a DEM to estimate, and correct for, the terrain differences between repeat ground tracks (Slobbe et al., 2008). A variant of this last method is also applicable to non-repeat measurements and is discussed in section 5.2.2.

All of the above methods are most applicable to ICESat data and less relevant to ICESat-2 data, when ICESat-2 data is acquired along repeated reference ground tracks. ICESat-2 has exceptionally precise pointing capabilities (Luthcke et al., 2021) that often negates the need for any “slope error” correction. ICESat-2 is also equipped with closely separated beam pairs that allow for easy translation of non-exact repeat measurements to a common reference ground track. This correction is applied on the ATL11 data product.

5.2.2. Methods for non-repeat observations and rough surfaces

Outside the polar regions, repeat tracks of ICESat/ICESat-2 are not close enough to be compared directly. Furthermore, the rougher surfaces of small glaciers cause greater uncertainties in individual elevation measurements. It is thus more practical to normalise all ICESat/ICESat-2 surface elevation measurements from several years with the help of a reference DEM surface. This method is described by Treichler (2017) and is suitable for mountain glacier studies. Thereby, individual laser altimetry measurements are compared to a reference DEM of a known date (Figure 7b), and only the resulting elevation differences are analysed. Surface elevation change over time (dh/dt) is then estimated by fitting a linear regression to dh from different years against time (Figure 7c). The result is a single dh/dt estimate for the analysed group of elevation samples. In the case of ICESat, given the sparse ground tracks, this is often a rather large area such as an entire mountain range. There are some caveats with this method: (1) the elevation differences to the reference DEM (dh) contain both real elevation changes between the DEM and laser altimetry data as well as uncertainties and potential bias in either the DEM, the laser altimeter data, or both; and (2) dh have to be binned spatially and filtered to remove outliers and make sure that they are representative for the glaciers in the sampled area. Careful preprocessing is vital to reach reliable results, in particular a robust assessment of biases and uncertainties in the reference DEM, elevation biases from snow cover during

ICESat/ICESat-2 acquisitions, and the elevation distribution of the laser altimetry samples (Treichler et al., 2019). This approach has been applied to the larger glacierized regions across the globe and in particular to High Mountain Asia, where glacier changes were poorly known before ICESat data became available (Farinotti et al., 2015; Treichler et al., 2019; Gardner et al., 2013; Kääb et al., 2012). The increased number of measurements provided by ICESat-2, relative to ICESat, significantly augment the utility and accuracy of this approach.

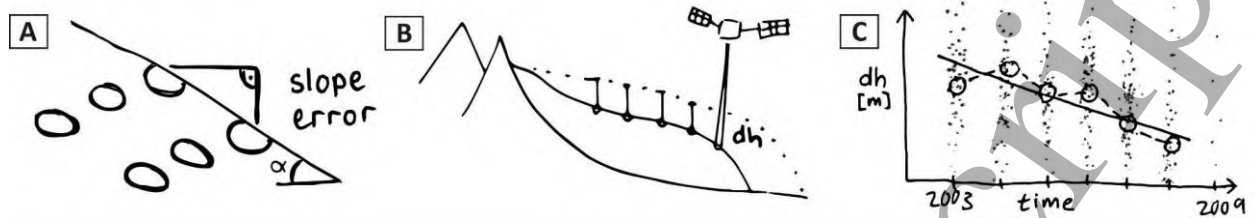


Figure 7: Calculating the regional rate of elevation changes from ICESat over steep terrain. (A) The offset of ICESat's quasi-repeat tracks causes a "slope error": a gentle slope of $\alpha=0.5^\circ$ combined with an across-track offset of 150 m results in 1.3 m elevation difference. This has to be accounted for when assessing glacier thickening/thinning from ICESat data. (B) When altimetry ground tracks do not overlap, elevation measurements within a spatial region are compared to a common reference DEM to calculate dh . (C) The resulting dh from several years of data are plotted against time and linear regression is used to estimate glacier thinning/thickening within that glacier region. (Source: from or modified from Treichler, 2017)

5.3. Outlook

New methods take time to develop for new products like ICESat-2, and as of this writing, there are relatively few results in the literature. It is expected that ICESat-2 data will contribute to new insights and a much better understanding of the entire cryosphere, including dynamical changes of the ice sheets (Smith et al., 2020) and improved monitoring of mountain glaciers (Wang et al., 2021; Fan et al., 2022), but also advances in related disciplines such as, snow depths on- and off-glacier (Treichler and Kääb, 2017), sea ice and ice shelf thickness (Kacimi and Kwok, 2020) or permafrost changes (Michaelides et al., 2021). In addition, the accurate elevation measurements of both ICESat and ICESat-2 provide a globally consistent reference elevation dataset that has the potential to greatly improve the quality and accuracy of existing and upcoming DEMs and other elevation data across the globe, which will directly benefit glacier volume change studies.

There are currently no funded Earth observing laser altimetry missions under development. However, the need for the continuation of cryosphere focused laser altimetry is highlighted in the 2018 Decadal Survey for Earth Science and Applications from Space, a guiding document for NASA's future Earth science investment, and has been recommended as one of seven observables to be completed as an Earth System Explorer class mission.

6. Gravimetry

The GRACE follow-on (FO) satellites are currently the only way to track mass redistribution on global scales. Launched in 2018, they continue the measurements of the GRACE mission, which was operational from 2002 to 2017 (Tapley et al., 2004; Landerer et al., 2020). Both missions

consist of a pair of satellites in the same orbit but separated by about 200 kilometres and are based on the same principle: given that the satellites are at different locations in their shared orbit, each of them will be affected differently by the Earth's gravitational field. For example, if the two satellites approach a mass anomaly on or within the Earth, such as a mountain range, the first satellite will experience its gravitational pull stronger and earlier than the other one. This results in an unequal acceleration of the satellites and changes their relative velocity, and consequently the inter-satellite distance. These extremely small changes in distance and velocity are measured by a very precise ranging system in the satellites. GPS receivers simultaneously record the location of the satellites, and the orientation of the satellites in space is derived from a star-camera system. Forces not related to the gravitational field, for example atmospheric drag and solar radiation pressure, are measured by on-board accelerometers which are precisely aligned with the centre of gravity of the satellites so that they only measure non-gravitational forces .

6.1. GRACE and GRACE-FO data

The Earth's gravitational field is described by the geopotential V , i.e. the potential energy per unit mass at a certain point. At a point above the Earth's surface, with spherical coordinates radius r , co-latitude θ and longitude λ , it can be expressed as a sum of Legendre functions:

$$V(r, \theta, \lambda) = \frac{GM}{a_e} \left\{ \sum_{l=0}^{\infty} \sum_{m=0}^l \left(\frac{a_e}{r} \right)^{l+1} P_{lm}(\cos \theta) \times (C_{lm} \cos m\lambda + S_{lm} \sin m\lambda) \right\}$$

where G is the gravitational constant, M the mass of the Earth and a_e denotes its mean equatorial radius. P_{lm} are the Legendre polynomials of degree l and order m , and C_{lm} and S_{lm} are spherical harmonic coefficients. For further details, we refer the reader to Wahr et al. (1998). As can be seen from the formula above, coefficients with a higher degree and order are related to increasingly smaller wavelengths. At the same time, the scaling by $(a_e/r)^{l+1}$ implies that the effect of these coefficients have a smaller contribution to the geopotential than the low order coefficients. In practice, this means that the orbit of the GRACE satellites are dominated by the large-scale mass distribution of the Earth and that small-scale features, such as glacier mass changes, are more challenging to measure than large-scale features, such as ice-sheet wide mass changes.

By collecting a sufficient amount of these range-rate observations, a model of the Earth's gravity field can be derived. The GRACE/GRACE-FO mission provides updated gravity fields typically every month, although weekly or even daily updates are available as well (at the cost of a lower resolution).

At seasonal to decadal time scales, variations in the gravity field are mainly induced by redistribution of water on the Earth's surface, although processes within its interior such as glacial isostatic adjustment may contribute as well, as we will see later on. Using an appropriate scaling (see Wahr et al., 1998 for details), variations in the geopotential can be expressed as variations in surface water loading. This is usually expressed in units of metre water equivalent height. It should be kept in mind that GRACE can only measure anomalies in surface water

loading, not the absolute weight of a glacier or ice sheet.

GRACE data are distributed by the GRACE science data centres, and other parties, as spherical harmonics (the C_{lm} and S_{lm} coefficients in the equation above). Since higher-order coefficients are increasingly affected by observational noise, only coefficients up to degrees and orders smaller than 60 or 90 are typically used in the derivation of the surface water loading anomalies, which corresponds to a maximum spatial resolution of approximately 200-300 km. A user-friendly alternative for the spherical harmonics are *mascons*, i.e. mass concentration blocks. These provide local mass variations on a regularly spaced grid. Compared to the spherical harmonics, they are less affected by noise and therefore require little or no post-processing. Mascons products are available with a grid resolution down to a few tens of kilometres, but it should be kept in mind that the inherent resolution is still in the order of a few hundred kilometres (in other words, the signal in adjacent grid cells will be correlated). Furthermore, once the grid cells are predefined by the processing centres, they do not always cover the area of interest exactly and may contain signals from neighbouring ice bodies (such as the Greenland Ice Sheet when studying the glaciers of the Canadian Archipelago or in Iceland (Sørensen et al., 2017)) or other non-glacier signals (e.g. groundwater and soil moisture signals in Patagonia or High Mountain Asia).

6.2. Glacier mass balance from GRACE

Figure 8 illustrates the linear trend in surface water load as observed by GRACE/GRACE-FO from 2002 to 2021. Together with the polar ice sheets, mountain glacier regions stand out with rates in the order of 20–50 cm/yr water equivalent mass loss in Alaska, the Arctic Archipelagos and Iceland.

To obtain the total mass balance for a region, the local surface mass anomalies need to be summed up over the region of interest. When working with mascons, this is relatively straightforward, but for the spherical harmonics some intermediate steps are required. If the Stokes coefficients were available up to an infinite degree l , we would be able to create a perfect region mask and could simply integrate the mass anomalies over the region. However, as mentioned earlier, the spherical harmonics are only provided up to a limited degree, typically 60 or 90. This, together with the postprocessing often applied to reduce noise in the higher degree coefficients, leads to attenuation and spreading of the signal (Swenson and Wahr, 2002). Here, spreading (or leakage) means that due to the limited resolution of the gravimetry data, mass variations from adjacent areas will spill into the region of interest. Likewise, part of the signal in the region of interest will be spread out beyond the boundaries of that region, e.g., in the ocean although recent mascon approaches minimise this effect compared to former spherical harmonic solutions (Wiese et al., 2016). Only considering the glacierized areas would therefore result in a biased estimate. Several methods have been proposed to circumvent these limitations. The most common approach is to place one or several unit mass loads in the glacierized areas of interest, represent these as Stokes coefficients with the same characteristics as the GRACE mass anomaly data (e.g. limited to the same maximum degree and applying a similar post processing) and finally applying a scaling to the mass loads so that the difference with the actual GRACE observations is minimised (Chen et al., 2013; Ciraci et al., 2020; Gardner

et al., 2013; Jacob et al., 2012; Wouters et al., 2008, 2019).

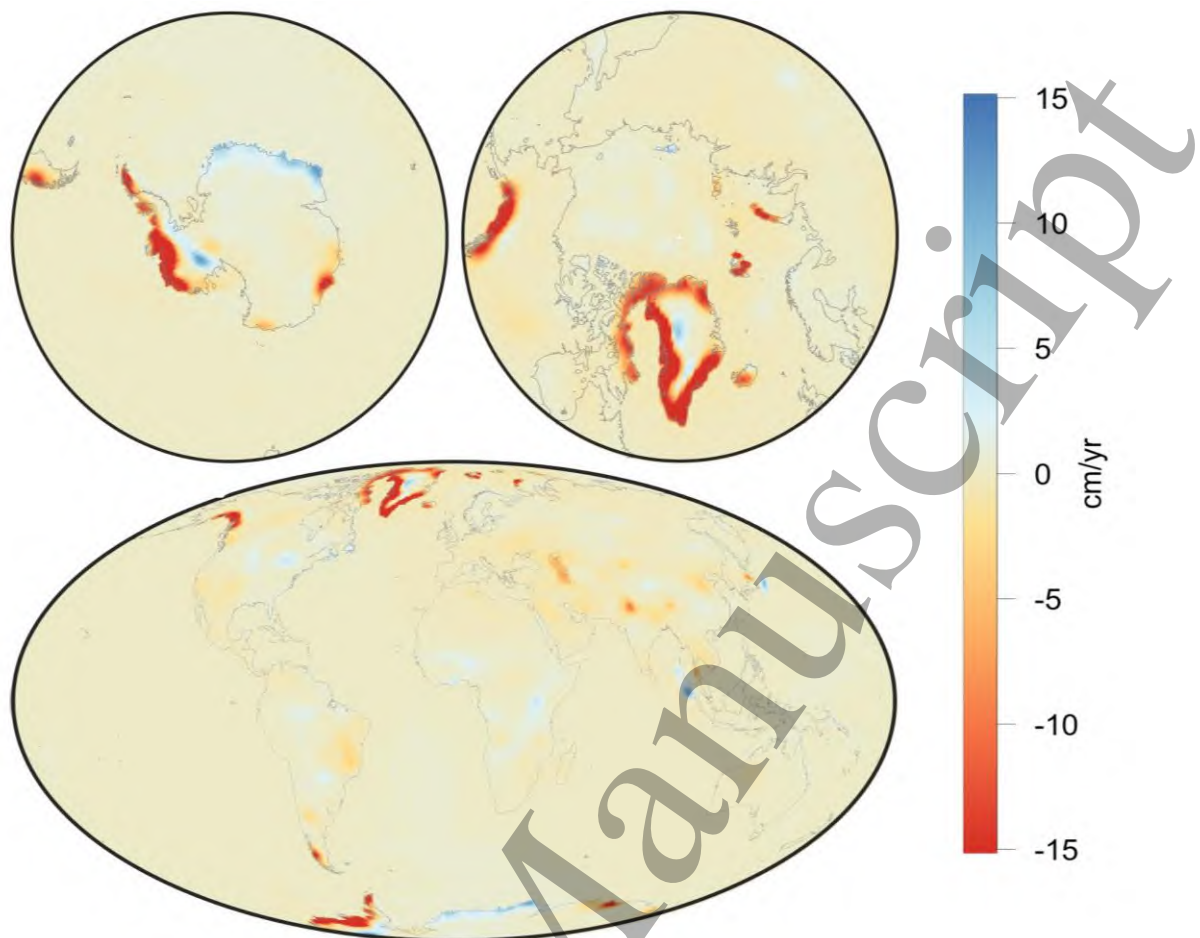


Figure 8: Trends in the global surface mass distribution between April 2002 and January 2021, expressed in centimetres equivalent water height per year, based on CSR mascons (Save et al., 2016). Yellow to red colours indicate a mass loss, with extreme values in the polar regions reaching -90 cm/yr.

6.3. Limitations and challenges

Just like any satellite observation, the GRACE data comes with noise, which reflects itself as random fluctuations in the mass anomaly time series in the order of a few gigatons. This means that in regions where the glacier mass change signal is small, the signal-to-noise ratio will be small, and the GRACE results should be interpreted with care. For the larger glacier regions, however, GRACE can capture mass variations with a high degree of confidence.

Even after extracting the mass changes in the glacier regions, there are confounding processes that need to be removed to isolate the glacier signal. Because GRACE has no vertical resolution, it senses the integrated sum of mass redistribution within its footprint, i.e. the sum of the water load changes at the surface and those in the subsurface. Many glaciers are located in regions that were widely covered by thick layers of ice during the Last Glacial Maximum (about 20 kyr ago), which depressed the Earth's surface and led to mass redistribution in the Earth's mantle. This ice has disappeared since, but the Earth's highly-viscous mantle material is still readjusting to the changes in surface load. The associated mass redistribution in the mantle will also be

1 observed by the GRACE satellites. Several models exist to correct for this process, called glacial
2 isostatic adjustment (GIA), which can be used to correct the GRACE data. Whereas models show
3 a wide spread in Antarctica (Martín-Español et al., 2016), they are fairly well constrained in
4 mountain glacier regions and the Arctic and GIA mass rates agree in most regions within a few
5 Gt/yr (Blazquez et al., 2018). Yet, when summed over all glacier regions globally, differences
6 become significant. For example, the GIA corrections used in two of the most recent GRACE-
7 based glacier mass balances studies, Ciraci et al. (2020) and Wouters et al. (2019) amounted to
8 58 ± 11 Gt/yr and 34 ± 21 Gt/yr, respectively ca. 18% and 13% of the total glacier mass change
9 signal (Figure 9). Furthermore, some regions with a low mantle viscosity are still adjusting to the
10 load changes related to the Little Ice Age (LIA) (Sørensen et al., 2017). A similar model-based
11 correction is applied for this, although these models are underconstrained in some areas and
12 not all studies include this correction. Another solid earth effect, i.e. mass redistribution
13 associated with earthquakes, is harder to correct for, but is mostly of small magnitude and
14 manifests itself as a step change in the mass time series followed by a slow recovery. In the few
15 cases where this affects glacier mass balance estimates, this can often be identified visually.

21
22 The coarse resolution of the GRACE observations also implies that, even after correcting for GIA,
23 the signal is a mix of mass changes related to glaciers and hydrological processes, such as
24 changes in the surface, canopy and soil moisture water storage, and in the groundwater table.
25 This is practically an issue in regions where glaciers are scattered and small compared to
26 GRACE's footprint, for example in Central Europe and the Caucasus. Furthermore, strong
27 hydrological variations outside the region of interest may affect the glacier mass balance
28 estimates through the leakage effect discussed earlier (An et al., 2021). Again, this is accounted
29 for using models, where it should be noted that most models only represent part of the
30 hydrological cycle, e.g. excluding groundwater storage changes and anthropogenic influences,
31 and tend to underestimate long-term changes in hydrological water storage (Scanlon et al.,
32 2018). Furthermore, the magnitude of corrections depends strongly on the choice of the model.
33 The global hydrology correction summed up to $+6 \pm 7$ Gt/yr in Ciraci et al. (2020) vs. -11 ± 6 Gt/yr
34 in Wouters et al. (2019) using a different model. Because of the disagreement between models,
35 some studies prefer to omit the correction and include it as an uncertainty (Reager et al., 2016).
36 Whereas the impact of hydrology is small in the polar regions, it is the major source of
37 uncertainty for most mid-latitude glacier systems. A further complication is that if part of the
38 glacial meltwater runs off in a proglacial lake, a nearby endorheic lake or an aquifer, the net
39 local mass change detected by the GRACE satellites will be smaller than the actual glacier mass
40 loss. Since such processes are currently not included in hydrological models, this will lead to an
41 underestimation of glacier mass balance. Finally, leakage of the glacier mass change signal in
42 the ocean can also be an issue for glacier regions fringing the ocean. This effect is reduced in the
43 mascon-based solutions.

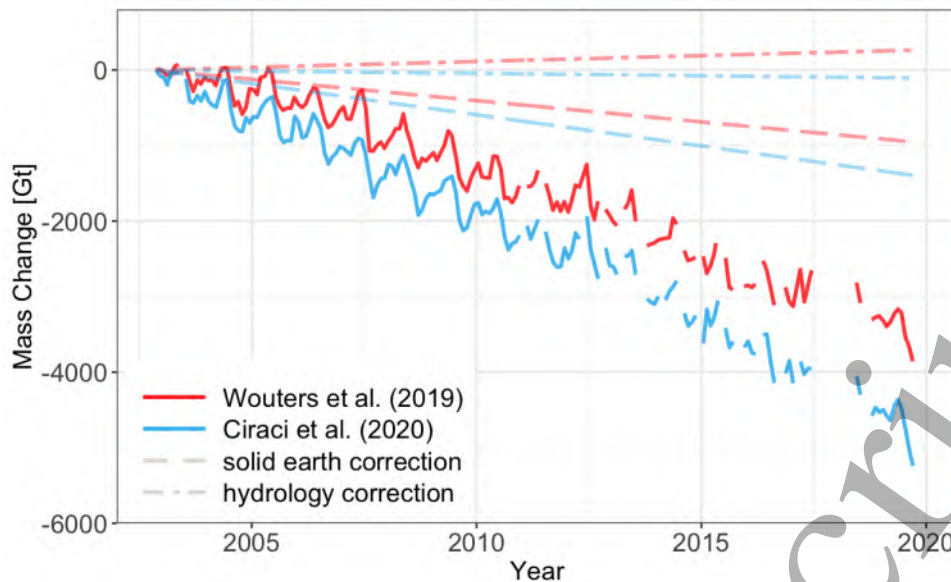


Figure 9: Global glacier mass change [Gt] time series for April 2002 - September 2019 from GRACE and GRACE Follow-On (Ciraci et al., 2020; Wouters et al., 2019). The thick lines show the cumulative mass change, the dashed lines the corrections for long-term hydrology (dashed-dot) and solid earth (long dashes) effects. The different corrections applied in the two studies explain for a large part the divergence of the glacier mass change time series.

6.4. Outlook

The GRACE-FO mission is currently our only tool to directly monitor glacier mass changes at a global scale, i.e. without a volume to mass conversion. Although it comes with its own limitations, it has proven to be essential to study the response of the larger glacier systems to climate variability. Likewise, the GRACE/GRACE-FO data has become an indispensable source of information in many other fields, and the importance of continued observations has been recognized by the wider scientific community and decision makers (Tapley et al., 2019). Several initiatives, including a joint effort of NASA and ESA, have recently emerged to study concepts for future gravity missions (respectively named Mass Change and MAGIC), consisting of one or more pairs of satellites. This would lead to an improved spatial and temporal resolution of the observations, and most importantly, continuity of this unique time series of global glacier mass balance that started in 2002 with the launch of the GRACE satellites.

7. Strengths and weaknesses of the different techniques

7.1. Comparison over the Vatnajökull Ice Cap - Iceland

The different methods presented in this review are applied to the Vatnajökull Ice Cap, a ~8,000 km² ice mass located in Southeast Iceland (Figure 10). The goal of this comparison is not to single out the best-performing technique or to provide a reconcile mass change estimate, but rather to illustrate the capabilities and characteristics of all these techniques in a concrete case study.

1 Vatnajökull is large enough so that each technique can (almost) resolve it spatially. Another
2 advantage is that comprehensive glaciological field surveys are available (Aðalgeirsdóttir et al.,
3 2020; Björnsson et al., 2013). These *in situ* data measure the surface mass balance (SMB) and have
4 been performed seasonally since September 1991. In Aðalgeirsdóttir et al. (2020), the SMB was
5 corrected for non-surface mass balance components and calving fluxes (Jóhannesson et al., 2020)
6 to calculate the total mass balance, the quantity directly comparable to the remote sensing
7 estimates. Applying or not this challenging correction leads to strikingly different results, this is
8 the reason why both time series (i.e. with/without non surface mass balance components) are
9 retained in Figure 11.

13 The dh/dt map derived from **InSAR TanDEM-X DEMs** for West Vatnajökull was shown in an
14 earlier section of this review (Figure 5). In principle, a complete coverage of the ice cap could be
15 derived from InSAR DEMs at high spatial resolution. Despite a shorter survey period (3.5 years),
16 the spatial pattern of elevation changes for West Vatnajökull is highly similar to the pattern
17 obtained from stereo-imagery and CryoSat-2 swath altimetry. The spatial resolution of the
18 InSAR dh/dt map (6 m) is an order of magnitude higher than the one from ASTER (100 m) and
19 almost two orders of magnitude higher than for CryoSat-2 (500 m). Fine details of the elevation
20 changes are captured in the InSAR map (e.g., the drainage of the Skafta cauldrons (Magnússon
21 et al., 2021)). If a complete map of elevation change was available from TanDEM-X DEMs, the
22 specific challenges to derive an unbiased estimate of the mass balance would be the need (i) to
23 account for temporal changes in X-band radar penetration and (ii) to correct the seasonal bias
24 due to the varying acquisition dates of the DEMs.

31 The dh/dt map based on **ASTER DEMs** (Figure 10a) has a 100-m posting to reduce computing
32 time in a recent global scale study (Hugonnet et al., 2021) but could potentially be derived at 30
33 m which is the posting of ASTER DEMs. The map is gap-free thanks to the relatively good
34 abundance of ASTER DEMs over Iceland compared to other regions on Earth. The massive
35 thinning toward glacier fronts and the surface expression of subglacial volcanic activities (such
36 as the Bárðarbunga caldera collapse (Gudmundsson et al., 2016)) are well captured. A larger
37 noise level is observed in the accumulation areas (where the thickening is less homogeneous,
38 noisier than for CryoSat-2), a consequence of the limited radiometric dynamic in the 8-bit
39 ASTER stereo-imagery over homogeneous snowfields (Figure 4). The time series of cumulative
40 mass change (Figure 11) exhibits a mean seasonal cycle of lower amplitude compared to other
41 techniques and only resolves the variability over periods longer than 4-5 years. One should note
42 that this continuous time series, obtained through Gaussian Process regression, is predicted at a
43 monthly time step but is derived from the temporal interpolation of moderate precision and
44 temporally inconsistent ASTER acquisitions (50 in 20 years, on average). Hence, the inter-annual
45 variability of the mass change, e.g. the positive mass balance during glaciological year 2014-
46 2015 or the strongly negative mass balance in 2009-2010 following the Eyjafjallajökull volcanic
47 eruption (Aðalgeirsdóttir et al., 2020), is not captured.

A. ASTER Jan 2010 to Dec 2019

B. CryoSat-2 Aug 2010 to Aug 2020

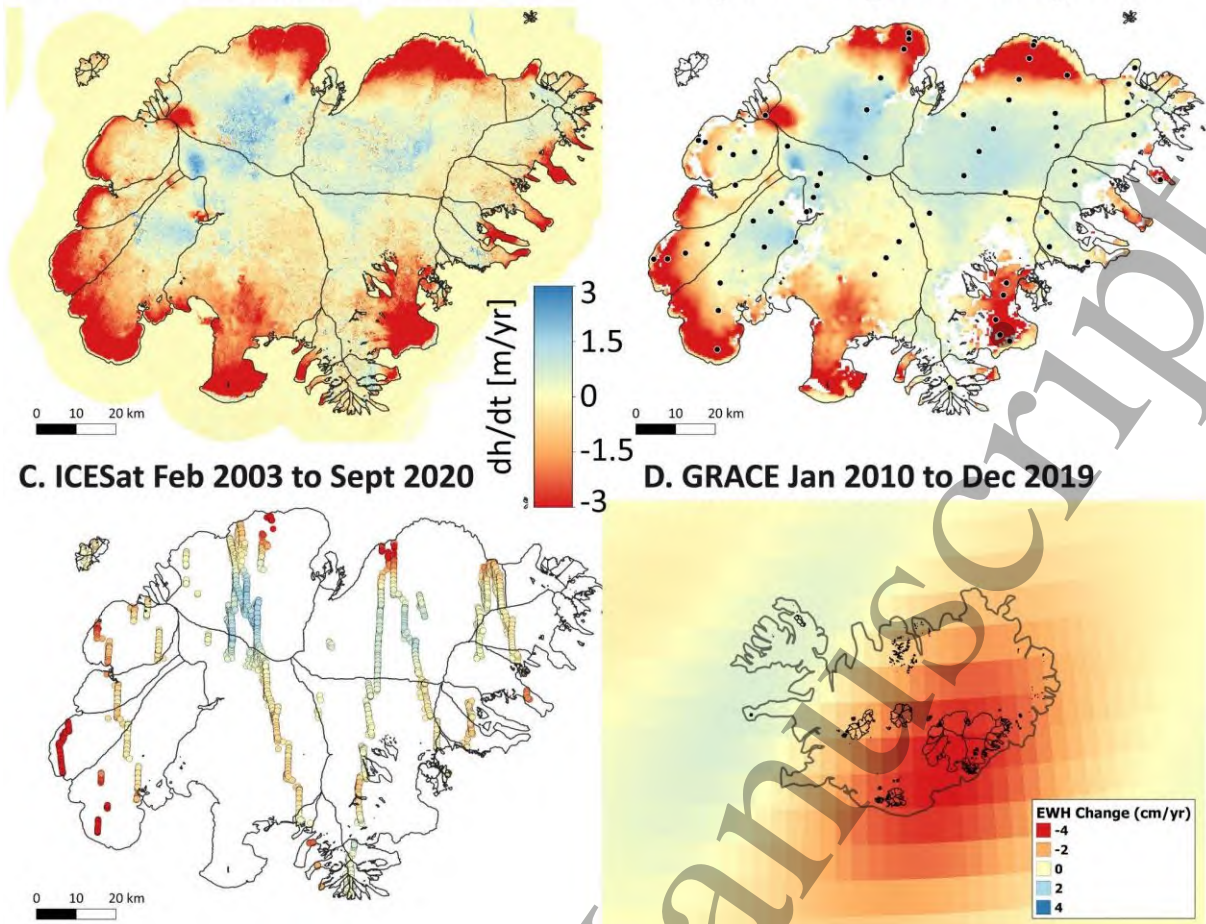


Figure 10: The elevation and mass changes estimates of the Vatnajökull Ice Cap (Iceland). The upper row shows dh/dt (A) applying Gaussian process regression to a time series of ASTER DEMs (Hugonnet et al., 2021) and (B) using CryoSat-2 swath processing (Foresta et al., 2016, updated). The lower panels show (C) dh/dt from ICESat and ICESat-2 (unpublished) and (D) the GRACE/GRACE-FO derived mass change anomaly for entire Iceland (Wouters et al., 2019, updated). For CryoSat-2, dh/dt is obtained by fitting a linear trend to the elevation time series, whereas for other methods it is derived as the difference between the end and start elevations, divided by the time separation. The InSAR dh/dt map for Western Vatnajökull is shown in Figure 5 with the same colour scale as panels A-C. The black dots in panel B locate in situ surface mass balance measurements performed by the University of Iceland (Aðalgeirsdóttir et al., 2020).

CryoSat-2 swath altimetry also provides an almost complete dh/dt map, covering 85% of the ice cap area (Figure 10b). To calculate an ice cap-wide mass balance, gaps are filled using the regional hypsometric approach (McNabb et al., 2019), i.e. using the mean elevation changes of the rest of the ice cap at the same altitude band. CryoSat-2 captures subtle changes in the ice cap interior as well as rapid changes related to the Bárðarbunga caldera collapse or strong thinning at the margins. There is some data loss over the steeper, marginal, parts of the ice cap, including the rapidly thinning margins. CryoSat-2 provides a smooth and continuous time series with monthly estimates thanks to the satellite's repeat period. The monthly repeat allows resolving the seasonal and inter-annual changes, with an amplitude in good agreement with GRACE (before 2016) and with the SMB measurements uncorrected for non surface-mass-balance processes.

1 **Laser altimetry** does not allow continuous temporal sampling due to the gap between ICESat
2 (ending in 2009) and ICESat-2 (launched in 2018). Figure 10c shows elevation change rates from
3 ICESat (GLAH06 L1B Global Elevation Data v34: Zwally et al., 2014) and ICESat-2 (ATL06 L3A Land
4 Ice Height, Version 3: Smith et al., 2021) data. The data span the period February 2003 to
5 September 2020. Rates of change are determined by solving least squares fits of offset, rate and
6 seasonality to elevation anomalies within a 480 m radius of solution points that are separated
7 by 480 m which explain the “stepwise” lines of measurements (Figure 10c). Elevation anomalies
8 are determined relative to the ArcticDEM 8-m Mosaicked DEM v3 (Porter et al., 2018). Despite a
9 rather scarce spatial sampling, laser altimetry is able to capture the main patterns of change,
10 with thinning in the lower reaches and slight thickening in the accumulation area of the two
11 largest outlets of northern Vatnajökull (Dyngjujökull and Bruarjökull). However, ICESat/ICESat-2
12 has no measurement below 450 m a.s.l. and misses the very strong thinning rate on the tongues
13 of the south and south-east flowing outlets. Given this sparse spatial sampling of a complex
14 pattern of elevation changes, we did not attempt here to estimate the total volume and mass
15 change of Vatnajökull. Hence, laser altimetry data are not plotted in Figure 11 and not listed in
16 Table 2.

17
18
19
20
21
22
23 Due to their coarse spatial resolution, **gravimetric** observations are not able to resolve
24 Vatnajökull mass change alone (Figure 10d). We corrected the GRACE-based mass change for
25 entire Iceland (updated from Wouters et al., 2019), with a scaling factor (0.68) deduced from an
26 analysis of glacier mass change for all major ice masses in Iceland, as 68% of the glacier mass
27 loss in Iceland from 2000/01 to 2018/19 originates from Vatnajökull (Aðalgeirsdóttir et al.,
28 2020). The processing of GRACE data was detailed in section 6. In Iceland, particular attention
29 needs to be paid to leakage from the Greenland Ice Sheet or to the ocean together with solid
30 Earth processes, related to mass load changes from glacial isostatic adjustment and little ice age
31 (Sørensen et al., 2011). The seasonal cycle is not as smooth as the one from CryoSat-2 with
32 spikes in the time series, due to measurement noise and the leakage from seasonal snow in the
33 surroundings of the ice cap. The GRACE time series also seems to diverge from the SMB-only in
34 situ and CryoSat-2 measurements after 2016, when it gets close to the ASTER-based results and
35 the glaciological measurements corrected for mass losses not occurring at the surface. Reasons
36 for these differences in the time series remain unclear. This may be explained by less reliable
37 measurements toward the end of the GRACE mission and the fact that GRACE/GRACE_FO also
38 captures the mass loss by other Icelandic ice caps. However, a recent study found a good
39 agreement between GRACE and Cryosat-2 mass balance time series for all icelandic ice caps
40 lumped together (Noël et al., 2022). Hence, a careful comparison of the Cryosat-2 time series
41 from different research groups is needed.

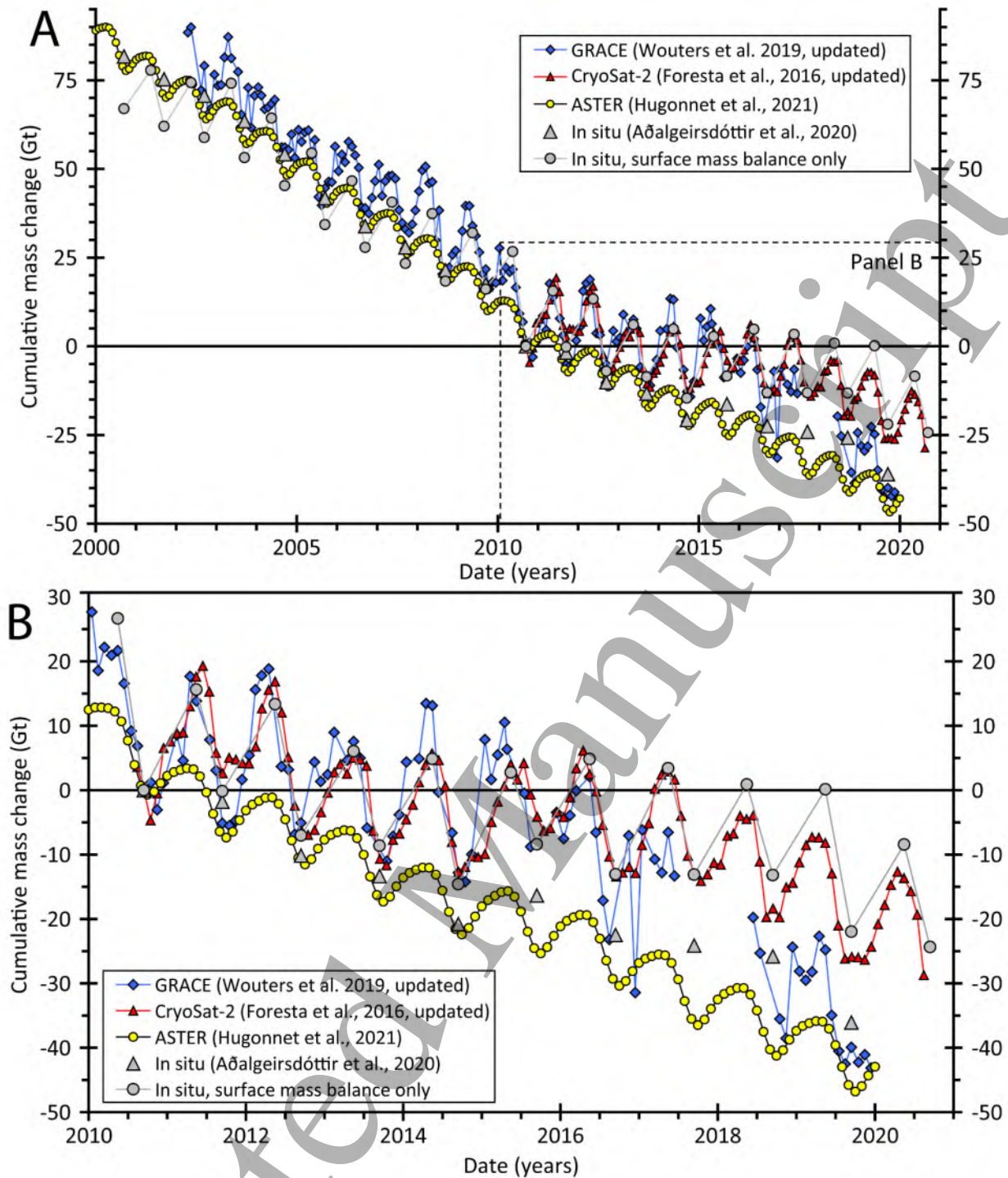


Figure 11: Time series of cumulative mass change (Gt) for Vatnajökull from the different techniques during 2000–2020 (upper panel). The lower panel zooms in over 2010 to 2020, the period common to most techniques. Cumulative mass changes are shown as anomalies compared to 15 September 2010. ICESat estimates are not included because the elevation difference measurements shown in Figure 10c cover a varying time stamp. The main text explains why two time series derived from in situ measurements are included (see beginning of section 7.1).

GRACE excluded, all satellite-based techniques include a conversion of the volume change to mass change, which is done here using an average value of 850 kg/m^3 (Huss, 2013). This value is in principle valid for periods of more than five years (ideally more) and more appropriate for negative mass balance years. This uncertain volume-to-mass conversion remains a major challenge and partly jeopardises the usage of geodetic observations at high temporal resolution. It can easily explain some of the observed differences with GRACE and the in situ

measurements, especially during years of balanced or positive mass budgets. Volcanic activity is another source of discrepancies: a striking example is the 65-m collapse ($\sim 2 \text{ km}^3$) of the Bárðarbunga caldera in 2014 in the northwest of Vatnajökull (Gudmundsson et al., 2016) that can be wrongly attributed to glacier change by elevation change methods.

The average rates of mass change for two different periods are compared in Table 2. Over the longest common period (15 September 2002 to 15 September 2019), the three available estimates show a satisfactory agreement, within $\sim 10\%$. However, over the shorter 9-year period (15 September 2010 to 15 September 2019), differences get larger ($\pm 25\%$) with reduced mass loss from CryoSat-2, higher mass loss from ASTER DEMs and intermediate values for GRACE and the “in situ” measurements corrected for the non-surface components (geothermal melting, volcanic eruptions, the energy dissipation in the flow of water and ice, and calving). Without this correction, in situ measurements are in agreement with Cryosat-2. It is beyond the scope of this review to conclude on the origin of these differences. Understanding them and providing a reconciled estimate of mass change require further work, in particular by examining individual glaciers of the ice cap.

Table 2. Summary of pluri-annual rates of mass changes (Gt/yr) of the Vatnajökull Ice Cap from different techniques. The non surface mass balance components amount to roughly -1.5 Gt/yr . Uncertainties are provided at the 95% confidence interval.

	DEM differencing (Hugonnet et al. 2021)	Gravimetry (Wouters et al., 2019, updated)	CryoSat-2 altimetry (Foresta et al., 2016 updated)	Glaciological, accounting for non-surface mass balance processes (Aðalgeirsdóttir et al., 2020)
sept-2002 to sept-2019	-6.5 ± 1.0	-7.0 ± 1.2	NaN	-6.3 ± 1.6
sept-2010 to sept-2019	-5.1 ± 1.0	-4.4 ± 1.3	-2.9 ± 1.1	-4.0 ± 1.6

7.2. Comparison over the Everest area - Himalaya

To complement the above case study over a large and flat arctic ice cap (Vatnajökull), we illustrate in Figure 12 the ability of the different elevation change methods to sample spatially and temporally glaciers in mountainous areas. The study area covers 100 km by 100 km around Mt Everest (Himalaya), which corresponds roughly to 1/10 of the GRACE resolution. This is why gravimetry data are not shown in this example, they simply cannot resolve glacier mass change at this scale.

DEM differencing resolves the changes of individual glaciers and provides an almost 50-yr long record albeit with a 5 to 10-yr resolution. There are large data gaps in the elevation change maps due to the lack of contrast, mostly in the upper accumulation areas. This is particularly the case when only two DEMs are compared (Fig. 12a). These gaps are reduced when processing a time series of ASTER DEMs (Fig 12b). Gaps would almost vanish if DEMs were derived from 11

or 12-bits modern stereo sensors as illustrated by the complete map of elevation differences for Mera Glacier (30 km south of Mt Everest) obtained by comparing Pléiades DEMs from 2012 and 2018 (Wagnon et al., 2021).

Altimetry data, from ICESat and CryoSat-2, are not able to resolve individual glaciers. They are only able to provide a region-wide mass balance estimate when aggregated over sufficiently large regions so that glaciers (in particular the different elevations bands) are well sampled. The denser sampling by CryoSat-2 swath altimetry and ICESat-2 allows resolving regions of 100 by 100 km and infer the seasonal elevation changes (Jakob et al., 2021; Wang et al., 2021). For ICESat, the spatial sampling was sparser and temporally more irregular so that mass loss estimates were mostly restricted to a single value (for the period 2003-2008) over large regions (Kääb et al., 2015).

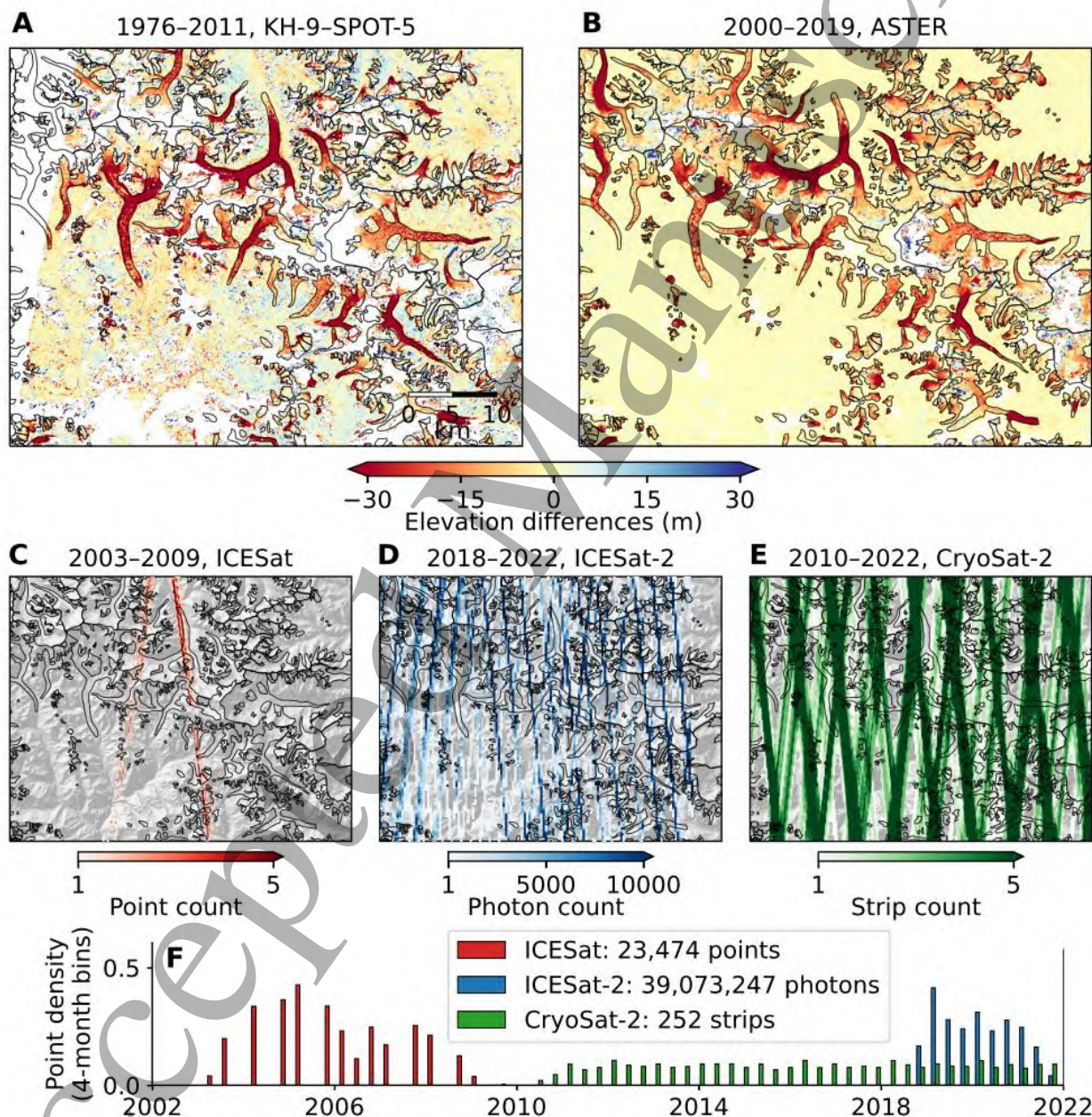


Figure 12. Spatiotemporal coverage and density of the different methods near Mount Everest. A-B, Spatial coverage and elevation change derived from (A) KH-9 Hexagon (Dehecq et al., 2020) and SPOT-5 DEMs (Gardelle et al., 2013), and (B) multiple ASTER DEMs processed using Gaussian Process regression (Hugonnet et al., 2021). Note that the DEMs have a single timestamp and, for ASTER time series, that the

temporal resolution is generally >5 years (statistically significant elevation change rate at the 95% confidence level). C-E, Spatial coverage and density from altimetry over the same area with (C) ICESat footprints, (D) ICESat-2 photons and (E) CryoSat-2 strips, rendered on top of a hillshade. A single CryoSat-2 strip includes, on average, 125 points for the geographic extent considered here. ICESat and ICESat-2 footprints are buffered by 200 m for visualisation purposes. CryoSat-2 swath width is fixed to an average of 1 km. Glacier outlines are shown in black. F, Temporal coverage and temporal density of altimetry measurements. Results of the gravimetry method are not shown due to its inability to resolve changes at this resolution.

7.3. Synthesis of the pros and cons of each method

Table 3 summarises the characteristics, strengths and weaknesses of the remote sensing methods to measure glacier mass changes. It includes some general and well-known limitations such as the dependence on cloud-free conditions for optical stereo-images and laser altimetry and, on the other hand, the need to account for time-variable radar penetration in snow and firn for SAR interferometry or radar altimetry.

As illustrated by our case studies in Iceland and Himalaya, the ability of these methods to resolve mass change depends on the glacier-type, their surrounding topography and the size and latitude of the area. Due to their high resolution (here decametric), DEM-based methods excel in mountainous regions hosting, mostly at low to middle latitudes, a myriad of glaciers of varying size, but generally less than 1000 km². Mass balance can be estimated for each individual glacier, albeit with larger uncertainties for smaller ice bodies. In these regions, the generous availability of stable terrain also facilitates the DEMs coregistration and bias correction. Conversely, the rough topography and modest mean glacier size result in a sparse sampling by laser or radar altimetry so that mass balance can be only computed over large regions, typically accounting 10³ to 10⁴ km² of glaciers. The gravimetric method will also be restricted to region-wide average, and the main challenge is to account for other natural and anthropogenic processes (hydrology, solid earth) influencing its mass change signal.

Over large icefields (Alaska, Patagonia) or Arctic ice caps, DEM differencing is more challenging to apply because of the scarcity of stable terrain, the need to mosaic multiple DEMs of different dates for a full coverage and, specifically for DEMs derived from pre-2010 optical images, the reduced contrasted in the flat accumulation areas. Laser and radar altimetry are well-suited providing a high temporal resolution, down to seasonal time scale. For laser altimetry this is particularly the case for polar areas where ground tracks are repeated exactly. GRACE also works well in principle, although here again the main challenge is to account properly for all non-glacier signals, generally through modelling.

A common limitation of all techniques is that none of them is able to “see” the loss (or gain) of ice below the waterline (sub-aqueous loss or gain) for water-terminating glaciers experiencing calving front migration. This omission does not matter (or very little) for estimating the sea-level contribution as the solid freshwater of the glacier tongue is displacing salted sea water (Seehaus et al., 2015).

Table 3: Capabilities of the different spaceborne techniques to estimate glacier mass change. The regional scale refers to entire RGI regions. The local scale refers to, typically an area of 50-100 km² (i.e. a large glacier or a group of glaciers).

Technique	DEM differencing		Altimetry		Gravimetry		
Sensor	Optical stereo-images	SAR images	Laser (ICESat, ICESat-2)	Radar (CryoSat-2)	GRACE & GRACE-FO		
Spatial resolution / posting	Individual glaciers resolved ; Down to a few metres with modern sensors		Track spacing at 60 deg: ~35 km for ICESat, 8/3.3/3.3 km (between three beam pairs) for ICESat-2	A few 100s m in moderate topography up to several km in extreme topography	~300 km		
Time span	Since 1960s	Since 2000	2003-2009 (ICESat) 2018- (ICESat-2)	Since 2010	2002-2017 (GRACE) 2018- (GRACE-FO)		
Temporal resolution	Typically multi-year at regional scale ; Down to seasonal resolution when high resolution DEMs are frequently available		Seasonal at regional scale	Monthly at large glacier/regional scale	Monthly at regional scale		
Coverage	Global with ASTER ; Local with other sensors	Potentially global with TanDEM-X ; Within 60°N-56°S for SRTM	Global	Global	Global		
Strengths	Associated imagery for interpretation ; Numerous sensors can be combined	All weather ; Associated amplitude and backscatter images for interpretation	Very accurate individual measurements	All weather ; continuous, homogeneous time series	Direct measurements of mass changes (no density assumption needed)		
Weaknesses	Most sensors are commercial, except ASTER not replaced after 2023 ; For 8-bit sensors only: noise in the accumulation areas ; clouds	Time variable penetration of the radar signal	Weather dependant ; no exact repeat ; Sparse or uneven sampling of ablation/accumulation areas often hampering glacier-wide estimates	Time variable penetration of the radar signal	Need to deconvolve other influencing factors (solid earth, hydrological signal) : Need models to bridge the gap between GRACE & GRACE-FO		
						Uncertain volume to mass conversion	
						Sub-aqueous ice losses not observed	

All these limitations and sources of uncertainties lead to a relatively large spread between the mass change estimates of the different techniques. This is well illustrated by a compilation for all glaciers and ice caps in the Russian Arctic updated from Tepes et al. (2021) (Figure 13, Table 4). For this large RGI region (covered by 51500 km² of glaciers), even using the same technique (Gravimetry or DEM differencing), the losses for similar time periods differ by a factor of almost

two (Table 4). Hence, a first step in an intercomparison exercise will consist in understanding the reasons behind the differences between similar techniques.

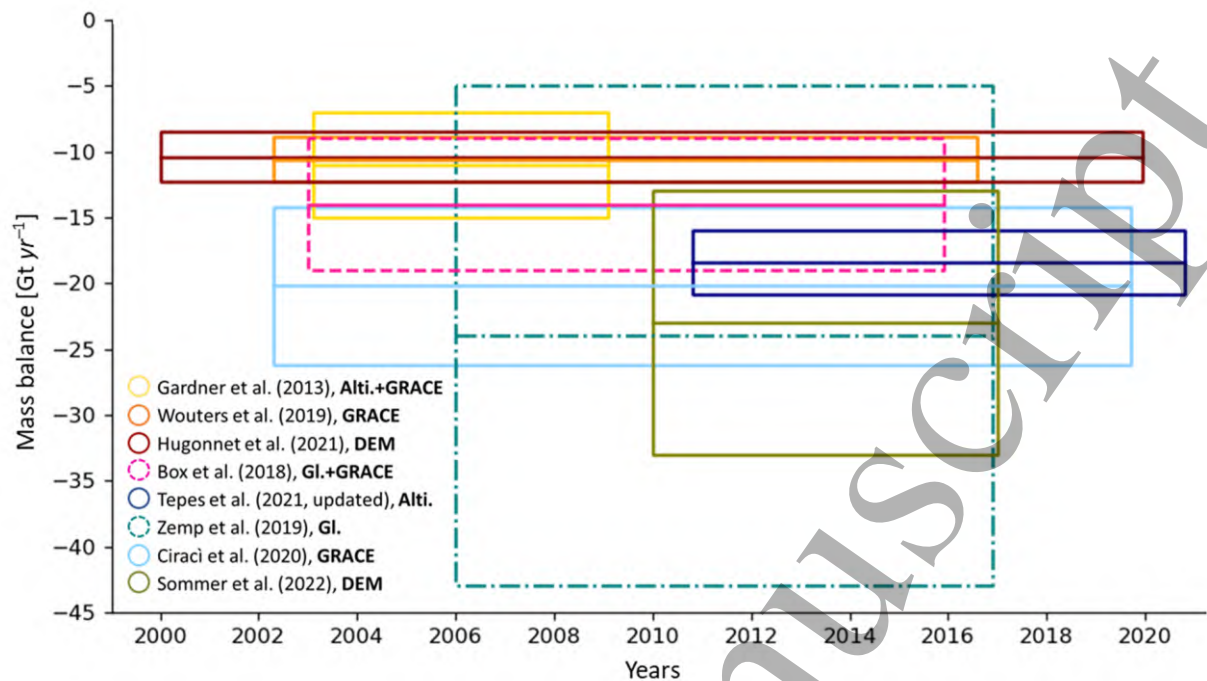


Figure 13: Mass change rates (Gt/yr) for glaciers and ice caps in the Russian Arctic (total glacier area = 51500 km²) since 2000. Estimates from remote sensing are shown with solid lines as opposed to the dashed lines for the other studies (Box et al., 2018; Zemp et al., 2019). The data/method used for each estimate is provided in the legend: Alti = Altimetry, GI = Glaciological, i.e. in situ data. Uncertainties are given at the 2-sigma confidence interval.

Table 4. Rates of mass changes (Gt/yr) in the Russian Arctic from DEM differencing and using the gravimetric method for two periods. The table illustrates how similar methods may lead to contending estimates for the same region and similar periods.

	Gravimetry		DEM differencing	
	Wouters et al., 2019	Ciraci et al., 2020	Stereo-images Hugonnet et al. 2021	InSAR Sommer et al. 2022
Jan 2003 to Dec 2019	-13.9 ± 1.3	-20.3 ± 6.5	-10.9 ± 0.9	
Jan 2011 to Dec 2017	-18.9 ± 2.5	-25.4 ± 7.4	-12.0 ± 2.9	-22.2 ± 6.4*

* For the period winter 2010-11 to winter 2017-18

8. Conclusion

In this review, we presented the different techniques able to measure glacier mass change from space: DEM differencing either from stereo-imagery or from SAR interferometry, laser and radar altimetry and space gravimetry. We illustrated how they perform to survey the mass change of a large Arctic ice body, the Vatnajökull Ice Cap (Iceland) and the smaller and steeper

1 glaciers in the Everest region (Himalaya), and discussed their strengths and weaknesses. We
2 highlighted some differences between the different mass change estimates, especially at short
3 time scales (seasonal or annual). For most main glacier regions, a spread exists between the
4 different techniques, even sometimes when the same technique is applied by different research
5 groups. At global scale, this leads to mass loss estimates varying by 20-30% (see Figure 3b in
6 Hugonnet et al., (2021)).
7
8

9
10 Ten years ago, a handful of field or geodetic measurements on a limited number of glaciers
11 were available and were extrapolated to the entire world. We have now entered a new era
12 where multiple regional, or even global, comprehensive estimates, yet not always in agreement,
13 are available. Understanding the reasons behind these discrepancies will require careful
14 intercomparison work. The range of size (spanning 7 orders of magnitude) and numbers (> 200
15 000) of glaciers is an additional complexity compared to ice sheets and implies that we can
16 hardly rely on a single method that would outperform the others. Instead, a combination of
17 sensors and methods is probably necessary to derive the best possible estimates and to cover
18 multiple time scales. Community efforts aiming at tackling these issues, such as RAGMAC⁶ are
19 eagerly needed.
20
21
22
23

24 A continuity of the underlying satellite missions, with an open data policy, is of the utmost
25 importance to maintain and improve the monitoring of the glaciers of the future, and should be
26 a top priority on the agenda of space agencies⁷. Free and easy scientific access to all satellite
27 data should be the rule for these future satellite missions (Pope et al., 2014). Among the
28 different techniques to measure glacier mass balance from space, continuity seems to be on-
29 track with forthcoming satellite missions such as Harmony for SAR interferometry and CRISTAL
30 for interferometric radar altimetry. Less clear is the continuity of the gravimetric measurements
31 after GRACE-FO, although China has recently launched its own experimental Tianqin-1 gravity
32 mission and NASA and ESA are investigating the options for a joint next-generation gravity
33 mission to be launched by the end of this decade. There are currently no funded laser altimetry
34 missions under development. To our knowledge, no satellite mission is funded to replace ASTER
35 and SPOT5-HRS in order to provide a global, frequent and open-access coverage of the
36 continents with optical stereo-images. A successor should be considered rapidly. Meanwhile,
37 releasing the stereo-images from past or ongoing commercial and defence satellites for
38 scientific use would help to mitigate the data gaps. Would it not make sense in view of the
39 climate crisis?
40
41
42
43
44
45
46
47
48
49

50 Acknowledgments

51 We dedicate this article to our colleague Jérémie Mougnot (CNRS Glaciologist at IGE,
52 Grenoble), who left us in September 2022, far too early. Anny Cazenave and Jérôme Benveniste
53 stimulated us to write this review. We also thank Maud Bernat and Jérôme Lebreton for
54 commenting on an earlier version of the manuscript. Comments by two anonymous referees
55
56
57
58
59

60
6 <https://cryosphericsscience.org/activities/wg-ragmac/>

7 <http://database.eohandbook.com/>

1 contributed to improve the article. Etienne Berthier acknowledges support from the France
2 Space Agency (CNES) through the TOSCA and Pléiades Glacier Observatory programs. The
3 contribution of Frank Paul, Désirée Treichler and Andreas Käab was supported by funding from
4 the ESA project Glaciers_cci+ (4000127593/19/I-NB) and in addition for A.K. ESA Harmony
5 (4000135083/21/NL/FF/ab). Noel Gourmelen acknowledges support from the European Space
6 Agency for the development and application of CryoSat-2 swath processing via projects CryoTop
7 (4000107394/12/I-NB), CryoTop Evolution (4000116874/16/I-NB), CS+ Mountain Glaciers
8 (4000114224/15/I-SBo), and CryoTEMPO EOLIS (4000128095/19/I-DT). Bert Wouters was
9 funded by NWO VIDI grant 016.Vidi.171.063. Dana Floricioiu and Lukas Krieger were supported
10 by the DLR project "Polar Monitor". Alex Gardner and Amaury Dehecq were funded by NASA's
11 Cryospheric Sciences and MEaSURES Programs. This is a contribution of the RAGMAC (Regional
12 Assessments of Glacier Mass Change) working group of the International Association of
13 Cryospheric Sciences.
14
15
16
17
18

19 **Author contribution statement**

20
21
22 EB designed the study and led the writing. DF, AG, NG, LJ, FrP, DT and BW led the writing of
23 specific sections. JB, AD, ID, RH, AK, LK, FiP, MZ contributed to data, to design the figures and to
24 the writing.
25
26
27
28
29
30
31
32
33
34
35
36
37
38
39
40
41
42
43
44
45
46
47
48
49
50
51
52
53
54
55
56
57
58
59
60

References

- Abdel Jaber, W., Rott, H., Floricioiu, D., Wuite, J., and Miranda, N.: Heterogeneous spatial and temporal pattern of surface elevation change and mass balance of the Patagonian ice fields between 2000 and 2016, *The Cryosphere*, 13, 2511–2535, <https://doi.org/10.5194/tc-13-2511-2019>, 2019.
- Abermann, J., Fischer, A., Lambrecht, A., and Geist, T.: On the potential of very high-resolution repeat DEMs in glacial and periglacial environments, *The Cryosphere*, 4, 53–65, <https://doi.org/10.5194/tc-4-53-2010>, 2010.
- Abshire, J. B., Sun, X., Riris, H., Sirota, J. M., McGarry, J. F., Palm, S., Yi, D., and Liiva, P.: Geoscience Laser Altimeter System (GLAS) on the ICESat Mission: On-orbit measurement performance, *Geophysical Research Letters*, 32, <https://doi.org/10.1029/2005GL024028>, 2005.
- Adalgeirsdóttir, G., Echelmeyer, K. A., and Harrison, W. D.: Elevation and volume changes on the Harding Icefield, Alaska, *J Glaciol*, 44, 570–582, 1998.
- Aðalgeirsdóttir, G., Magnússon, E., Pálsson, F., Thorsteinsson, T., Belart, J. M. C., Jóhannesson, T., Hannesdóttir, H., Sigurðsson, O., Gunnarsson, A., Einarsson, B., Berthier, E., Schmidt, L. S., Haraldsson, H. H., and Björnsson, H.: Glacier Changes in Iceland From ~1890 to 2019, *Frontiers in Earth Science*, 8, 520, <https://doi.org/10.3389/feart.2020.523646>, 2020.
- AlRousan, N., Cheng, P., Petrie, G., Toutin, T., and Zoj, M. J. V.: Automated DEM extraction and orthoimage generation from SPOT Level 1B imagery, *Photogrammetric Engineering and Remote Sensing*, 63, 965–974, 1997.
- An, L., Wang, J., Huang, J., Pokhrel, Y., Hugonnet, R., Wada, Y., Cáceres, D., Müller Schmied, H., Song, C., Berthier, E., Yu, H., and Zhang, G.: Divergent Causes of Terrestrial Water Storage Decline Between Drylands and Humid Regions Globally, *Geophysical Research Letters*, 48, e2021GL095035, <https://doi.org/10.1029/2021GL095035>, 2021.
- Andreassen, L. M., Elvehøy, H., Kjøllmoen, B., and Engeset, R. V.: Reanalysis of long-term series of glaciological and geodetic mass balance for 10 Norwegian glaciers, *The Cryosphere*, 10, 535–552, <https://doi.org/10.5194/tc-10-535-2016>, 2016.
- Arendt, A. A., Echelmeyer, K. A., Harrison, W. D., Lingle, C. S., and Valentine, V. B.: Rapid wastage of Alaska glaciers and their contribution to rising sea level, *Science*, 297, 382–386, 2002.
- Bader, H.: Sorge's law of densification of snow on high polar glaciers, *Journal of Glaciology*, 2, 319–323, 1954.
- Bamber, J. L. and Rivera, A.: A review of remote sensing methods for glacier mass balance determination, *Global and Planetary Change*, 59, 138–148, <https://doi.org/10.1016/j.gloplacha.2006.11.031>, 2007.
- Bamber, J. L., Westaway, R. M., Marzeion, B., and Wouters, B.: The land ice contribution to sea level during the satellite era, *Environmental Research Letters*, 13, 063008, 2018.
- Bamler, R. and Hartl, P.: Synthetic aperture radar interferometry, *Inverse Problems*, 14, R1–R54, <https://doi.org/10.1088/0266-5611/14/4/001>, 1998.
- Barandun, M., Pohl, E., Naegeli, K., McNabb, R., Huss, M., Berthier, E., Saks, T., and Hoelzle, M.: Hot Spots of Glacier Mass Balance Variability in Central Asia, *Geophysical Research Letters*, 48, e2020GL092084, <https://doi.org/10.1029/2020GL092084>, 2021.
- Bayr, K. J., Hall, D. K., and Kovalick, W. M.: Observations on glaciers in the eastern Austrian Alps using satellite data, *Journal of Glaciology*, 15, 1733–1742, <https://doi.org/10.1080/01431169408954205>, 1994.
- Belart, J. M. C., Berthier, E., Magnússon, E., Anderson, L. S., Pálsson, F., Thorsteinsson, T., Howat, I. M., Aðalgeirsdóttir, G., Jóhannesson, T., and Jarosch, A. H.: Winter mass balance of Drangajökull ice cap (NW Iceland) derived from satellite sub-meter stereo images, *The Cryosphere*, 11, 1501–1517, <https://doi.org/10.5194/tc-11-1501-2017>, 2017.
- Belart, J. M. C., Magnússon, E., Berthier, E., Pálsson, F., Adalgeirsdóttir, G., and Jóhannesson, T.: The geodetic mass balance of Eyjafjallajökull ice cap for 1945–2014: processing guidelines and relation to climate, *J Glaciol*, 65, 395–409, <https://doi.org/10.1017/jog.2019.16>, 2019.
- Beraud, L., Cusicanqui, D., Rabatel, A., Brun, F., Vincent, C., and Six, D.: Glacier-wide seasonal and annual geodetic mass balances from Pléiades stereo images: application to the Glacier d'Argentière, French Alps, *Journal of Glaciology*, 1–13, <https://doi.org/10.1017/jog.2022.79>, 2022.
- Berthier, E. and Brun, F.: Karakoram geodetic glacier mass balances between 2008 and 2016: persistence of the anomaly and influence of a large rock avalanche on Siachen Glacier, *J Glaciol*, 65, 494–507,

<https://doi.org/10.1017/jog.2019.32>, 2019.

- Berthier, E., Arnaud, Y., Baratoux, D., Vincent, C., and Remy, F.: Recent rapid thinning of the "Mer de Glace" glacier derived from satellite optical images, *Geophysical Research Letters*, 31, L17401, <https://doi.org/10.1029/2004GL020706>, 2004.
- Berthier, E., Vincent, C., Magnússon, E., Gunnlaugsson, Á. Þ., Pitte, P., Le Meur, E., Masiokas, M., Ruiz, L., Pálsson, F., Belart, J. M. C., and Wagnon, P.: Glacier topography and elevation changes derived from Pléiades sub-meter stereo images, *Cryosphere*, 8, 2275–2291, <https://doi.org/10.5194/tc-8-2275-2014>, 2014.
- Beyer, R. A., Alexandrov, O., and McMichael, S.: The Ames Stereo Pipeline: NASA's Open Source Software for Deriving and Processing Terrain Data, *Earth and Space Science*, 5, 537–548, <https://doi.org/10.1029/2018EA000409>, 2018.
- Björnsson, H., Pálsson, F., Guðmundsson, S., Magnússon, E., Aðalgeirsdóttir, G., Jóhannesson, T., Berthier, E., Sigurðsson, O., and Thorsteinsson, T.: Contribution of Icelandic ice caps to sea level rise: trends and variability since the Little Ice Age, *Geophys. Res. Lett.*, 40, 1–5, <https://doi.org/10.1002/grl.50278>, 2013.
- Błaszczuk, M., Jania, J. A., and Hagen, J. O.: Tidewater glaciers of Svalbard: Recent changes and estimates of calving fluxes, *Polish Polar Research*, 30, 85–142, 2009.
- Blazquez, A., Meyssignac, B., Lemoine, J., Berthier, E., Ribes, A., and Cazenave, A.: Exploring the uncertainty in GRACE estimates of the mass redistributions at the Earth surface: implications for the global water and sea level budgets, *Geophysical Journal International*, 215, 415–430, <https://doi.org/10.1093/gji/ggy293>, 2018.
- Bojinski, S., Verstraete, M., Peterson, T. C., Richter, C., Simmons, A., and Zemp, M.: The Concept of Essential Climate Variables in Support of Climate Research, Applications, and Policy, *Bulletin of the American Meteorological Society*, 95, 1431–1443, <https://doi.org/10.1175/BAMS-D-13-00047.1>, 2014.
- Bolch, T., Buchroithner, M., Pieczonka, T., and Kunert, A.: Planimetric and volumetric glacier changes in the Khumbu Himal, Nepal, since 1962 using Corona, Landsat TM and ASTER data, *Journal of Glaciology*, 54, 592–600, 2008.
- Bolch, T., Menounos, B., and Wheate, R.: Landsat-based inventory of glaciers in western Canada, 1985–2005, *Remote Sensing of Environment*, 114, 127–137, 2010.
- Box, J. E., Colgan, W. T., Wouters, B., Burgess, D. O., O'Neel, S., Thomson, L. I., and Mernild, S. H.: Global sea-level contribution from Arctic land ice: 1971–2017, *Environmental Research Letters*, 13, 125012, <https://doi.org/10.1088/1748-9326/aaf2ed>, 2018.
- Braithwaite, R. J. and Raper, S. C. B.: Estimating equilibrium-line altitude (ELA) from glacier inventory data, *Annals of Glaciology*, 50, 127–132, <https://doi.org/10.3189/172756410790595930>, 2009.
- Braun, M. H., Malz, P., Sommer, C., Fariás-Barahona, D., Sauter, T., Casassa, G., Soruco, A., Skvarca, P., and Seehaus, T. C.: Constraining glacier elevation and mass changes in South America, *Nature Climate Change*, 9, 130–136, <https://doi.org/10.1038/s41558-018-0375-7>, 2019.
- Brenner, A. C., Blöndschadler, R. A., Thomas, R. H., and Zwally, H. J.: Slope-induced errors in radar altimetry over continental ice sheets, *Journal of Geophysical Research: Oceans*, 88, 1617–1623, <https://doi.org/10.1029/JC088iC03p01617>, 1983.
- Brenner, A. C., DiMarzio, J. P., and Zwally, H. J.: Precision and Accuracy of Satellite Radar and Laser Altimeter Data Over the Continental Ice Sheets, *IEEE Transactions on Geoscience and Remote Sensing*, 45, 321–331, <https://doi.org/10.1109/TGRS.2006.887172>, 2007.
- Burgess, D. O. and Danielson, B. D.: Meighen Ice Cap: changes in geometry, mass, and climatic response since 1959, *Can. J. Earth Sci.*, 1–13, <https://doi.org/10.1139/cjes-2021-0126>, 2022.
- Carturan, L., Rastner, P., and Paul, F.: On the disequilibrium response and climate change vulnerability of the mass-balance glaciers in the Alps, *Journal of Glaciology*, 1–17, <https://doi.org/10.1017/jog.2020.71>, 2020.
- Cauvy-Fraunié, S. and Dangles, O.: A global synthesis of biodiversity responses to glacier retreat, *Nature Ecology & Evolution*, <https://doi.org/10.1038/s41559-019-1042-8>, 2019.
- Cazenave, A., Meyssignac, B., Ablain, M., Balmaseda, M., Bamber, J., Barletta, V., Beckley, B., Benveniste, J., Berthier, E., Blazquez, A., Boyer, T., Caceres, D., Chambers, D., Champollion, N., Chao, B., Chen, J., Cheng, L., Church, J. A., Chuter, S., Cogley, J. G., Dangendorf, S., Desbruyeres, D., Doell, P., Domingues, C., Falk, U., Famiglietti, J., Fenoglio-Marc, L., Forsberg, R., Galassi, G., Gardner, A.,

- Groh, A., Hamlington, B., Hogg, A., Horwath, M., Humphrey, V., Husson, L., Ishii, M., Jaeggi, A., Jevrejeva, S., Johnson, G., Kolodziejczyk, N., Kusche, J., Lambeck, K., Landerer, F., Leclercq, P., Legresy, B., Leuliette, E., Llovel, W., Longuevergne, L., Loomis, B. D., Luthcke, S. B., Marcos, M., Marzeion, B., Merchant, C., Merrifield, M., Milne, G., Mitchum, G., Mohajerani, Y., Monier, M., Monselesan, D., Nerem, S., Palanisamy, H., Paul, F., Perez, B., Piecuch, C. G., Ponte, R. M., Purkey, S. G., Reager, J. T., Rietbroek, R., Rignot, E., Riva, R., Roemmich, D. H., Sorensen, L. S., Sasgen, I., Schrama, E. J. O., Seneviratne, S. I., Shum, C. K., Spada, G., Stammer, D., van de Wal, R., Velicogna, I., von Schuckmann, K., Wada, Y., Wang, Y., Watson, C., Wiese, D., Wijffels, S., Westaway, R., Woppelmann, G., and Wouters, B.: Global sea-level budget 1993-present, *Earth Syst Sci Data*, 10, 1551–1590, <https://doi.org/10.5194/essd-10-1551-2018>, 2018.
- Chen, J. L., Wilson, C. R., and Tapley, B. D.: Contribution of ice sheet and mountain glacier melt to recent sea level rise, *Nature Geoscience*, 6, 549–552, <https://doi.org/10.1038/ngeo1829>, 2013.
- Ciraci, E., Velicogna, I., and Swenson, S.: Continuity of the Mass Loss of the World's Glaciers and Ice Caps From the GRACE and GRACE Follow-On Missions, *Geophysical Research Letters*, 47, e2019GL086926, <https://doi.org/10.1029/2019GL086926>, 2020.
- Cogley, J. G., Arendt, A. A., Bauder, A., Braithwaite, R. J., Hock, R., Jansson, P., Kaser, G., Moller, M., Nicholson, L., Rasmussen, L. A., and Zemp, M.: Glossary of glacier mass balance and related terms, International Hydrological Programme, Paris, France, 2011.
- Cuffey, K. M. and Paterson, W. S. B.: *The physics of glaciers*, Academic Press Inc, Amsterdam, 2010.
- Dall, J.: InSAR Elevation Bias Caused by Penetration Into Uniform Volumes, *IEEE Transactions on Geoscience and Remote Sensing*, 45, 2319–2324, <https://doi.org/10.1109/TGRS.2007.896613>, 2007.
- Davaze, L., Rabatel, A., Dufour, A., Hugonnet, R., and Arnaud, Y.: Region-Wide Annual Glacier Surface Mass Balance for the European Alps From 2000 to 2016, *Frontiers in Earth Science*, 8, 149, <https://doi.org/10.3389/feart.2020.00149>, 2020.
- Davis, C. H. and Moore, R. K.: A combined surface-and volume-scattering model for ice-sheet radar altimetry, *Journal of Glaciology*, 39, 675–686, <https://doi.org/10.3189/S0022143000016579>, 1993.
- Davis, C. H. and Segura, D. M.: An algorithm for time series analysis of ice sheet surface elevations from satellite altimetry, *IEEE Transactions on Geoscience and Remote Sensing*, 39, 202–206, <https://doi.org/10.1109/36.898686>, 2001.
- Dehecq, A., Gourmelen, N., Shepherd, A., Cullen, R., and Trouvé, E.: Evaluation of CryoSat-2 for height retrieval over the Himalayan range, in: *CryoSat-2 third user workshop*, Dresden, Germany, 2013.
- Dehecq, A., Millan, R., Berthier, E., Gourmelen, N., and Trouve, E.: Elevation changes inferred from TanDEM-X data over the Mont-Blanc area: Impact of the X-band interferometric bias, *IEEE J. Sel. Top. Appl. Earth. Obs. Remote Sens.*, 9, 3870–3882, <https://doi.org/10.1109/JSTARS.2016.2581482>, 2016.
- Dehecq, A., Gardner, A. S., Alexandrov, O., McMichael, S., Hugonnet, R., Shean, D., and Marty, M.: Automated Processing of Declassified KH-9 Hexagon Satellite Images for Global Elevation Change Analysis Since the 1970s, *Frontiers in Earth Science*, 8, 516, <https://doi.org/10.3389/feart.2020.566802>, 2020.
- DLR-EOC: TanDEM-X Ground Segment – DEM Products Specification Document, 2018.
- Dubayah, R., Blair, J. B., Goetz, S., Fatoyinbo, L., Hansen, M., Healey, S., Hofton, M., Hurtt, G., Kellner, J., Luthcke, S., Armston, J., Tang, H., Duncanson, L., Hancock, S., Jantz, P., Marselis, S., Patterson, P. L., Qi, W., and Silva, C.: The Global Ecosystem Dynamics Investigation: High-resolution laser ranging of the Earth's forests and topography, *Science of Remote Sensing*, 1, 100002, <https://doi.org/10.1016/j.srs.2020.100002>, 2020.
- Dussaillant, I., Berthier, E., Brun, F., Masiokas, M., Hugonnet, R., Favier, V., Rabatel, A., Pitte, P., and Ruiz, L.: Two decades of glacier mass loss along the Andes, *Nature Geoscience*, 12, 802–808, <https://doi.org/10.1038/s41561-019-0432-5>, 2019.
- Echelmeyer, K. A., Harrison, W. D., Larsen, C. F., Sapiano, J., Mitchell, J. E., DeMallie, J., Rabus, B., Adalgeirsdottir, G., and Sombardier, L.: Airborne surface profiling of glaciers: A case-study in Alaska, *Journal of Glaciology*, 42, 538–547, 1996.
- Fair, Z., Flanner, M., Brunt, K. M., Fricker, H. A., and Gardner, A.: Using ICESat-2 and Operation IceBridge altimetry for supraglacial lake depth retrievals, *The Cryosphere*, 14, 4253–4263, <https://doi.org/10.5194/tc-14-4253-2020>, 2020.

- 1 Fan, Y., Ke, C.-Q., Zhou, X., Shen, X., Yu, X., and Lhakpa, D.: Glacier mass-balance estimates over High
2 Mountain Asia from 2000 to 2021 based on ICESat-2 and NASADEM, *Journal of Glaciology*, 1–13,
3 <https://doi.org/10.1017/jog.2022.78>, 2022.
- 4 Farinotti, D., Longuevergne, L., Moholdt, G., Duethmann, D., Molg, T., Bolch, T., Vorogushyn, S., and
5 Guntner, A.: Substantial glacier mass loss in the Tien Shan over the past 50 years, *Nature Geosci*, 8,
6 716–722, 2015.
- 7 Farinotti, D., Huss, M., Fürst, J. J., Landmann, J., Machguth, H., Maussion, F., and Pandit, A.: A consensus
8 estimate for the ice thickness distribution of all glaciers on Earth, *Nature Geoscience*,
9 <https://doi.org/10.1038/s41561-019-0300-3>, 2019.
- 10 Farr, T. G., Rosen, P. A., Caro, E., Crippen, R., Duren, R., Hensley, S., Kobrick, M., Paller, M., Rodriguez, E.,
11 Roth, L., Seal, D., Shaffer, S., Shimada, J., Umland, J., Werner, M., Oskin, M., Burbank, D., and
12 Alsdorf, D.: The Shuttle Radar Topography Mission, *Rev. Geophys.*, 45, RG2004,
13 <https://doi.org/10.1029/2005RG000183>, 2007.
- 14 Ferri, L., Dussaillant, I., Zalazar, L., Masiokas, M. H., Ruiz, L., Pitte, P., Gargantini, H., Castro, M., Berthier,
15 E., and Villalba, R.: Ice Mass Loss in the Central Andes of Argentina Between 2000 and 2018
16 Derived From a New Glacier Inventory and Satellite Stereo-Imagery, *Frontiers in Earth Science*, 8,
17 596, <https://doi.org/10.3389/feart.2020.530997>, 2020.
- 18 Finsterwalder, R.: Photogrammetry and glacier research with special reference to glacier retreat in the
19 eastern Alps, *Journal of Glaciology*, 2, 306–315, 1954.
- 20 Fischer, M., Huss, M., and Hoelzle, M.: Surface elevation and mass changes of all Swiss glaciers 1980–
21 2010, *Cryosphere*, 9, 525–540, <https://doi.org/10.5194/tc-9-525-2015>, 2015.
- 22 Foresta, L., Gourmelen, N., Pálsson, F., Nienow, P., Björnsson, H., and Shepherd, A.: Surface elevation
23 change and mass balance of Icelandic ice caps derived from swath mode CryoSat-2 altimetry,
24 *Geophysical Research Letters*, 43, 12,138–12,145, <https://doi.org/10.1002/2016GL071485>, 2016.
- 25 Foresta, L., Gourmelen, N., Weissgerber, F., Nienow, P., Williams, J. J., Shepherd, A., Drinkwater, M. R.,
26 and Plummer, S.: Heterogeneous and rapid ice loss over the Patagonian Ice Fields revealed by
27 CryoSat-2 swath radar altimetry, *Remote Sensing of Environment*, 211, 441–455,
28 <https://doi.org/10.1016/j.rse.2018.03.041>, 2018.
- 29 Frederikse, T., Landerer, F., Caron, L., Adhikari, S., Parkes, D., Humphrey, V. W., Dangendorf, S., Hogarth,
30 P., Zanna, L., Cheng, L., and Wu, Y.-H.: The causes of sea-level rise since 1900, *Nature*, 584, 393–
31 397, <https://doi.org/10.1038/s41586-020-2591-3>, 2020.
- 32 Frey, H., Paul, F., and Strozzi, T.: Compilation of a glacier inventory for the western Himalayas from
33 satellite data: methods, challenges, and results, *Remote Sensing of Environment*, 124, 832–843,
34 <https://doi.org/10.1016/j.rse.2012.06.020>, 2012.
- 35 Fricker, H. A. and Padman, L.: Tides on Filchner-Ronne Ice Shelf from ERS radar altimetry, *Geophysical
36 Research Letters*, 29, 2002.
- 37 Gardelle, J., Berthier, E., and Arnaud, Y.: Impact of resolution and radar penetration on glacier elevation
38 changes computed from multi-temporal DEMs, *Journal of Glaciology*, 58, 419–422, 2012.
- 39 Gardelle, J., Berthier, E., Arnaud, Y., and Käab, A.: Region-wide glacier mass balances over the Pamir-
40 Karakoram-Himalaya during 1999–2011, *Cryosphere*, 7, 1263–1286, <https://doi.org/10.5194/tc-7-1263-2013>, 2013.
- 41 Gardner, A. S., Moholdt, G., Wouters, B., Wolken, G. J., Burgess, D. O., Sharp, M. J., Cogley, J. G., Braun,
42 C., and Labine, C.: Sharply increased mass loss from glaciers and ice caps in the Canadian Arctic
43 Archipelago, *Nature*, 473, 357–360, 2011.
- 44 Gardner, A. S., Moholdt, G., Cogley, J. G., Wouters, B., Arendt, A. A., Wahr, J., Berthier, E., Hock, R.,
45 Pfeffer, W. T., Kaser, G., Ligtenberg, S. R. M., Bolch, T., Sharp, M. J., Hagen, J. O., van den Broeke,
46 M. R., and Paul, F.: A Reconciled Estimate of Glacier Contributions to Sea Level Rise: 2003 to 2009,
47 *Science*, 340, 852–857, <https://doi.org/10.1126/science.1234532>, 2013.
- 48 Ghuffar, S., Bolch, T., Rupnik, E., and Bhattacharya, A.: A pipeline for automated processing of
49 declassified Corona KH-4 (1962–1972) stereo imagery, *IEEE Transactions on Geoscience and
50 Remote Sensing*, 1–1, <https://doi.org/10.1109/TGRS.2022.3200151>, 2022.
- 51 Girod, L., Nuth, C., Käab, A., McNabb, R., and Galland, O.: MMASTER: Improved ASTER DEMs for
52 Elevation Change Monitoring, *Remote Sensing*, 9, <https://doi.org/10.3390/rs9070704>, 2017.
- 53 Gleyzes, M. A., Perret, L., and Kubik, P.: Pléiades system architecture and main performances, *Int. Arch.
54 Photogrammetry, Remote Sens. Spatial Informat. Sci.*, 39, 537–542, 2012.

- 1 Gourmelen, N., Escorihuela, M. J., Shepherd, A., Foresta, L., Muir, A., Garcia-Mondéjar, A., Roca, M.,
2 Baker, S. G., and Drinkwater, M. R.: CryoSat-2 swath interferometric altimetry for mapping ice
3 elevation and elevation change, *Advances in Space Research*, 62, 1226–1242,
4 <https://doi.org/10.1016/j.asr.2017.11.014>, 2018.
- 5 Gray, L., Burgess, D., Copland, L., Cullen, R., Galin, N., Hawley, R., and Helm, V.: Interferometric swath
6 processing of Cryosat data for glacial ice topography, *The Cryosphere*, 7, 1857–1867,
7 <https://doi.org/10.5194/tc-7-1857-2013>, 2013.
- 8 Gray, L., Burgess, D., Copland, L., Demuth, M. N., Dunse, T., Langley, K., and Schuler, T. V.: CryoSat-2
9 delivers monthly and inter-annual surface elevation change for Arctic ice caps, *The Cryosphere*, 9,
10 1895–1913, <https://doi.org/10.5194/tc-9-1895-2015>, 2015.
- 11 Gray, L., Burgess, D., Copland, L., Langley, K., Gogineni, P., Paden, J., Leuschen, C., van As, D., Fausto, R.,
12 Joughin, I., and Smith, B.: Measuring Height Change Around the Periphery of the Greenland Ice
13 Sheet With Radar Altimetry, *Frontiers in Earth Science*, 7, 146,
14 <https://doi.org/10.3389/feart.2019.00146>, 2019.
- 15 Gudmundsson, M. T., Jónsdóttir, K., Hooper, A., Holohan, E. P., Halldórsson, S. A., Ófeigsson, B. G., Cesca,
16 S., Vogfjörð, K. S., Sigmundsson, F., Högnadóttir, T., Einarsson, P., Sigmarsson, O., Jarosch, A. H.,
17 Jónasson, K., Magnússon, E., Hreinsdóttir, S., Bagnardi, M., Parks, M. M., Hjörleifsdóttir, V.,
18 Pálsson, F., Walter, T. R., Schöpfer, M. P. J., Heimann, S., Reynolds, H. I., Dumont, S., Bali, E.,
19 Gudfinnsson, G. H., Dahm, T., Roberts, M. J., Hensch, M., Belart, J. M. C., Spaans, K., Jakobsson, S.,
20 Gudmundsson, G. B., Fridriksdóttir, H. M., Drouin, V., Dürig, T., Aðalgeirsdóttir, G., Riishuus, M. S.,
21 Pedersen, G. B. M., van Boeckel, T., Oddsson, B., Pfeffer, M. A., Barsotti, S., Bergsson, B., Donovan,
22 A., Burton, M. R., and Aiuppa, A.: Gradual caldera collapse at Bárðarbunga volcano, Iceland,
23 regulated by lateral magma outflow, *Science*, 353, <https://doi.org/10.1126/science.aaf8988>, 2016.
- 24 Guo, W., Liu, S., Xu, J., Wu, L., Shangguan, D., Yao, X., Wei, J., Bao, W., Yu, P., Liu, Q., and Jiang, Z.: The
25 second Chinese glacier inventory: data, methods and results, *Journal of Glaciology*, 61, 357–372,
26 <https://doi.org/10.3189/2015JoG14J209>, 2015.
- 27 Haag, W., Braun, L., Uvarov, V., and Makarevich, K.: A comparison of three methods of mass-balance
28 determination in the Tuyuksu glacier region, Tien Shan, Central Asia, *Journal of Glaciology*, 50,
29 505–510, <https://doi.org/10.3189/172756504781829783>, 2004.
- 30 Haeberli, W. and Hoelzle, M.: Application of inventory data for estimating characteristics of and regional
31 climate-change effects on mountain glaciers: a pilot study with the European Alps, *Annals of
32 Glaciology*, 21, 206–212, <https://doi.org/10.3189/S0260305500015834>, 1995.
- 33 Haeberli, W. and Whiteman, C.: *Snow and Ice-Related Hazards, Risks, and Disasters*, 2nd ed., Elsevier,
34 784 pp., 2015.
- 35 Haeberli, W., Huggel, C., Paul, F., and Zemp, M.: The Response of Glaciers to Climate Change:
36 Observations and Impacts☆, in: *Reference Module in Earth Systems and Environmental Sciences*,
37 Elsevier, <https://doi.org/10.1016/B978-0-12-818234-5.00011-0>, 2021.
- 38 Hall, D. K., Ormsby, J. P., Bindschadler, R. A., and Siddalingaiah, H.: Characterization of Snow and Ice
39 Reflectance Zones On Glaciers Using Landsat Thematic Mapper Data, *Annals of Glaciology*, 9, 104–
40 108, <https://doi.org/10.3189/S0260305500000471>, 1987.
- 41 Hawley, R. L., Shepherd, A., Cullen, R., Helm, V., and Wingham, D. J.: Ice-sheet elevations from across-
42 track processing of airborne interferometric radar altimetry, *Geophysical Research Letters*, 36,
43 <https://doi.org/10.1029/2009GL040416>, 2009.
- 44 Herreid, S. and Pellicciotti, F.: The state of rock debris covering Earth's glaciers, *Nature Geoscience*,
45 <https://doi.org/10.1038/s41561-020-0615-0>, 2020.
- 46 Herzfeld, U. C., Trantow, T., Lawson, M., Hans, J., and Medley, G.: Surface heights and crevasse
47 morphologies of surging and fast-moving glaciers from ICESat-2 laser altimeter data - Application
48 of the density-dimension algorithm (DDA-ice) and evaluation using airborne altimeter and Planet
49 SkySat data, *Science of Remote Sensing*, 3, 100013, <https://doi.org/10.1016/j.srs.2020.100013>,
50 2021.
- 51 Hirano, A., Welch, R., and Lang, H.: Mapping from ASTER stereo image data: DEM validation and
52 accuracy assessment, *ISPRS Journal of Photogrammetry and Remote Sensing*, 57, 356–370,
53 [https://doi.org/10.1016/S0924-2716\(02\)00164-8](https://doi.org/10.1016/S0924-2716(02)00164-8), 2003.
- 54 Holzer, N., Vijay, S., Yao, T., Xu, B., Buchroithner, M., and Bolch, T.: Four decades of glacier variations at
55 Muztagh Ata (eastern Pamir): a multi-sensor study including Hexagon KH-9 and Pléiades data, *The*
56
57
58
59
60

Cryosphere, 9, 2071–2088, <https://doi.org/10.5194/tc-9-2071-2015>, 2015.

- 1
2 Howat, I. M., Smith, B. E., Joughin, I., and Scambos, T. A.: Rates of southeast Greenland ice volume loss
3 from combined ICESat and ASTER observations, *Geophys Res Lett*, 35, 2008.
- 4 Howat, I. M., Porter, C., Smith, B. E., Noh, M.-J., and Morin, P.: The Reference Elevation Model of
5 Antarctica, *The Cryosphere*, 13, 665–674, <https://doi.org/10.5194/tc-13-665-2019>, 2019.
- 6 Hugonnet, R., McNabb, R., Berthier, E., Menounos, B., Nuth, C., Girod, L., Farinotti, D., Huss, M.,
7 Dussailant, I., Brun, F., and Kääb, A.: Accelerated global glacier mass loss in the early twenty-first
8 century, *Nature*, 592, 726–731, <https://doi.org/10.1038/s41586-021-03436-z>, 2021.
- 9 Huss, M.: Density assumptions for converting geodetic glacier volume change to mass change,
10 *Cryosphere*, 7, 877–887, <https://doi.org/10.5194/tc-7-877-2013>, 2013.
- 11 Huss, M. and Hock, R.: Global-scale hydrological response to future glacier mass loss, *Nat. Clim. Change*,
12 8, 135–140, <https://doi.org/10.1038/s41558-017-0049-x>, 2018.
- 13 IGOS: Integrated Global Observing Strategy Cryosphere Theme Report: For the Monitoring of our
14 Environment from Space and from Earth, 2007.
- 15 Iliopoulos, C., Mallet, J. P., Laurent, L., Thierry, M., Jérôme, L., Laubier, D., Michaud, J., Juan, V.-S., Le
16 Corre, S., Dusseux, P., Kääb, A., Yesou, H., Mouginot, J., Battiston, S., Clandillon, S., Bergsma, E.,
17 Lucas, A., Dejoux, J.-F., Delvit, J.-M., Dedieu, G., Ferrant, S., Sheeren, D., Lefevre, A., Cantou, J.-P.,
18 Crétaux, J.-F., Almar, R., Berthier, E., Lelong, C., Maurel, P., Faure, J.-F., Nabucet, J., Corpetti, T.,
19 Herrault, P.-A., Puissant, A., Hagolle, O., and Michel, J.: Sentinel-HR Phase 0 Report, CNES - Centre
20 national d'études spatiales, CESBIO, 2022.
- 21 Jacob, T., Wahr, J., Pfeffer, W. T., and Swenson, S.: Recent contributions of glaciers and ice caps to sea
22 level rise, *Nature*, 482, 514–518, <https://doi.org/10.1038/nature10847>, 2012.
- 23 Jakob, L., Gourmelen, N., Ewart, M., and Plummer, S.: Spatially and temporally resolved ice loss in High
24 Mountain Asia and the Gulf of Alaska observed by CryoSat-2 swath altimetry between 2010 and
25 2019, *The Cryosphere*, 15, 1845–1862, <https://doi.org/10.5194/tc-15-1845-2021>, 2021.
- 26 Janke, J. R., Bellisario, A. C., and Ferrando, F. A.: Classification of debris-covered glaciers and rock glaciers
27 in the Andes of central Chile, *Geomorphology*, 241, 98–121,
28 <https://doi.org/10.1016/j.geomorph.2015.03.034>, 2015.
- 29 Jóhannesson, T., Pálmason, B., Hjartarson, Á., Jarosch, A. H., Magnússon, E., Belart, J. M. C., and
30 Gudmundsson, M. T.: Non-surface mass balance of glaciers in Iceland, *Journal of Glaciology*, 66,
31 685–697, <https://doi.org/10.1017/jog.2020.37>, 2020.
- 32 Kääb, A.: Monitoring high-mountain terrain deformation from repeated air- and spaceborne optical data:
33 examples using digital aerial imagery and ASTER data, *ISPRS J Photogramm*, 57, 39–52, 2002.
- 34 Kääb, A.: Glacier volume changes using ASTER satellite stereo and ICESat GLAS laser altimetry. A test
35 study on Edgeøya, Eastern Svalbard, *IEEE Transactions on Geoscience and Remote Sensing*, 46,
36 2823–2830, 2008.
- 37 Kääb, A., Berthier, E., Nuth, C., Gardelle, J., and Arnaud, Y.: Contrasting patterns of early 21st century
38 glacier mass change in the Himalaya, *Nature*, 488, 495–498, <https://doi.org/10.1038/nature11324>,
39 2012.
- 40 Kääb, A., Treichler, D., Nuth, C., and Berthier, E.: Brief Communication: Contending estimates of 2003–
41 2008 glacier mass balance over the Pamir–Karakoram–Himalaya, *Cryosphere*, 9, 557–564,
42 <https://doi.org/10.5194/tc-9-557-2015>, 2015.
- 43 Kääb, A., Winsvold, S. H., Altena, B., Nuth, C., Nagler, T., and Wuite, J.: Glacier Remote Sensing Using
44 Sentinel-2. Part I: Radiometric and Geometric Performance, and Application to Ice Velocity,
45 *Remote Sensing*, 8, <https://doi.org/10.3390/rs8070598>, 2016.
- 46 Kacimi, S. and Kwok, R.: The Antarctic sea ice cover from ICESat-2 and CryoSat-2: freeboard, snow depth,
47 and ice thickness, *The Cryosphere*, 14, 4453–4474, <https://doi.org/10.5194/tc-14-4453-2020>,
48 2020.
- 49 Kargel, J. S., Abrams, M. J., Bishop, M. P., Bush, A., Hamilton, G., Jiskoot, H., Kääb, A., Kieffer, H. H., Lee,
50 E. M., Paul, F., Rau, F., Raup, B., Shroder, J. F., Soltesz, D., Stainforth, D., Stearns, L., and Wessels,
51 R.: Multispectral imaging contributions to global land ice measurements from space, *Remote
52 Sensing of Environment*, 99, 187–219, 2005.
- 53 Kargel, J. S., Leonard, G. L., Wheate, R., and Edwards, B.: ASTER and DEM change assessment of glaciers
54 near Hoodoo Mountain, British Columbia, Canada, in: *Global Land Ice Measurements from Space*,
55 Kargel J. S., Leonard G. J., Bishop M. P., Kääb A. and Raup B., Berlin Heidelberg, 353–373, 2014.
- 56
57
58
59
60

- 1 Kaser, G., Cogley, J. G., Dyurgerov, M. B., Meier, M. F., and Ohmura, A.: Mass balance of glaciers and ice
2 caps: Consensus estimates for 1961–2004, *Geophysical Research Letters*, 33, L19501, 2006.
- 3 Kern, M., Cullen, R., Berruti, B., Bouffard, J., Casal, T., Drinkwater, M. R., Gabriele, A., Lecuyot, A., Ludwig,
4 M., Midthassel, R., Navas Traver, I., Parrinello, T., Ressler, G., Andersson, E., Martin-Puig, C.,
5 Andersen, O., Bartsch, A., Farrell, S., Fleury, S., Gascoïn, S., Guillot, A., Humbert, A., Rinne, E.,
6 Shepherd, A., van den Broeke, M. R., and Yackel, J.: The Copernicus Polar Ice and Snow
7 Topography Altimeter (CRISTAL) high-priority candidate mission, *The Cryosphere*, 14, 2235–2251,
8 <https://doi.org/10.5194/tc-14-2235-2020>, 2020.
- 9 Kienholz, C., Herreid, S., Rich, J. L., Arendt, A. A., Hock, R., and Burgess, E. W.: Derivation and analysis of a
10 complete modern-date glacier inventory for Alaska and northwest Canada, *Journal of Glaciology*,
11 61, 403–420, <https://doi.org/10.3189/2015JoG14J230>, 2015.
- 12 Kochtitzky, W., Copland, L., Van Wychen, W., Hugonnet, R., Hock, R., Dowdeswell, J. A., Benham, T.,
13 Strozzi, T., Glazovsky, A., Lavrentiev, I., Rounce, D. R., Millan, R., Cook, A., Dalton, A., Jiskoót, H.,
14 Cooley, J., Jania, J., and Navarro, F.: The unquantified mass loss of Northern Hemisphere marine-
15 terminating glaciers from 2000–2020, *Nat Commun*, 13, 5835, [https://doi.org/10.1038/s41467-
16 022-33231-x](https://doi.org/10.1038/s41467-022-33231-x), 2022.
- 17 Korona, J., Berthier, E., Bernard, M., Remy, F., and Thouvenot, E.: SPIRIT. SPOT 5 stereoscopic survey of
18 Polar Ice: Reference Images and Topographies during the fourth International Polar Year (2007-
19 2009), *ISPRS J. Photogramm.*, 64, 204–212, <https://doi.org/10.1016/j.isprsjprs.2008.10.005>, 2009.
- 20 Krieger, G., Moreira, A., Fiedler, H., Hajnsek, I., Werner, M., Younis, M., and Zink, M.: TanDEM-X: A
21 satellite formation for high-resolution SAR interferometry, *IEEE Transactions on Geoscience and
22 Remote Sensing*, 45, 3317–3341, 2007.
- 23 Krieger, G., Zonno, M., Mittermayer, J., Moreira, A., Huber, S., and Rodriguez-Cassola, M.: MirrorSAR: A
24 Fractionated Space Transponder Concept for the Implementation of Low-Cost Multistatic SAR
25 Missions, in: *Proceedings of the European Conference on Synthetic Aperture Radar, EUSAR,*
26 *Aachen, Germany, 1359–1364, 2018.*
- 27 Krieger, L., Strößenreuther, U., Helm, V., Floricioiu, D., and Horwath, M.: Synergistic Use of Single-Pass
28 Interferometry and Radar Altimetry to Measure Mass Loss of NEGIS Outlet Glaciers between 2011
29 and 2014, *Remote Sensing*, 12, <https://doi.org/10.3390/rs12060996>, 2020.
- 30 Lambrecht, A., Mayer, C., Wendt, A., Floricioiu, D., and Völkse, C.: Elevation change of Fedchenko
31 Glacier, Pamir Mountains, from GNSS field measurements and TanDEM-X elevation models, with a
32 focus on the upper glacier, *J Glaciol*, 64, 637–648, <https://doi.org/10.1017/jog.2018.52>, 2018.
- 33 Lamsal, D., Sawagaki, T., and Watanabe, T.: Digital Terrain Modelling Using Corona and ALOS PRISM Data
34 to Investigate the Distal Part of Imja Glacier, Khumbu Himal, Nepal, *Journal of Mountain Science*,
35 8, 390–402, <https://doi.org/10.1007/s11629-011-2064-0>, 2011.
- 36 Landerer, F. W., Flechtner, F. M., Save, H., Webb, F. H., Bandikova, T., Bertiger, W. I., Bettadpur, S. V.,
37 Byun, S. H., Dahle, C., Dobslaw, H., Fahnestock, E., Harvey, N., Kang, Z., Kruizinga, G. L. H., Loomis,
38 B. D., McCullough, C., Murböck, M., Nagel, P., Paik, M., Pie, N., Poole, S., Strelakov, D., Tamisiea,
39 M. E., Wang, F., Watkins, M. M., Wen, H.-Y., Wiese, D. N., and Yuan, D.-N.: Extending the Global
40 Mass Change Data Record: GRACE Follow-On Instrument and Science Data Performance,
41 *Geophysical Research Letters*, 47, e2020GL088306, <https://doi.org/10.1029/2020GL088306>, 2020.
- 42 Li, J., Li, Z.-W., Hu, J., Wu, L.-X., Li, X., Guo, L., Liu, Z., Miao, Z.-L., Wang, W., and Chen, J.-L.: Investigating
43 the bias of TanDEM-X digital elevation models of glaciers on the Tibetan Plateau: impacting factors
44 and potential effects on geodetic mass-balance measurements, *Journal of Glaciology*, 1–14,
45 <https://doi.org/10.1017/jog.2021.15>, 2021.
- 46 Luthcke, S. B., Thomas, T. C., Pennington, T. A., Rebold, T. W., Nicholas, J. B., Rowlands, D. D., Gardner, A.
47 S., and Bae, S.: ICESat-2 Pointing Calibration and Geolocation Performance, *Earth and Space
48 Science*, 8, e2020EA001494, <https://doi.org/10.1029/2020EA001494>, 2021.
- 49 MacGregor, J. A., Boisvert, L. N., Medley, B., Petty, A. A., Harbeck, J. P., Bell, R. E., Blair, J. B., Blanchard-
50 Wrigglesworth, E., Buckley, E. M., Christoffersen, M. S., Cochran, J. R., Csathó, B. M., De Marco, E.
51 L., Dominguez, R. T., Fahnestock, M. A., Farrell, S. L., Gogineni, S. P., Greenbaum, J. S., Hansen, C.
52 M., Hofton, M. A., Holt, J. W., Jezek, K. C., Koenig, L. S., Kurtz, N. T., Kwok, R., Larsen, C. F.,
53 Leuschen, C. J., Locke, C. D., Manizade, S. S., Martin, S., Neumann, T. A., Nowicki, S. M. J., Paden, J.
54 D., Richter-Menge, J. A., Rignot, E. J., Rodríguez-Morales, F., Siegfried, M. R., Smith, B. E., Sonntag,
55 J. G., Studinger, M., Tinto, K. J., Truffer, M., Wagner, T. P., Woods, J. E., Young, D. A., and Yungel, J.

- 1 K.: The Scientific Legacy of NASA's Operation IceBridge, *Reviews of Geophysics*, 59,
2 e2020RG000712, <https://doi.org/10.1029/2020RG000712>, 2021.
- 3 Magnússon, E., Pálsson, F., Gudmundsson, M. T., Högnadóttir, T., Rossi, C., Thorsteinsson, T., Ófeigsson,
4 B. G., Sturkell, E., and Jóhannesson, T.: Development of a subglacial lake monitored with radio-
5 echo sounding: case study from the eastern Skaftá cauldron in the Vatnajökull ice cap, Iceland,
6 *The Cryosphere*, 15, 3731–3749, <https://doi.org/10.5194/tc-15-3731-2021>, 2021.
- 7 Magruder, L., Brunt, K., Neumann, T., Klotz, B., and Alonzo, M.: Passive Ground-Based Optical
8 Techniques for Monitoring the On-Orbit ICESat-2 Altimeter Geolocation and Footprint Diameter,
9 *Earth and Space Science*, 8, e2020EA001414, <https://doi.org/10.1029/2020EA001414>, 2021.
- 10 Malczyk, G., Gourmelen, N., Goldberg, D., Wuite, J., and Nagler, T.: Repeat Subglacial Lake Drainage and
11 Filling Beneath Thwaites Glacier, *Geophysical Research Letters*, 47, e2020GL089658,
12 <https://doi.org/10.1029/2020GL089658>, 2020.
- 13 Malz, P., Meier, W., Casassa, G., Jaña, R., Skvarca, P., and Braun, H. M.: Elevation and Mass Changes of
14 the Southern Patagonia Icefield Derived from TanDEM-X and SRTM Data, *Remote Sensing*, 10,
15 <https://doi.org/10.3390/rs10020188>, 2018.
- 16 Markus, T., Neumann, T., Martino, A., Abdalati, W., Brunt, K., Csatho, B., Farrell, S., Fricker, H., Gardner,
17 A., Harding, D., Jasinski, M., Kwok, R., Magruder, L., Lubin, D., Luthcke, S., Morison, J., Nelson, R.,
18 Neuenschwander, A., Palm, S., Popescu, S., Shum, C., Schutz, B. E., Smith, B., Yang, Y., and Zwally,
19 J.: The Ice, Cloud, and land Elevation Satellite-2 (ICESat-2): Science requirements, concept, and
20 implementation, *Remote Sensing of Environment*, 190, 260–273,
21 <https://doi.org/10.1016/j.rse.2016.12.029>, 2017.
- 22 Martin, T. V., Zwally, H. J., Brenner, A. C., and Bindschadler, R. A.: Analysis and retracking of continental
23 ice sheet radar altimeter waveforms, *Journal of Geophysical Research: Oceans*, 88, 1608–1616,
24 <https://doi.org/10.1029/JC088iC03p01608>, 1983.
- 25 Martín-Español, A., King, M. A., Zammit-Mangion, A., Andrews, S. B., Moore, P., and Bamber, J. L.: An
26 assessment of forward and inverse GIA solutions for Antarctica, *Journal of Geophysical Research:*
27 *Solid Earth*, 121, 6947–6965, <https://doi.org/10.1002/2016JB013154>, 2016.
- 28 Marzeion, B., Cogley, J. G., Richter, K., and Parkes, D.: Attribution of global glacier mass loss to
29 anthropogenic and natural causes, *Science*, 345, 919–921,
30 <https://doi.org/10.1126/science.1254702>, 2014.
- 31 Marzeion, B., Champollion, N., Haeberli, W., Langley, K., Leclercq, P., and Paul, F.: Observation-Based
32 Estimates of Global Glacier Mass Change and Its Contribution to Sea-Level Change, *Surveys in*
33 *Geophysics*, 38, 105–130, <https://doi.org/10.1007/s10712-016-9394-y>, 2017.
- 34 Maurer, J. and Rupper, S.: Tapping into the Hexagon spy imagery database: a new automated workflow
35 for geomorphic change detection, *ISPRS Journal of Photogrammetry and Remote Sensing*, 108,
36 113–127, 2015.
- 37 Maurer, J. M., Schaefer, J. M., Rupper, S., and Corley, A.: Acceleration of ice loss across the Himalayas
38 over the past 40 years, *Sci Adv*, 5, eaav7266, <https://doi.org/10.1126/sciadv.aav7266>, 2019.
- 39 McMillan, M., Shepherd, A., Gourmelen, N., Dehecq, A., Leeson, A., Ridout, A., Flament, T., Hogg, A.,
40 Gilbert, L., Benham, T., van den Broeke, M., Dowdeswell, J. A., Fettweis, X., Noël, B., and Strozzi,
41 T.: Rapid dynamic activation of a marine-based Arctic ice cap, *Geophysical Research Letters*, 41,
42 8902–8909, <https://doi.org/10.1002/2014GL062255>, 2014.
- 43 McNabb, R., Nuth, C., Käab, A., and Girod, L.: Sensitivity of glacier volume change estimation to DEM
44 void interpolation, *Cryosphere*, 13, 895–910, <https://doi.org/10.5194/tc-13-895-2019>, 2019.
- 45 McNabb, R. W., Hock, R., and Huss, M.: Variations in Alaska tidewater glacier frontal ablation, 1985–
46 2013, *Journal of Geophysical Research: Earth Surface*, 120, 120–136,
47 <https://doi.org/10.1002/2014JF003276>, 2015.
- 48 Meier, M. F.: Contribution of Small Glaciers to Global Sea Level, *Science*, 226, 1418–1421, 1984.
- 49 Michaelides, R. J., Bryant, M. B., Siegfried, M. R., and Borsa, A. A.: Quantifying Surface-Height Change
50 Over a Periglacial Environment With ICESat-2 Laser Altimetry, *Earth and Space Science*, 8,
51 e2020EA001538, <https://doi.org/10.1029/2020EA001538>, 2021.
- 52 Millan, R., Mouginot, J., Rabatel, A., and Morlighem, M.: Ice velocity and thickness of the world's
53 glaciers, *Nature Geoscience*, 15, 124–129, <https://doi.org/10.1038/s41561-021-00885-z>, 2022.
- 54 Moholdt, G., Nuth, C., Hagen, J. O., and Kohler, J.: Recent elevation changes of Svalbard glaciers derived
55 from repeat track ICESat altimetry, *Remote Sensing of the Environment*, 114, 2756–2767, 2010.

- 1
2
3
4
5
6
7
8
9
10
11
12
13
14
15
16
17
18
19
20
21
22
23
24
25
26
27
28
29
30
31
32
33
34
35
36
37
38
39
40
41
42
43
44
45
46
47
48
49
50
51
52
53
54
55
56
57
58
59
60
- Moreira, A., Zink, M., Bartusch, M., Quiroz, A. E. N., and Stettner, S.: German Spaceborne SAR Missions, in: 2021 IEEE Radar Conference (RadarConf21), 2021 IEEE Radar Conference (RadarConf21), journalAbbreviation: 2021 IEEE Radar Conference (RadarConf21), 1–6, <https://doi.org/10.1109/RadarConf2147009.2021.9455326>, 2021.
- Morris, A., Moholdt, G., and Gray, L.: Spread of Svalbard Glacier Mass Loss to Barents Sea Margins Revealed by CryoSat-2, *Journal of Geophysical Research: Earth Surface*, 125, e2019JF005357, <https://doi.org/10.1029/2019JF005357>, 2020.
- Morris, A., Moholdt, G., Gray, L., Schuler, T. V., and Eiken, T.: CryoSat-2 interferometric mode calibration and validation: A case study from the Austfonna ice cap, Svalbard, *Remote Sensing of Environment*, 269, 112805, <https://doi.org/10.1016/j.rse.2021.112805>, 2022.
- Neumann, T. A., Martino, A. J., Markus, T., Bae, S., Bock, M. R., Brenner, A. C., Brunt, K. M., Cavanaugh, J., Fernandes, S. T., Hancock, D. W., Harbeck, K., Lee, J., Kurtz, N. T., Luers, P. J., Luthcke, S. B., Magruder, L., Pennington, T. A., Ramos-Izquierdo, L., Rebold, T., Skoog, J., and Thomas, T. C.: The Ice, Cloud, and Land Elevation Satellite – 2 mission: A global geolocated photon product derived from the Advanced Topographic Laser Altimeter System, *Remote Sensing of Environment*, 233, 111325, <https://doi.org/10.1016/j.rse.2019.111325>, 2019.
- Nilsson, J., Vallenga, P., Simonsen, S. B., Sørensen, L. S., Forsberg, R., Dahl-Jensen, D., Hirabayashi, M., Goto-Azuma, K., Hvidberg, C. S., Kjær, H. A., and Satow, K.: Greenland 2012 melt event effects on CryoSat-2 radar altimetry, *Geophysical Research Letters*, 42, 3919–3926, <https://doi.org/10.1002/2015GL063296>, 2015a.
- Nilsson, J., Sandberg Sørensen, L., Barletta, V. R., and Forsberg, R.: Mass changes in Arctic ice caps and glaciers: implications of regionalizing elevation changes, *The Cryosphere*, 9, 139–150, <https://doi.org/10.5194/tc-9-139-2015>, 2015b.
- Nilsson, J., Gardner, A., Sandberg Sørensen, L., and Forsberg, R.: Improved retrieval of land ice topography from CryoSat-2 data and its impact for volume-change estimation of the Greenland Ice Sheet, *The Cryosphere*, 10, 2953–2969, <https://doi.org/10.5194/tc-10-2953-2016>, 2016.
- Noël, B., van de Berg, W. J., Lhermitte, S., Wouters, B., Schaffer, N., and van den Broeke, M. R.: Six Decades of Glacial Mass Loss in the Canadian Arctic Archipelago, *Journal of Geophysical Research: Earth Surface*, 123, 1430–1449, <https://doi.org/10.1029/2017JF004304>, 2018.
- Noël, B., Aðalgeirsdóttir, G., Pálsson, F., Wouters, B., Lhermitte, S., Haacker, J. M., and van den Broeke, M. R.: North Atlantic Cooling is Slowing Down Mass Loss of Icelandic Glaciers, *Geophysical Research Letters*, 49, e2021GL095697, <https://doi.org/10.1029/2021GL095697>, 2022.
- Noh, M.-J. and Howat, I. M.: Automated stereo-photogrammetric DEM generation at high latitudes: Surface Extraction with TIN-based Search-space Minimization (SETSM) validation and demonstration over glaciated regions, *GIScience & Remote Sensing*, 52, 198–217, <https://doi.org/10.1080/15481603.2015.1008621>, 2015.
- Nuimura, T., Fujita, K., Yamaguchi, S., and Sharma, R. R.: Elevation changes of glaciers revealed by multitemporal digital elevation models calibrated by GPS survey in the Khumbu region, Nepal Himalaya, 1992–2008, *Journal of Glaciology*, 58, 648–656, <https://doi.org/10.3189/2012JoG11J061>, 2012.
- Nuth, C. and Kääb, A.: Co-registration and bias corrections of satellite elevation data sets for quantifying glacier thickness change, *Cryosphere*, 5, 271–290, <https://doi.org/10.5194/tcd-4-2013-2010>, 2011.
- Nuth, C., Kohler, J., Aas, H. F., Brandt, O., and Hagen, J. O.: Glacier geometry and elevation changes on Svalbard (1936–90): a baseline dataset, *Ann Glaciol*, 46, 106–116, 2007.
- Oerlemans, J.: *Glaciers and climate change*, edited by: Oerlemans, J., A. A. Balkema Publishers, Rotterdam, 2001.
- Oerlemans, J.: Extracting a climate signal from 169 glacier records, *Science*, 308, 675–677, 2005.
- Ohmura, A., Kasser, P., and Funk, M.: Climate at the Equilibrium Line of Glaciers, *Journal of Glaciology*, 38, 397–411, <https://doi.org/10.3189/S0022143000002276>, 1992.
- Pálsson, F., Gudmundsson, Sv., Björnsson, H., Berthier, E., Magnússon, E., Gudmundsson, Sn., and Haraldsson, H.: Mass and volume changes of Langjökull ice cap, Iceland, ~1890 to 2009, deduced from old maps, satellite images and in situ mass balance measurements, *Jökull*, 62, 81–96, 2012.
- Paul, F., Kääb, A., Maisch, M., Kellenberger, T., and Haeberli, W.: The new remote-sensing-derived swiss glacier inventory: I. Methods, *Annals of Glaciology*, 34, 355–361, 2002.
- Paul, F., Barrand, N. E., Berthier, E., Bolch, T., Casey, K., Frey, H., Joshi, S. P., Konovalov, V., Le Bris, R.,

- 1 Moelg, N., Nuth, C., Pope, A., Racoviteanu, A., Rastner, P., Raup, B., Scharrer, K., Steffen, S., and
2 Winswold, S.: On the accuracy of glacier outlines derived from remote sensing data, *Ann. Glaciol.*,
3 54, 171–182, <https://doi.org/10.3189/2013AoG63A296>, 2013.
- 4 Paul, F., Winsvold, S. H., Käab, A., Nagler, T., and Schwaizer, G.: Glacier Remote Sensing Using Sentinel-2.
5 Part II: Mapping Glacier Extents and Surface Facies, and Comparison to Landsat 8, *Remote*
6 *Sensing*, 8, <https://doi.org/10.3390/rs8070575>, 2016.
- 7 Paul, F., Rastner, P., Azzoni, R. S., Diolaiuti, G., Fugazza, D., Le Bris, R., Nemeč, J., Rabatel, A., Ramusovic,
8 M., Schwaizer, G., and Smiraglia, C.: Glacier shrinkage in the Alps continues unabated as revealed
9 by a new glacier inventory from Sentinel-2, *Earth Syst. Sci. Data*, 12, 1805–1821,
10 <https://doi.org/10.5194/essd-12-1805-2020>, 2020.
- 11 Pelto, M. S.: Forecasting temperate alpine glacier survival from accumulation zone observations,
12 *Cryosphere*, 4, 67–75, 2010.
- 13 Pfeffer, W. T., Arendt, A. A., Bliss, A., Bolch, T., Cogley, J. G., Gardner, A. S., Hagen, J.-O., Hock, R., Kaser,
14 G., Kienholz, C., Miles, E. S., Moholdt, G., Moelg, N., Paul, F., Radic, V., Rastner, P., Raup, B. H.,
15 Rich, J., Sharp, M. J., Andeassen, L. M., Bajracharya, S., Barrand, N. E., Beedle, M. J., Berthier, E.,
16 Bhabri, R., Brown, I., Burgess, D. O., Burgess, E. W., Cawkwell, F., Chinn, T., Copland, L., Cullen, N.
17 J., Davies, B., De Angelis, H., Fountain, A. G., Frey, H., Giffen, B. A., Glasser, N. F., Gurney, S. D.,
18 Hagg, W., Hall, D. K., Haritashya, U. K., Hartmann, G., Herreid, S., Howat, I., Jiskoot, H., Khromova,
19 T. E., Klein, A., Kohler, J., König, M., Kriegel, D., Kutuzov, S., Lavrentiev, I., Le Bris, R., Li, X., Manley,
20 W. F., Mayer, C., Menounos, B., Mercer, A., Mool, P., Negrete, A., Nosenko, G., Nuth, C., Osmonov,
21 A., Pettersson, R., Racoviteanu, A., Ranzi, R., Sarikaya, M. A., Schneider, C., Sigurdsson, O., Sirguey,
22 P., Stokes, C. R., Wheate, R., Wolken, G. J., Wu, L. Z., and Wyatt, F. R.: The Randolph Glacier
23 Inventory: a globally complete inventory of glaciers, *J. Glaciol.*, 60, 537–552,
24 <https://doi.org/10.3189/2014JoG13J176>, 2014.
- 25 Pieczonka, T., Bolch, T., and Buchroithner, M.: Generation and evaluation of multitemporal digital terrain
26 models of the Mt. Everest area from different optical sensors, *ISPRS Journal of Photogrammetry*
27 *and Remote Sensing*, 66, 927–940, <https://doi.org/10.1016/j.isprsjprs.2011.07.003>, 2011.
- 28 Pope, A., Rees, W. G., Fox, A. J., and Fleming, A.: Open Access Data in Polar and Cryospheric Remote
29 Sensing, *Remote Sensing*, 6, 6183–6220, <https://doi.org/10.3390/rs6076183>, 2014.
- 30 Porter, C., Morin, P., Howat, I., Noh, M.-J., Bates, B., Peterman, K., Keeseey, S., Schlenk, M., Gardiner, J.,
31 Tomko, K., Willis, M., Kelleher, C., Cloutier, M., Husby, E., Foga, S., Nakamura, H., Platson, M.,
32 Wethington, M., Jr., Williamson, C., Bauer, G., Enos, J., Arnold, G., Kramer, W., Becker, P., Doshi,
33 A., D'Souza, C., Cummins, P., Laurier, F., and Bojesen, M.: ArcticDEM, ,
34 <https://doi.org/10.7910/DVN/OHHUKH>, 2018.
- 35 Portner, H.-O., Roberts, D. C., Masson-Delmotte, V., Zhai, P., Tignor, M., Poloczanska, E., Mintenbeck, K.,
36 Alegría, A., Nicolai, M., Okem, A., Petzold, J., Rama, B., and Weyer, N. M.: IPCC Special Report on
37 the Ocean and Cryosphere in a Changing Climate, 2019.
- 38 Pritchard, H. D.: Asia's shrinking glaciers protect large populations from drought stress, *Nature*, 569,
39 649–654, <https://doi.org/10.1038/s41586-019-1240-1>, 2019.
- 40 Pritchard, H. D., Arthern, R. J., Vaughan, D. G., and Edwards, L. A.: Extensive dynamic thinning on the
41 margins of the Greenland and Antarctic ice sheets, *Nature*, 461, 971–975, 2009.
- 42 Racoviteanu, A. E., Nicholson, L., Glasser, N. F., Miles, E., Harrison, S., and Reynolds, J. M.: Debris-
43 covered glacier systems and associated glacial lake outburst flood hazards: challenges and
44 prospects, *Journal of the Geological Society*, 179, jgs2021-084, <https://doi.org/10.1144/jgs2021-084>, 2022.
- 45 Ragettli, S., Bolch, T., and Pellicciotti, F.: Heterogeneous glacier thinning patterns over the last 40 years
46 in Langtang Himal, Nepal, *Cryosphere*, 10, 2075–2097, <https://doi.org/10.5194/tc-10-2075-2016>,
47 2016.
- 48 Raup, B. H., Kieffer, H. H., Hare, T. M., and Kargel, J. S.: Generation of data acquisition requests for the
49 ASTER satellite instrument for monitoring a globally distributed target: Glaciers, *IEEE Transactions*
50 *on Geoscience and Remote Sensing*, 38, 1105–1112, <https://doi.org/10.1109/36.841989>, 2000.
- 51 Reager, J. T., Gardner, A. S., Famiglietti, J. S., Wiese, D. N., Eicker, A., and Lo, M.-H.: A decade of sea level
52 rise slowed by climate-driven hydrology, *Science*, 351, 699,
53 <https://doi.org/10.1126/science.aad8386>, 2016.
- 54 RGI Consortium: Randolph Glacier Inventory – A Dataset of Global Glacier Outlines: Version 6.0, 2017.

- 1 Rignot, E., Rivera, A., and Casassa, G.: Contribution of the Patagonia Icefields of South America to sea
2 level rise, *Science*, 302, 434–437, 2003.
- 3 Rizzoli, P., Martone, M., Gonzalez, C., Wecklich, C., Borla Tridon, D., Bräutigam, B., Bachmann, M.,
4 Schulze, D., Fritz, T., Huber, M., Wessel, B., Krieger, G., Zink, M., and Moreira, A.: Generation and
5 performance assessment of the global TanDEM-X digital elevation model, *ISPRS Journal of*
6 *Photogrammetry and Remote Sensing*, 132, 119–139,
7 <https://doi.org/10.1016/j.isprsjprs.2017.08.008>, 2017.
- 8 Rosen, P. A., Hensley, S., Joughin, I. R., Li, F. K., Madsen, S. N., Rodriguez, E., and Goldstein, R. M.:
9 Synthetic aperture radar interferometry, *Proceedings of the IEEE*, 88, 333–382,
10 <https://doi.org/10.1109/5.838084>, 2000.
- 11 Rossi, C., Rodriguez Gonzalez, F., Fritz, T., Yague-Martinez, N., and Eineder, M.: TanDEM-X calibrated Raw
12 DEM generation, *ISPRS Journal of Photogrammetry and Remote Sensing*, 73, 12–20,
13 <https://doi.org/10.1016/j.isprsjprs.2012.05.014>, 2012.
- 14 Rott, H., Scheiblauer, S., Wuite, J., Krieger, L., Floricioiu, D., Rizzoli, P., Libert, L., and Nagler, T.:
15 Penetration of interferometric radar signals in Antarctic snow, *The Cryosphere*, 15, 4399–4419,
16 <https://doi.org/10.5194/tc-15-4399-2021>, 2021.
- 17 Rupnik, E., Pierrot-Deseilligny, M., and Delorme, A.: 3D reconstruction from multi-view VHR-satellite
18 images in MicMac, *ISPRS Journal of Photogrammetry and Remote Sensing*, 139, 201–211,
19 <https://doi.org/10.1016/j.isprsjprs.2018.03.016>, 2018.
- 20 Sakai, A., Nuimura, T., Fujita, K., Takenaka, S., Nagai, H., and Lamsal, D.: Climate regime of Asian glaciers
21 revealed by GAMDAM glacier inventory, *The Cryosphere*, 9, 865–880, [https://doi.org/10.5194/tc-](https://doi.org/10.5194/tc-9-865-2015)
22 [9-865-2015](https://doi.org/10.5194/tc-9-865-2015), 2015.
- 23 Salim, E., Ravel, L., Bourdeau, P., and Deline, P.: Glacier tourism and climate change: effects,
24 adaptations, and perspectives in the Alps, *Regional Environmental Change*, 21, 120,
25 <https://doi.org/10.1007/s10113-021-01849-0>, 2021.
- 26 Save, H., Bettadpur, S., and Tapley, B. D.: High-resolution CSR GRACE RL05 mascons, *Journal of*
27 *Geophysical Research: Solid Earth*, 121, 7547–7569, <https://doi.org/10.1002/2016JB013007>, 2016.
- 28 Scanlon, B. R., Zhang, Z., Save, H., Sun, A. Y., Müller Schmied, H., van Beek, L. P. H., Wiese, D. N., Wada,
29 Y., Long, D., Reedy, R. C., Longuevergne, L., Döll, P., and Bierkens, M. F. P.: Global models
30 underestimate large decadal declining and rising water storage trends relative to GRACE satellite
31 data, *Proc Natl Acad Sci USA*, 115, E1080, <https://doi.org/10.1073/pnas.1704665115>, 2018.
- 32 Schenk, T. and Csatho, B.: A New Methodology for Detecting Ice Sheet Surface Elevation Changes From
33 Laser Altimetry Data, *IEEE Transactions on Geoscience and Remote Sensing*, 50, 3302–3316,
34 <https://doi.org/10.1109/TGRS.2011.2182357>, 2012.
- 35 Scherler, D., Wulf, H., and Gorelick, N.: Global Assessment of Supraglacial Debris-Cover Extents,
36 *Geophysical Research Letters*, 45, 11,798–11,805, <https://doi.org/10.1029/2018GL080158>, 2018.
- 37 Schutz, B. E., Zwally, H. J., Shuman, C. A., Hancock, D., and DiMarzio, J. P.: Overview of the ICESat
38 Mission, *Geophysical Research Letters*, 32, 2005.
- 39 Schwitter, M. P. and Raymond, C. F.: Changes in the Longitudinal Profiles of Glaciers during Advance and
40 Retreat, *Journal of Glaciology*, 39, 582–590, 1993.
- 41 Seehaus, T., Marinsek, S., Helm, V., Skvarca, P., and Braun, M.: Changes in ice dynamics, elevation and
42 mass discharge of Dinsmoor-Bombardier-Edgeworth glacier system, Antarctic Peninsula, *Earth and*
43 *Planetary Science Letters*, 427, 125–135, <https://doi.org/10.1016/j.epsl.2015.06.047>, 2015.
- 44 Seehaus, T., Morgenshtern, V. I., Hübner, F., Bänsch, E., and Braun, M. H.: Novel Techniques for Void
45 Filling in Glacier Elevation Change Data Sets, *Remote Sensing*, 12,
46 <https://doi.org/10.3390/rs12233917>, 2020.
- 47 Shean, D. E., Alexandrov, O., Moratto, Z. M., Smith, B. E., Joughin, I. R., Porter, C., and Morin, P.: An
48 automated, open-source pipeline for mass production of digital elevation models (DEMs) from
49 very-high-resolution commercial stereo satellite imagery, *ISPRS J. Photogramm.*, 116, 101–117,
50 <https://doi.org/10.1016/j.isprsjprs.2016.03.012>, 2016.
- 51 Shean, D. E., Bhushan, S., Montesano, P., Rounce, D. R., Arendt, A., and Osmanoglu, B.: A Systematic,
52 Regional Assessment of High Mountain Asia Glacier Mass Balance, *Frontiers in Earth Science*, 7,
53 363, <https://doi.org/10.3389/feart.2019.00363>, 2020.
- 54 Slobbe, D. C., Lindenbergh, R. C., and Ditmar, P.: Estimation of volume change rates of Greenland's ice
55 sheet from ICESat data using overlapping footprints, *Remote Sensing of Environment*, 112, 4204–
56

4213, 2008.

- 1 Smith, B., Fricker, H. A., Gardner, A. S., Medley, B., Nilsson, J., Paolo, F. S., Holschuh, N., Adusumilli, S.,
2 Brunt, K., Csatho, B., Harbeck, K., Markus, T., Neumann, T., Siegfried, M. R., and Zwally, H. J.:
3 Pervasive ice sheet mass loss reflects competing ocean and atmosphere processes, *Science*, 368,
4 1239, <https://doi.org/10.1126/science.aaz5845>, 2020.
- 5
6 Smith, B., Fricker, H. A., Gardner, A., Siegfried, M. R., Adusumilli, S., Csatho, B. M., Holschuh, N., Nilsson,
7 J., Paolo, F. S., and ICESat-2 Science Team: ATLAS/ICESat-2 L3A Land Ice Height, Version 3, Boulder,
8 Colorado USA., <https://doi.org/10.5067/ATLAS/ATL06.003>, 2021.
- 9 Smith, B. E., Gardner, A., Schneider, A., and Flanner, M.: Modeling biases in laser-altimetry
10 measurements caused by scattering of green light in snow, *Remote Sensing of Environment*, 215,
11 398–410, <https://doi.org/10.1016/j.rse.2018.06.012>, 2018.
- 12 Sommer, C., Seehaus, T., Glazovsky, A., and Braun, M. H.: Brief communication: Increased glacier mass
13 loss in the Russian High Arctic (2010–2017), *The Cryosphere*, 16, 35–42,
14 <https://doi.org/10.5194/tc-16-35-2022>, 2022.
- 15 Sørensen, L. S., Simonsen, S. B., Nielsen, K., Lucas-Picher, P., Spada, G., Adalgeirsdóttir, G., Forsberg, R.,
16 and Hvidberg, C. S.: Mass balance of the Greenland ice sheet (2003–2008) from ICESat data – the
17 impact of interpolation, sampling and firn density, *The Cryosphere*, 5, 173–186,
18 <https://doi.org/10.5194/tc-5-173-2011>, 2011.
- 19 Sørensen, L. S., Jarosch, A. H., Aðalgeirsdóttir, G., Barletta, V. R., Forsberg, R., Pálsson, F., Björnsson, H.,
20 and Jóhannesson, T.: The effect of signal leakage and glacial isostatic rebound on GRACE-derived
21 ice mass changes in Iceland, *Geophysical Journal International*, 209, 226–233,
22 <https://doi.org/10.1093/gji/ggx008>, 2017.
- 23 Surazakov, A. B. and Aizen, V. B.: Positional accuracy evaluation of declassified Hexagon KH-9 mapping
24 camera imagery, *Photogrammetric Engineering & Remote Sensing*, 76, 603–608, 2010.
- 25 Swenson, S. and Wahr, J.: Methods for inferring regional surface-mass anomalies from Gravity Recovery
26 and Climate Experiment (GRACE) measurements of time-variable gravity, *Journal of Geophysical
27 Research: Solid Earth*, 107, ETG 3-1, <https://doi.org/10.1029/2001JB000576>, 2002.
- 28 Tapley, B. D., Bettadpur, S., Ries, J. C., Thompson, P. F., and Watkins, M. M.: GRACE Measurements of
29 Mass Variability in the Earth System, *Science*, 305, 503–505,
30 <https://doi.org/10.1126/science.1099192>, 2004.
- 31 Tapley, B. D., Watkins, M. M., Flechtner, F., Reigber, C., Bettadpur, S., Rodell, M., Sasgen, I., Famiglietti, J.
32 S., Landerer, F. W., Chambers, D. P., Reager, J. T., Gardner, A. S., Save, H., Ivins, E. R., Swenson, S.
33 C., Boening, C., Dahle, C., Wiese, D. N., Dobslaw, H., Tamisiea, M. E., and Velicogna, I.:
34 Contributions of GRACE to understanding climate change, *Nature Climate Change*,
35 <https://doi.org/10.1038/s41558-019-0456-2>, 2019.
- 36 Taylor, L. S., Quincey, D. J., Smith, M. W., Baumhoer, C. A., McMillan, M., and Mansell, D. T.: Remote
37 sensing of the mountain cryosphere: Current capabilities and future opportunities for research,
38 *Progress in Physical Geography: Earth and Environment*, 45, 931–964,
39 <https://doi.org/10.1177/03091333211023690>, 2021.
- 40 Tepes, P., Gourmelen, N., Nienow, P., Tsamados, M., Shepherd, A., and Weissgerber, F.: Changes in
41 elevation and mass of Arctic glaciers and ice caps, 2010–2017, *Remote Sensing of Environment*,
42 261, 112481, <https://doi.org/10.1016/j.rse.2021.112481>, 2021.
- 43 The IMBIE Team: Mass balance of the Greenland Ice Sheet from 1992 to 2018, *Nature*, 579, 233–239,
44 <https://doi.org/10.1038/s41586-019-1855-2>, 2020.
- 45 Thibert, E., Blanc, R., Vincent, C., and Eckert, N.: Glaciological and volumetric mass-balance
46 measurements: error analysis over 51 years for Glacier de Sarennes, French Alps, *Journal of
47 Glaciology*, 54, 522–532, 2008.
- 48 Toutin, T.: Elevation modelling from satellite visible and infrared (VIR) data, *International Journal of
49 Remote Sensing*, 22, 1097–1125, 2001.
- 50 Treichler, D.: Measuring mountain glaciers and snow with a spaceborne laser, PhD thesis, Department of
51 Geosciences, University of Oslo, Norway, 2017.
- 52 Treichler, D. and Käab, A.: Snow depth from ICESat laser altimetry — A test study in southern Norway,
53 *Remote Sensing of Environment*, 191, 389–401, <https://doi.org/10.1016/j.rse.2017.01.022>, 2017.
- 54 Treichler, D., Käab, A., Salzmann, N., and Xu, C.-Y.: Recent glacier and lake changes in High Mountain Asia
55 and their relation to precipitation changes, *The Cryosphere*, 13, 2977–3005,

<https://doi.org/10.5194/tc-13-2977-2019>, 2019.

- Trewin, B., Cazenave, A., Howell, S., Huss, M., Isensee, K., Palmer, M. D., Tarasova, O., and Vermeulen, A.: *Headline Indicators for Global Climate Monitoring*, *Bulletin of the American Meteorological Society*, 102, E20–E37, <https://doi.org/10.1175/BAMS-D-19-0196.1>, 2021.
- Van Wychen, W., Davis, J., Burgess, D. O., Copland, L., Gray, L., Sharp, M., and Mortimer, C.: *Characterizing interannual variability of glacier dynamics and dynamic discharge (1999–2015) for the ice masses of Ellesmere and Axel Heiberg Islands, Nunavut, Canada*, *Journal of Geophysical Research: Earth Surface*, 121, 39–63, <https://doi.org/10.1002/2015JF003708>, 2016.
- Wagnon, P., Brun, F., Khadka, A., Berthier, E., Shrestha, D., Vincent, C., Arnaud, Y., Six, D., Dehecq, A., Ménégoz, M., and Jomelli, V.: *Reanalysing the 2007–19 glaciological mass-balance series of Mera Glacier, Nepal, Central Himalaya, using geodetic mass balance*, *Journal of Glaciology*, 67, 117–125, <https://doi.org/10.1017/jog.2020.88>, 2021.
- Wahr, J., Molenaar, M., and Bryan, F.: *Time variability of the Earth's gravity field: Hydrological and oceanic effects and their possible detection using GRACE*, *Journal of Geophysical Research: Solid Earth*, 103, 30205–30229, <https://doi.org/10.1029/98JB02844>, 1998.
- Wang, Q., Yi, S., and Sun, W.: *Continuous Estimates of Glacier Mass Balance in High Mountain Asia Based on ICESat-1,2 and GRACE/GRACE Follow-On Data*, *Geophysical Research Letters*, 48, e2020GL090954, <https://doi.org/10.1029/2020GL090954>, 2021.
- Wessel, B., Huber, M., Wohlfart, C., Marschalk, U., Kosmann, D., and Roth, A.: *Accuracy assessment of the global TanDEM-X Digital Elevation Model with GPS data*, *ISPRS Journal of Photogrammetry and Remote Sensing*, 139, 171–182, <https://doi.org/10.1016/j.isprsjprs.2018.02.017>, 2018.
- Willis, M. J., Melkonian, A. K., Pritchard, M. E., and Ramage, J. A.: *Ice loss rates at the Northern Patagonian Icefield derived using a decade of satellite remote sensing*, *Remote Sensing of Environment*, 117, 184–198, 2012.
- Wingham, D. J., Rapley, C. G., and Griffiths, H.: *New techniques in satellite altimeter tracking systems*, in: *Proceedings of IGARSS 88 Symposium, Zurich, Switzerland*, 1339–1344, 1986.
- Wingham, D. J., Francis, C. R., Baker, S., Bouzinac, C., Brockley, D., Cullen, R., de Chateau-Thierry, P., Laxon, S. W., Mallow, U., Mavrocordatos, C., Phalippou, L., Ratier, G., Rey, L., Rostan, F., Viau, P., and Wallis, D. W.: *CryoSat: A mission to determine the fluctuations in Earth's land and marine ice fields*, *Advances in Space Research*, 37, 841–871, <https://doi.org/10.1016/j.asr.2005.07.027>, 2006.
- Wouters, B., Chambers, D., and Schrama, E. J. O.: *GRACE observes small-scale mass loss in Greenland*, *Geophysical Research Letters*, 35, L20501, <https://doi.org/10.1029/2008GL034816>, 2008.
- Wouters, B., Gardner, A. S., and Moholdt, G.: *Global Glacier Mass Loss During the GRACE Satellite Mission (2002-2016)*, *Front. Earth Sci.*, 7, 96, <https://doi.org/10.3389/feart.2019.00096>, 2019.
- Wulder, M. A., Masek, J. G., Cohen, W. B., Loveland, T. R., and Woodcock, C. E.: *Opening the archive: How free data has enabled the science and monitoring promise of Landsat*, *Remote Sensing of Environment*, 122, 2–10, <https://doi.org/10.1016/j.rse.2012.01.010>, 2012.
- Zemp, M., Thibert, E., Huss, M., Stumm, D., Rolstad Denby, C., Nuth, C., Nussbaumer, S. U., Moholdt, G., Mercer, A., Mayer, C., Joerg, P. C., Jansson, P., Hynek, B., Fischer, A., Escher-Vetter, H., Elvehøy, H., and Andreassen, L. M.: *Reanalysing glacier mass balance measurement series*, *Cryosphere*, 7, 1227–1245, <https://doi.org/10.5194/tc-7-1227-2013>, 2013.
- Zemp, M., Frey, H., Gaertner-Roer, I., Nussbaumer, S. U., Hoelzle, M., Paul, F., Haeberli, W., Denzinger, F., Ahlstrom, A. P., Anderson, B., Bajracharya, S., Baroni, C., Braun, L. N., Caceres, B. E., Casassa, G., Cobos, G., Davila, L. R., Delgado Granados, H., Demuth, M. N., Espizua, L., Fischer, A., Fujita, K., Gadek, B., Ghazanfar, A., Hagen, J. O., Holmlund, P., Karimi, N., Li, Z., Pelto, M., Pitte, P., Popovnin, V. V., Portocarrero, C. A., Prinz, R., Sangewar, C. V., Severskiy, I., Sigurosson, O., Soruco, A., Usabaliev, R., and Vincent, C.: *Historically unprecedented global glacier decline in the early 21st century*, *J. Glaciol.*, 61, 745–+, <https://doi.org/10.3189/2015JoG15J017>, 2015.
- Zemp, M., Huss, M., Thibert, E., Eckert, N., McNabb, R., Huber, J., Barandun, M., Machguth, H., Nussbaumer, S. U., Gärtner-Roer, I., Thomson, L., Paul, F., Maussion, F., Kutuzov, S., and Cogley, J. G.: *Global glacier mass changes and their contributions to sea-level rise from 1961 to 2016*, *Nature*, 568, 382–386, <https://doi.org/10.1038/s41586-019-1071-0>, 2019.
- Zemp, M., Huss, M., Eckert, N., Thibert, E., Paul, F., Nussbaumer, S. U., and Gärtner-Roer, I.: *Brief communication: Ad hoc estimation of glacier contributions to sea-level rise from the latest glaciological observations*, *The Cryosphere*, 14, 1043–1050, <https://doi.org/10.5194/tc-14-1043->

2020, 2020.

Zhou, Y., Li, Z., Li, J., Zhao, R., and Ding, X.: Glacier mass balance in the Qinghai–Tibet Plateau and its surroundings from the mid-1970s to 2000 based on Hexagon KH-9 and SRTM DEMs, *Remote Sensing of Environment*, 210, 96–112, <https://doi.org/10.1016/j.rse.2018.03.020>, 2018.

Zwally, H. J., Schutz, R., DiMarzio, J. P., and Hancock, D.: GLAS/ICESat L1B Global Elevation Data (HDF5), Version 34, Boulder, Colorado, USA, <https://doi.org/10.5067/ICESAT/GLAS/DATA109>, 2014.

Accepted Manuscript